POLITECNICO DI MILANO
School of Industrial and Information Engineering

Laurea Magistrale in Mechanical Engineering

DESIGN ANALYSIS FOR THE EMERGENCY VENTILATION REQUIREMENTS OF RAILWAY TUNNELS

–

THE CASE STUDY OF KHOR FAKKAN TUNNEL.

Supervisor: Prof. Claudio Somaschini
Co-Supervisor: Ing. Gabriele D'Uva

Master's degree thesis by:
Muhammad Rizwanullah Shaik
883090

Academic Year 2019/20

To my family.

Acknowledgement

First and foremost, praise be to Almighty God who bestowed me with the strength both physically and mentally in order to carry out successfully the thesis work. This thesis became a reality with the support and help of many individuals, whose names may not all be enumerated.

This thesis would have not been possible without the continuous support and patience of my principal supervisor, Prof. Claudio Somaschini, providing me with invaluable guidance, suggestions and comments throughout the thesis work, pushing me further than I thought I could go.

I would like to thank my company supervisor Ing. Gabriele D'Uva, at Italferr S.p.A., who believed in me and gave me the opportunity to carry out this project work. I am truly grateful for his unwavering support and encouragement. His enthusiasm and unlimited zeal have been the major driving force that helped me forge this work. I am indebted and grateful to him for sharing his wisdom and experience and being available at all times to solve all of my doubts and confusions.

A very special thanks to Gorghinian Debora Brigit, at Italferr S.p.A., for guiding and helping me understand the functions and activities of the organization from time to time. I would also like to extend my warmest gratitude to the entire team of Italferr S.p.A. for making me part of the family. My sincere thanks to Simone Ascrizzi, Francesca Barbera and Angelo Dimasi.

Also, I would like to thank my friends Raghupathi Nirajankumar and Akhif Rasheed for their support and motivation. Finally, my deepest appreciation belongs to my family, my parents, Kareemulla and Nazeem; and my sisters Tanzeem and Aeysha for helping me survive all the stress, for their moral support and most importantly not letting me give up.

Table of Contents

List of Figures

List of Tables

About the Company: Italferr

The following thesis work was carried out in collaboration with Italferr S.p.A., an engineering company of the Ferrovie dello Stato Italiane Group, that provides multi-disciplinary services and comprehensive designs in the field of the transportation sector according to the very latest technological and safety standards.

Established in the year 1984, its main competences lie in the field of engineering with large-scale infrastructure projects both in the conventional and high-speed rail sectors, metropolitan and road transport and port and station design both in Italy as well as other countries. Italferr offers expertise ranging from engineering design to contracting, from construction site management and supervision to the acceptance testing and commissioning of railway lines, stations, intermodal and logistics facilities, from project management to organisational consultancy work, from training to the transfer of specialist know-how.

Italferr became the driving force behind the most important acceleration process for railway investments ever to take place in Italy, designing most of the large-scale projects like the design and construction of both the HS/HC lines. This project brought a dramatic change in the railway infrastructure, where Italferr played a significant role in the modernization of the infrastructure. Conventional systems were also gradually upgraded for improving traffic flows in all the most important Italian hubs.

Italferr's success story is not only contained within Italy but also different parts of the world that include contracts for designing the new rail link between Jeddah and Al Jubail in Saudi Arabia, "The Saudi Land bridge Railway Project", the "Doha Metro Red Line Underground" in Qatar, the supervision of the construction work of the Eurasia Tunnel in Turkey together with the designs for the airport link between Esenboga International Airport and Ankara, etc.. Italferr has also been working on projects in different parts of India, Australia and even the United States of America with the objective of setting up a high-speed network.

The current thesis work deals with the preliminary analysis of evaluating the effectiveness and efficiency of the ventilation system of a tunnel – Khor Fakkan Tunnel, situated in the UAE. The analysis is strictly based on the latest design standards of the tunnel ventilation system that emphasizes on the safety and security of the people by maintaining a tenable environment throughout its operation, both, in the normal operating conditions and in case of an emergency situation.

Abstract

Tunnels are an integral part of the transportation system playing a significant role both in people and freight transportation. Many countries around the world have developed hundreds of kilometres of these channels and networks connecting different points passing through plains and areas having varying slopes and also potential natural obstructions. The focus on tunnel safety has increased significantly over the years pertaining to various catastrophic accidents. In case of a fire inside the tunnel, hot smoke and combustion products rise and reach the ceiling, wherein depending upon the ventilation conditions, either are pushed outside the tunnel or lead to a phenomenon of reverse flow in the direction opposite to the ventilation thrust called as backlayering with the minimum ventilation velocity needed to prevent this flow called as the critical velocity.

The current work analyses the ventilation requirements for Khor Fakkan Tunnel (KFK) situated in the United Arab Emirates, passing through the Hajar mountains, and is verified using both the 1D and 3D analysis with the softwares – *IDA Tunnel* and *ANSYS Fluent*. The section TK1 of the KFK tunnel is focussed, wherein critical sections are identified pertaining to wind and stack effects and the thermal and visibility parameters are evaluated in coherence with the NFPA 130 standard. A preliminary study is carried out where the critical velocity is calculated using both the NFPA 502-2017 and NFPA 502-2020 standards for the two fire sizes selected based on the NFPA 92 standard. The results of the 1D analysis provide the groundwork for the CFD simulation and the modelling is carried out to visualize the varying gradients of both the temperature and velocity. The results reveal the existence of the backlayering phenomenon inside the tunnel with the ventilation velocity being lower than that of the minimum needed. The thermal properties along the egress pathway for evacuation are also checked so as to ensure tenability along the route of escape.

Chapter 1

Introduction

1.1. Introduction

Tunnels are passages used in transportation systems for carrying people, freight, water, sewage, etc. The technology of constructing tunnels has developed over the past few decades. Tunnels are being built under cities to relieve surface congestion. Many cities across the world have hundreds of kilometres of underground tunnels as part of the road and rail transportation systems. Also, they represent a vital part of the transportation system in regions with mountainous ranges, varying slopes, and other natural obstructions. Therefore, tunnel maintenance is very important in order to maintain a tenable environment with minimum quantity of pollutants. The development of fire in a tunnel poses a huge threat. In recent years, the focus on fire safety issues in tunnels have increased dramatically following numerous catastrophic tunnel fires and accidents like the King's Cross underground station in 1987, Baku Underground fire in 1995, Gotthard Tunnel in 2001, Tauern Tunnel in 1999, Mont Blanc Tunnel in 1999, Frejus Tunnel in 2005 and Channel tunnel fires in 1996, 2006 and 2008. The appearance of large amounts of toxic smoke makes it very difficult to evacuate people and to operate by the rescue teams. The limited space of the tunnel also means that the temperatures and heat fluxes are rapidly increasing.

All these accidents have raised questions about maintaining the optimum conditions inside the tunnel, the need for the design and development of safe evacuation pathway in case of such events, and identification of the best suitable ventilation strategy that could eliminate the risk of spread of the fire and toxic smoke. The tunnel ventilation system plays an important role in tunnel safety for both the normal operating conditions and during emergency fire scenario. During the normal operating conditions, the ventilation system has to maintain the proposed air quality levels by standards by diluting the contaminant particles. Whereas, in case of a fire outbreak the ventilation system has to be strategized with proper techniques of fire and smoke management. The ventilation system should be designed in such a way that the events of the emergency conditions have a least impact on the evacuation routes. The first attempt of a tunnel ventilation system was based on Natural ventilation that relied on meteorological conditions and piston effect generated from the moving traffic inside the tunnel to guarantee acceptable environmental conditions.

The effectiveness of this system is compromised in the presence of traffic conditions. Also, due to the absence of mechanical ventilation components the smoke naturally stratifies and spreads inside the tunnel making it riskier for adoption in long tunnels. Nowadays, tunnels employ either the Longitudinal or Transverse ventilation systems that generate the ventilation flow either by injection or extraction of air using fans at different points along the tunnel. Longitudinal thrust can be achieved using Saccardo nozzles located in the vicinity of the tunnel portals or by using a series of axial jet fans installed individually or in pairs along the tunnel ceiling. The typical ventilation strategy adopted in longitudinally ventilated tunnel (Figure 1.1) require the ventilation system to push the smoke downstream of the fire, avoiding the smoke spreading against the ventilation flow. However, the effects of reverse flow totally depend on the applied ventilation velocity and the minimum velocity that prevents such a flow phenomenon is called critical velocity. In comparison to other complex ventilation systems longitudinal ventilation systems

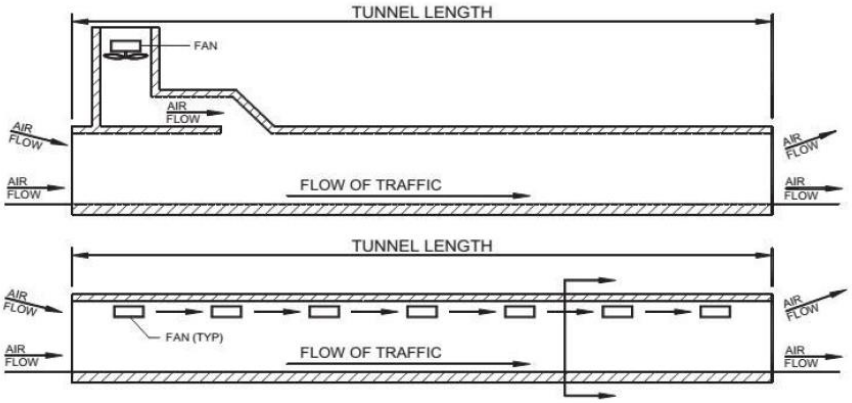

Figure 1.1. Longitudinal Ventilation System: Saccardo Ventilation System (top) & Jet-Fan Ventilation System (bottom) [5].

require less space for ventilation building and ductworks, and a lower capital investment. The other method of ventilation system is realized by means of full-length ducts.

These supply ducts are usually located above the ceiling and are connected to the tunnel environment through dampers that can be automatically opened. The ducts are connected to a central ventilation station comprising of axial fans that generate the necessary thrust. Transverse ventilation systems (Figure 1.2) are used in order to avoid the spreading of smoke by promoting smoke confinement, stratification, and extraction. The smoke is extracted through dampers which are opened during the outbreak of a fire. These are preferred in case of a bi-directional traffic operation. The investment cost is higher compared to the longitudinal scheme. Fire detection and localization also are critical issues for transverse ventilation system. Apart from these systems there are other ventilation schemes like the semi-transverse ventilation system or even a hybrid ventilation scheme depending upon the severity of requirements and other environmental conditions. [6]

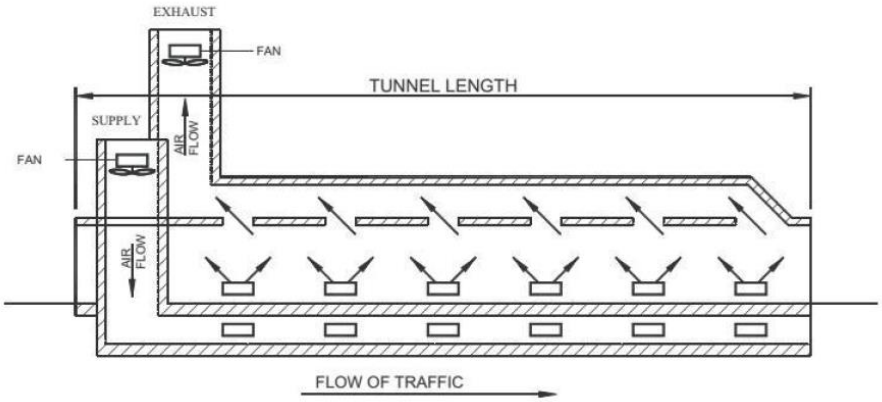

Figure 1.2. Fully Transverse Ventilation System [5].

Basically, a tunnel and the corresponding ventilation system constitute as a single system where its behaviour is affected by factors like pressure fluctuations at portals, tunnel slope, traffic conditions. Apart from this the fire dynamics, smoke movement, stratification and dilution, heat transfer with the tunnel ceiling are also coupled with the ventilation flows. Therefore, a good understanding of the interaction between the

ventilation and fire is vital when developing a fire safety strategy as this interaction controls the movement of smoke and also supplies the fire with the oxidizer.

In this project work the ventilation scheme for the Khor Fakkan Tunnel located in United Arab Emirates is evaluated. The tunnel for the railway line passes through mountainous range that is proposed to carry freight linking the Khor Fakkan Port. A preliminary analysis is carried out where the critical velocity is calculated using both the standards, NFPA 502-2017 [1] and NFPA 502-2020 [2] and a comparison is drawn. The ventilation scheme is then developed by studying the behaviour for different scenarios wherein a fire breaks out inside the tunnel and the possibility of generation of a potential backlayering is checked using both the 1D and 3D analysis on *IDA Tunnel* and *ANSYS Fluent*. Based on these results the effects of fire and smoke spread along the egress passage is verified in order to ensure a safe and tenable environment for the evacuation of passengers.

1.2. Literature Review

The present work is based on the standards – NFPA 130-17 [3], NFPA 502-2017 and NFPA 502-2020 prepared by the Technical Committee on Road Tunnel and Highway Fire Protection. These standards provide the minimum fire protection and fire life safety requirements that need to be followed to maintain a tenable environment. Chapter 2 uses these calculations for determining the critical velocity that are proposed in these standards which are based on the works of Thomas, Li et.al. and Ingason and other researchers. In 2019, R.K. Haddad and Zambri Harun [7] compiled a State-of-the-Art review for the critical velocity and backlayering conditions in railway tunnels. The article showcases the evolution of calculations that have been obtained from the initial works of Thomas in 1958 [8], until the recently implemented ones from Li et.al. and Ingason.

Over the past few decades there have been lots of books, articles and research publications enlightening the potential effects of a tunnel fire. Each of these articles and journals led to the establishment of newer terms and parameters that paved the way to increased safety levels and allowed engineers to come up with better, stringent emergency plans in case of an outbreak. The experiments were carried out using different methods like Numerical modelling using commercial CFD softwares, Full scale fire tests, etc., replicating the real fire breakout scenario in a tunnel. The content of CFD modelling of the fire phenomenon is pretty huge to be treated in a single literature review. As a result, in this section only the most relevant research material related to the CFD modelling of ventilation system and fire scenario is discussed.

In 1996 Woodburn and Britter from the Engineering Department at Cambridge University presented a sensitivity study of CFD simulations of a fire in the test tunnel, 366m in length, at Buxton, UK, [9] and [10]. The simulations were carried out using the commercial software *Flow-3D* for a 2.7 MW fire scenario wherein the tunnel was supported by a longitudinal ventilation system. The standard k-ε turbulence model was used, and the combustion was modelled using the eddy break-up model. They analysed the effects of the results upon the variation of ventilation velocity, turbulence model and heat input rate. They found that length of the reverse flow is sensitive to the ventilation velocity and other input data like the turbulence model and fire size. However, their

results were overpredicted downstream from the fire source showing larger deviations from that of the experimental results.

Wu and Bakar in 2000 performed an analysis for two fire scenarios 1.4 KW and 28 KW in small scale tunnel of length equal to 10.4 m. These scaled fire sizes were equivalent to 2.5 and 50 MW. They carried out the analysis on *ANSYS Fluent* wherein a standard k-ε model was adopted. A mixture fraction model was used to represent the combustion source and the radiation heat transfer was neglected. The comparison of the results to the experimental data shows that the CFD analysis underpredicts the critical velocity. However, the analysis did confirm a presence of a potential backlayering but the velocity profiles in this region is also underpredicted. The temperature on the other side were overpredicted which the authors deemed to be due to the selection of the mixture fraction combustion model [11].

Again, in the same year of 2000, a numerical model for an 800m long tunnel using COMPACT- 3D was developed by Karki and Patankar. The analysis was compared to the experimental data from the Memorial Tunnel Fire Ventilation Test Program (MTFVTP) case 606A – 10MW fire and case 615B – 100MW fire. A standard k-ε model was again implemented also considering the effects of buoyancy. They did not use any conventional combustion model to represent the fire but rather modelled it as a volumetric source of heat and smoke. The jet fans were also modelled and were based on the same mass conservation principle of sources and sinks. Both the analysis showed pretty good agreements with the experimental values with an average 20% deviation in the values of both the temperature and velocities [12].

Haukur Ingason and Fredric Seco carried out a numerical simulation for a model scale tunnel fire test and drew comparisons with the CFD simulations for the same model using *ANSYS Fluent* [13]. The length of the model was 20 m and also consisted of a tunnel ventilation shaft 11.5 m from the entrance of the tunnel. The model scale tunnel used kerosene as a fire source. On *Fluent* a k-ε model with full buoyancy effects was selected. The mixture material was activated, and kerosene-air was taken along with the selection of a combustion model wherein carbon monoxide, soot and NO_x were neglected. Rosseland radiation model was selected too. They also modified the under-relaxation factors so as to fasten the calculation times. The results of the simulations show the presence of backlayering roughly 7.5 m in length. The results were similar to that of the experiments with some minor deviations in the thermal properties near the vicinity of the fire. They figured the reason to be a poorly refined mesh and the choice of the radiation model.

In 2005, Hwang and Edwards provided detailed descriptions of the CFD modelling procedure adopting the open source CFD package FDS to simulate the flow and temperature fields for two different tunnels. The first was a 4.9 m long small-scale tunnel for a 3.3 kW fire. The full-scale experimental data was taken from the MTFVTP for a 50 MW fire with longitudinal ventilation conditions. The authors reported a good agreement between the predicted and experimental critical velocity for both the tunnels. Detailed flow field data show a satisfactory qualitative and quantitative agreement between experimental and numerical data for the small-scale tunnel in the downstream region. In the upstream region velocities are overpredicted. The full-scale simulations show a qualitative agreement to the experiments, but higher deviations are recorded too [14].

In the 2006, Abanto et.al. conducted a numerical analysis on *ANSYS Fluent* for the Louis-Hippolyte-Lafontaine tunnel in Montreal. They used a combustion model as well as represented the fire source as a volumetric heat sink. k-ε model was used for both the cases. The results were not compared with any experimental data. The simulation results were questionable with temperatures reaching above 3000 K in certain regions [15].

Rafael Ballesteros-Tajadura et.al. in the year 2005 published a journal in the Tunnelling and Underground Space Technology about the influence of slope in an urban tunnel of length equal to 1535 m with a slope of 2% upgrade. *ANSYS Fluent* was used again with a finely adopted mesh with a mesh density approximately 163 cells/m. However, the results were satisfactory and were not validated with any experiments. The presence of slope showed a predominant progression of smoke in the upstream ascending area [16].

Galdo Vega et.al. later in 2007 performed an analysis for the Memorial Tunnel Fire Ventilation Test Program (MTFVTP) for three cases Test 606A, Test 612B and Test 611 for 10 MW and 50 MW source. The simulations were carried out for a tunnel length of 850 m with the presence of jet fans and the heat source modelled as volumetric sink which emits heat and smoke. The mass fractions of the emitting species were calculated using mass balances linking the maximum temperature of the fire obtained from PIARC 1999. Radiation modelling was neglected, and this was shown by reducing heat source by 35%. k-ε model was implemented and a time step of 1 second was selected and the simulation was run until a steady state solution was reached. The results showed total agreement between the numerical scheme and that of the experimental data pointing out the usefulness of CFD simulations in order to predict the effectiveness of the tunnel ventilation system. Some significant discrepancies were found for the temperatures around the regions of fire wherein the authors reveal the reason to be the absence of a radiation model [17].

Eduardo Blanco et.al. in 2010 investigated the effects of backlayering in the Memorial Tunnel test, 853 m in length, using *ANSYS Fluent*. The fire sources were of 10, 50 and 100 MW. They used a longitudinal symmetrical condition for the geometry in order to reduce the computational effort. Here a volumetric heat sink is used rather than a combustion source and the smoke is represented by a mixture of air and carbon dioxide species. The concentrations were obtained by applying mass conservation principles. k-omega model was chosen and a time step of 1 second was imposed. The results of the model show that the critical velocity obtained was quite in agreement with the experimental ones for the low and medium heat release rates. The results, however deviated for the higher heat release rate [18].

A detailed analysis for several fire occurrences has been described in the thesis work of Francesco Colella in 2010. He used different numerical techniques to represent the case studies that includes 1D models, CFD models and also multiscale models and validated these results with those of the experiments. For example, the 1D model for the analysis of Frejus Tunnel was able to predict with good accuracy the ventilation conditions in the tunnel. However, the author also stresses on the fact that 1D are not suitable to see the fluid behaviour especially in regions characterised by high velocity and temperature gradients, close to the proximity of the fire. For the CFD simulations *ANSYS Fluent* was used and validated with the work studied by Wu and Bakar for the two small scale tunnels. Again, a standard k-ε model was used and the fire source was modelled as a heat sink releasing hot combustion products from the top surface of the slab. The simulations achieved a significant level of accuracy for the predictions of the critical velocity with

average deviations between 17-25%. The author further states the disadvantage of using CFD simulations pointing out the reason to be the huge computational time and the ability to see the behavior only in the regions close to fire source. He then delves into the concept of multiscale modelling which is basically a hybrid of 1D and CFD methods. The concept of multi scale modelling has not been used extensively for tunnel research. Colella shows that with the application of such technique the entire domain could analyzed with lead times lower than that of CFD simulations [6].

Hot smoke tests were carried out for the Laliki Tunnel in Poland by Aleksander Król et.al. The experimental results were then validated by a numerical model on *ANSYS Fluent*. The bidirectional tunnel was 678m in length with slope of 4% and was supported with a longitudinal ventilation system. The design fire sizes for tests were taken as 750 and 1500 KW, respectively. The experiments were recorded, and the results were validated with the numerical model to a sufficient level of accuracy. However, the temperatures at a region far from the fire were not precise and had severe deviations. The results showed that the region filled with hot gases poses a deadly threat to people [19].

Helmut Steiner et.al. carried out an analysis to determine the temperature gradients for the escape doors of the tunnels of the Koralm Railway line. A CFD model was created and the setup was tested for two HRR of 75 MW and 100 MW. The results were also compared to the full-scale fire tests. A k-ε model was chosen for turbulence with enhanced wall functions. The fire is represented as a volumetric source of heat using conservation laws. The results were slightly underpredicted when compared to the experiments with area averaged temperatures of 860 °C at the escape doors [20].

Therefore, the CFD models of tunnel fires are able to predict critical velocity, and backlayering phenomenon with an acceptable level of accuracy with deviations smaller than 30%. The fluid flow data, for example temperature gradients, are also accurately predicted with deviations of roughly 20% with respect to the experimental values [6]. The literature review over the past few years in the field of prediction of flow for a tunnel fire scenario show a variety of different approaches and techniques which have also influenced the work carried out in this project work. Most of the work shows that the prediction of local velocity and temperature fields in the vicinity of the fire source, can be affected by a higher error when compared to the experimental measurements. It is also evident that the CFD analysis of a fire phenomenon within tunnels suffers from the limitations set by the size of the computational domain. This leads to large mesh sizes and sometimes becomes impractical for engineering purposes, even for the case of short tunnels with lengths less than 500 m. Also, in most of the cases the computational domain is limited to the region close to the proximity of the fire. This is one of the limitation where a potential de-coupling could arise between the location of the fire and the overall ventilation system. As a result, assumptions are made in the best possible way to replicate the environment of the tunnel ventilation system by extrapolating accurate data for those near the portals and use some constants and safety factors to account for the MEP systems inside the tunnel.

1.3. Case Study – Khor Fakkan Tunnel (KFK)

The objective of this project is to determine the ventilation requirements for Khor Fakkan Tunnel (KFK), situated at the Hajar Mountains in the United Arab Emirates. The tunnel is basically made up of two elements - Tunnel TK1, which runs 5.9 kilometers in length, and Tunnel TK2 which is 0.72 kilometers, respectively. The tunnel section TK1 is found to be the most critical one taking into consideration the wind and thermal stack effects and would be the basis of this report where 1D and 3D simulations will be carried out. The tunnel profile sits on an elevated pathway with varying slopes along its chainage as see from Figure 3. A single bore tunnel has been developed to accommodate a single railway track arrangement allowing sufficient space for escape and maintenance walkway on each sides of the tunnel, rolling stock clearances and the required Mechanical Electrical Plumbing (MEP) installations. Table 1.1 summarizes the two cross-sections in the TK1 tunnel.

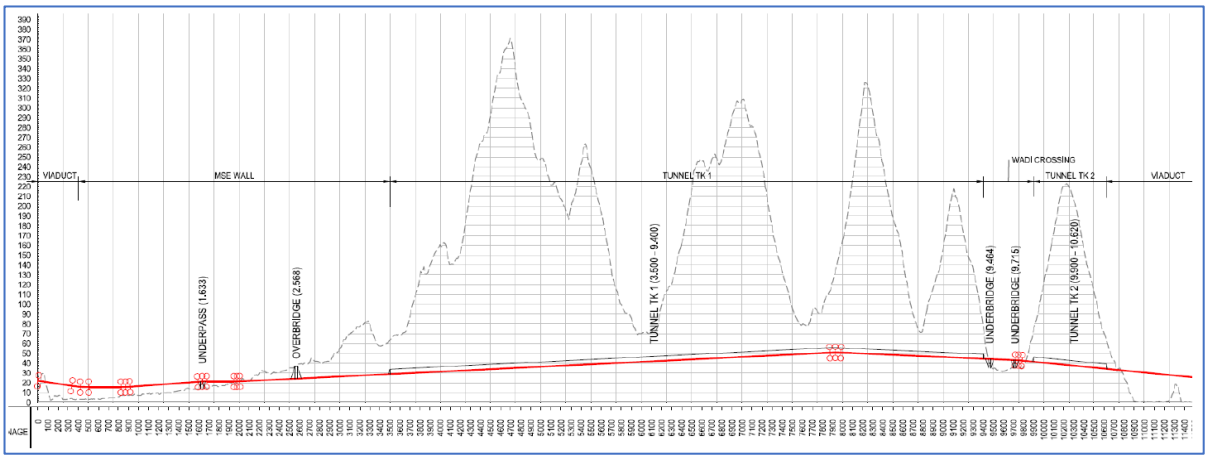

Figure 1.3. Layout of Khor Fakkan Tunnel (KFK).

Tunnel No	Ch. Start (m)	Ch. End (m)	Length (m)	Max depth (m)
Tk 1	3+500	9+400	5900	335
Tk 2	9+900	10+620	720	185

Table 1.1. Sections of the Khor Fakkan Tunnel (KFK).

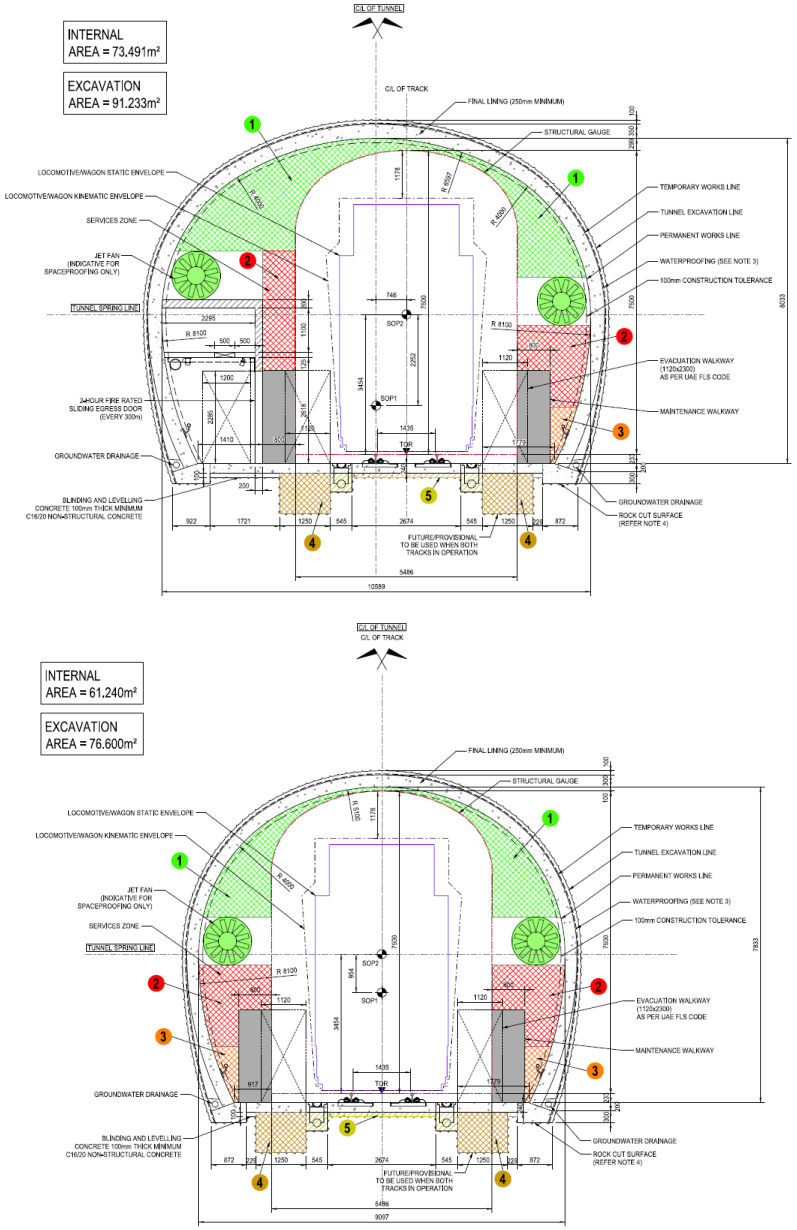

Figure 1.4. Cross-Sections of Tunnel TK1: CS-1 with LEP (top) and CS-2 without LEP (bottom).

The tunnel TK1 profile has two sections as shown in Figure 1.4 and also Table 1.2, the first one consists of a pathway – Longitudinal Egress Passage stretching from chainage 3+500 until 5+400. This passage is useful for evacuation upon incidents of a fire outbreak inside the tunnel. This section is followed by a change in cross-section at chainage 5+400 until the end of the tunnel at chainage 9+400. The tunnel section sits on an elevated plain with the ground elevation increasing steadily from the entry portal, and the peak elevation of the first mountain ridge is +350 m NADD (National Abu Dhabi Datum) at chainage 4+750. The elevation gradually falls back down to approximately 70m NADD where the first of three wadi channels in this section is encountered at chainage 6+000. The wadi channel is approximately 200m wide and forms a major channel, snaking west back into the Hajar Mountain which it drains.

The alignment then passes into the second mountain ridge which has an approximate peak elevation of +300m NADD at chainage 7+000. The elevation falls to approximately +80m NADD at chainage 7+700 where another wadi is encountered. This wadi is of similar width compared to the first wadi, at about 250m width, however it has a much smaller catchment compared to the first one. The third mountain ridge has a peak elevation on alignment of +320m NADD at chainage 8+250. The third wadi channel has similar characteristics to the second, with an elevation of about +70m NADD at chainage 8+750. The fourth ridge is smaller, with a peak elevation of approximately +210m NADD at chainage 9+100. The exit portal of tunnel TK1 is set up at chainage 9+400. Tunnel TK1 also has a tunnel ventilation shaft (TVS) situated at chainage 6+150 and four ventilation and escape adits (VEA) at chainages 6+400, 7+150, 7+900 and 8+650.

Tunnel	Cross-section	Chainage	Remarks
TK1	CS-1	From 3+500 to 5+400	**Section with Longitudinal Egress Passage (LEP)** Area=64.45 m^2 P=32.48 m D_h=7.94 m H=8.00 m W=7.2 m
	CS-2	From 5+400 to 9+400	**Section without LEP** Area=61.15 m^2 P=28.69 m D_h=8.53 m H=7.80 m W=7.3 m

Table 1.2. Properties of the TK1 Section of the Khor Fakkan Tunnel (KFK).

A longitudinal ventilation system is proposed for the environmental control of Tunnel TK1. It consists of jet fans mounted along the walls above the egress walkways and blows air longitudinally into the tunnel. Considering the fact that a single bore tunnel has been developed, the jet fans (36 in total) are installed in pairs along the sidewalls of the tunnel with a spacing of about 330-350 meters. The ventilation station consists of three axial fans with motorized dampers. The dampers open and close upon the requirement of the minimum ventilation velocity required in order to maintain a tenable environment. This kind of longitudinal ventilation system is the most space-efficient system because no ducts are required within the tunnel. The ventilation requirement drives several aspects of the tunnel design but has specific impact on the tunnel cross-sectional area. Typically for railway tunnels, the sizing of the ventilation system is determined by air flow requirements during emergency scenario i.e. fire. If a fire is detected or reported when a train is travelling through the tunnels, the default strategy is for the train to continue to travel until it is clear of the tunnels. In the event of a fire that disables a train within the tunnels, driver/occupants can leave the train and use the side walkway to evacuate safely from the fire. In order to study the effectiveness and overall performance of the tunnel ventilation system four scenarios are considered.

These scenarios use two of the most critical locations one at 5+100 and the other at 6+450 as a result of wind and thermal stack effects.

For the analysis, the following four scenarios are considered:

a) Train on fire in an intermediate section of tunnel equipped with LEP, at chainage 5+100, with heat release rate equal to 20 MW;
b) Train on fire in an intermediate section of tunnel equipped with LEP, at chainage 5+100, with heat release rate equal to 250 MW;
c) Train on fire in an intermediate section of tunnel without LEP, at chainage 6+450, with heat release rate equal to 20 MW;
d) Train on fire in an intermediate section of tunnel without LEP, at chainage 6+450, with heat release rate equal to 250 MW;

In the following chapters the analysis carried out on *IDA Tunnel* and *ANSYS Fluent* are described in detail. But before that a preliminary analysis is carried out in determining the critical velocities using both the NFPA 502-2017 and NFPA 502-2020 standards. These calculations predict the minimum critical velocity needed in order to avoid the reverse flow phenomenon of smoke and combustion products inside the tunnel. Using these analyses, the tenable conditions along the egress passage are checked to see if the evacuation conditions are viable.

Chapter 2

Critical Velocity and Backlayering

2.1. Critical Velocity and Backlayering in tunnels

Generally, when a fire breaks out in a tunnel, it rises above and entrains the surrounding area into a plume. This plume forms two streams flowing in the opposite directions along the surface of the ceiling. The smoke which spreads in the upstream direction of the fire is called Backlayering and the minimum ventilation velocity that could prevent this flow is called the Critical Velocity, which according to the NFPA 502 Standard for Road Tunnels, Bridges, and Other Limited Access Highways defines it as "The minimum steady-state velocity of the ventilation airflow moving toward the fire, within a tunnel or passageway, that is required to prevent backlayering at the fire site" [1].

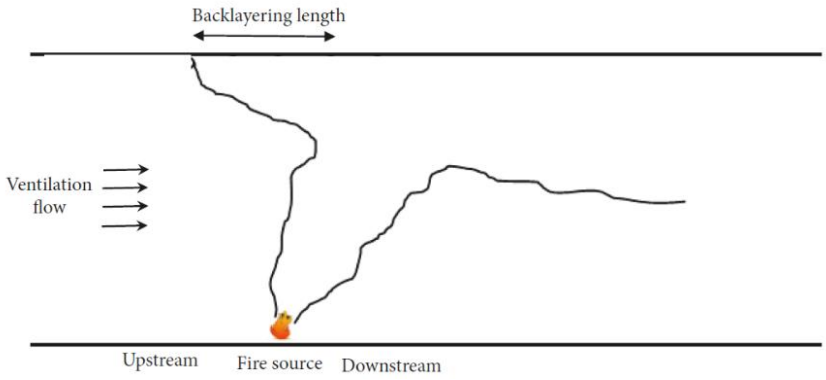

Figure 2.1. Backlayering Phenomenon in a longitudinal ventilation tunnel [7].

The risk from accidental fires and the smoke movement depends largely on this applied ventilation airflow. Therefore, it is of practical importance to understand the physical parameters and flow conditions under which the reverse stratified flow can be prevented. The characteristics of the smoke movement is highly dependent on the air velocity supplied inside the tunnel. In order to understand more clearly three typical ranges of air velocity are identified:

- For the case of a low forced air velocity range, the smoke stratification is higher in the vicinity of the fire source. The common scenario for this group includes tunnels with natural ventilation. The back-layering distance of the smoke is relatively long, and in some cases the smoke travels nearly uniformly in both directions (Figure 2.2.a). When the velocity increases gradually back-layering of the smoke occurs upstream of the fire source (Figure 2.2.b) [5].

- In the moderately forced air velocity range, the smoke stratification in the vicinity of the fire is strongly affected by the air velocity, particularly at the higher velocities. This group normally includes tunnels equipped with natural ventilation or forced ventilation systems. The back-layering distance can vary and usually stationary backlayering can be visualized (Figure 2.2.c) [5].

- Finally, for the high forced air velocity group, there is usually low or negligible stratification of the smoke and most importantly no back-layering (Figure 2.2.d). This group normally includes tunnels with forced ventilation with ventilation velocity, equal to the 'critical velocity' [5].

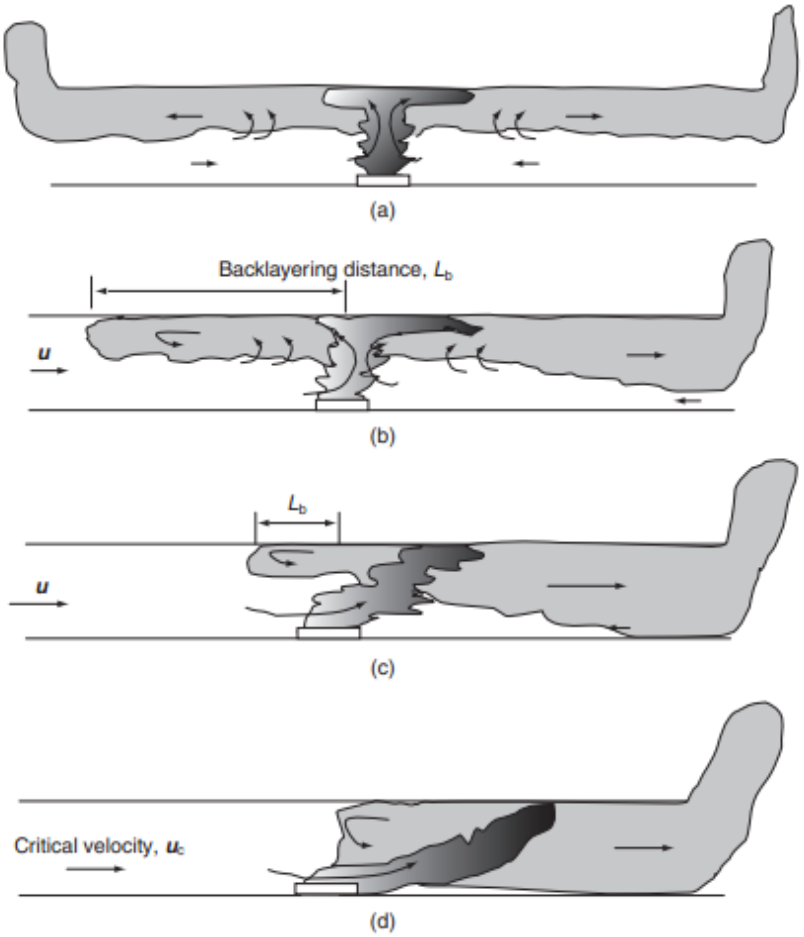

Figure 2.2. Smoke stratification with varying ventilation velocities [5].

Many experiments and theoretical analyses were carried out in order to study the critical velocity along with the back-layering length in tunnel fires. These experiments defined the correlations for critical velocity that comply well with the experimental data. The back-layering length was related to the ratio of longitudinal ventilation velocity to critical velocity. The experimental data shows that the ratio of the ventilation velocity to the critical velocity and the dimensionless back layering length follows an exponential relation. A correlation based on experimental data to predict the back-layering length has been proposed in the NFPA 502, 2020 edition.

In this section the critical velocity for the fire scenarios of 20 and 250 MW are calculated according to the NFPA 502 – 2017 and the latest NFPA 502 – 2020 edition. The latest edition of calculations is based on the research activity of Li.et.al, where they proposed that the predicted critical velocity by the previous models was low and investigated the critical velocity with the effect on the backlayering length.

2.1.1. Critical velocity

Critical velocity, as defined earlier, is an important parameter to be calculated for any fire size represented by Heat release rate in a longitudinal ventilation system. The methods for the prediction of the values of the critical ventilation velocity for various fire sizes are mainly based on empirical relationships obtained from the Froude number conservation using experimental data. The Froude number is defined as the ratio between the buoyancy forces generated by the fire and the inertia forces due to the ventilation air flow [7].

$$Fr = \frac{V^2}{gD} = \frac{\text{Inertia Forces}}{\text{Gravity forces}}$$

The earliest investigation dates back to 1968 where, the Froude number conservation was applied by Thomas [8], where he studied the effect of ventilation velocity on fire flow in underground tunnels, taking the Froude number as unity. Thomas derived the following semi-empirical relation for the critical velocity:

$$V_C \approx \left(\frac{gHQ}{\rho_0 C_p T_0 A}\right)^{1/3}$$

From the relationship shown above it is evident that the critical velocities are related to the cube root of the heat release for all values of the heat release rate. The work of Thomas laid a foundation for analyzing different parameters that can influence the critical velocity, including the tunnel geometry, tunnel slope, or plume flow, is the frequent factor in these studies. Hinkley [21] in 1970, based on Thomas's theory, derived a formula for calculating the smoke velocity moving along the roof and proposed a similar cubic root relationship, as mentioned earlier, between the velocity of hot stream along the ceiling and the heat release rate. Hinkley established a formula for calculating the depth of the hot smoke layer beneath the ceiling and found that the depth of the layer is proportional to the perimeter of the fire and is inversely proportional to the velocity of the layer and the width of the mall. Heselden [7], then in 1976, derived another formula based on Hinkleys theory for calculating the critical ventilation velocity as:

$$V_C = CK\left(\frac{gQT}{\rho_0 C_p T_0^2 B}\right)^{1/3}$$

The constants C and K are obtained from the experiments in a disused rail tunnel. This relationship was widely used to predict the critical velocity, but a simpler relationship was later developed by Danziger and Kennedy [22] and is based on the relationship of the increase in the smoke temperature and the convective heat release rate. The Danziger and Kennedy model also varies with the one-third power of HRR as depicted by Thomas and Hinkley, but the difference is that it has a grade correction factor for an elevated/sloped tunnel. These relations that assume critical velocities are related to the cubic root of the heat release are not accurate when the fire impinges the ceiling. As a result, this issue should be considered separately, as very large rates of heat release are produced by vehicle fires resulting from an accident.

Oka and Atkinson [23] then developed the work using a dimensional analysis to solve this problem. The objective of their work was to measure the critical velocities for a model tunnel fire and test the scaling procedures used. They used tunnel height as the characteristic length and derived a simpler relation to predict the critical velocity, that can be applied to both small and large fires. They concluded that for lower rates of heat release the critical velocity varies by the cube root of the HRR. But, at higher rates of heat release the dependence on the HRR falls off rapidly until it becomes independent. The dimensionless critical velocity and HRR are:

$$Q^* = \frac{Q}{\rho_0 C_p T_a g^{1/2} H^{5/2}}$$

$$U_C^* = \frac{U_C}{\sqrt{gH}}$$

With the following replacements,

$$U_C^* = \begin{cases} 0.35(0.124)^{-1/3}(Q^*)^{1/3} & for\ Q^* \leq 0.124 \\ 0.35 & for\ Q^* > 0.124 \end{cases}$$

But the formulae proposed by Oka and Atkinson cannot correlate the experimental results from various cross-sectional tunnel shapes into a single form on the ground and tunnel height is used as the characteristic length in the analysis. Therefore, these formulae should not be used for tunnels with different cross-sections.

Wu and Bakar [24] in 2000, carried out a series of experimental tests on five tunnel models with same height but different cross-sections to investigate the effect of tunnel geometry on the critical velocity. Based on their results, they proposed to use 'hydraulic tunnel height' to replace the tunnel height as the characteristic length in the analysis. The formulae proposed by Wu and Bakar, however, confirmed the one-third power law by Oka and Atkinson and all the experimental results could be correlated into a single form. Therefore, it was possible to derive a universal correlation for predicting the critical ventilation velocity for tunnels with various cross-sectional shapes.

The new dimensionless critical ventilation velocity, U^*_C, and new dimensionless heat release, Q^*, are defined as,

$$Q^* = \frac{Q}{\rho_0 C_p T_a g^{1/2} \overline{H}^{5/2}}$$

$$U_C^* = \frac{U_C}{\sqrt{g\overline{H}}}$$

The critical velocity calculations proposed in the standard – NFPA 502 – 2017 edition are based on these above equations.

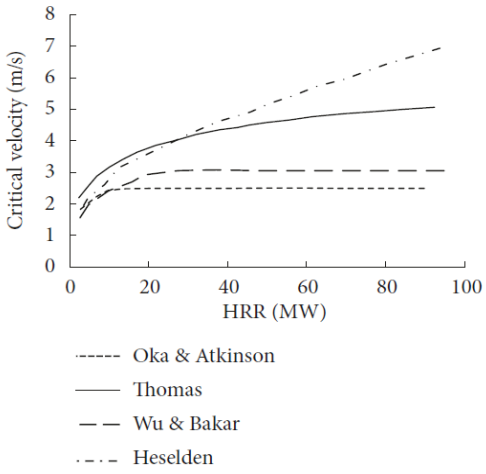

Figure 2.3. Critical Velocity comparison of different empirical models [7].

Experimental analyses were then conducted by Li et. al. [25] to investigate the critical velocity along with the behaviour of backlayering phenomenon in tunnel fires. The backlayering length was measured by measuring the gas temperature and they proposed a correlation between the dimensionless critical velocity and the dimensionless HRR using the tunnel height as the characteristic length, respectively. The suggested equations are:

$$U_C^* = \begin{cases} 0.81(Q^*)^{1/3} & for\ Q^* \leq 0.15 \\ 0.43 & for\ Q^* \geq 0.15 \end{cases}$$

Li's results were evaluated with results from the largescale tests and found good agreement between model-scale tests and large-scale tests. The predicted critical velocity proposed by Oka and Atkinson and the equations proposed by Wu and Bakar are lower than that of the experimental data of the critical velocity, especially for HRR below 0.15.

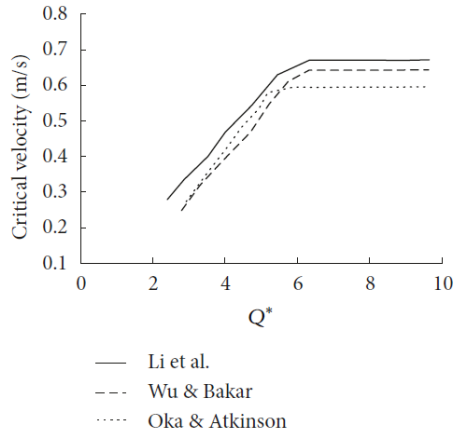

Figure 2.4. Comparison of Critical Velocities from different publications [7].

Li and Ingason [28] then examined the influence of cross section of the tunnel on the critical velocity. They analysed the previous models established for critical velocity and concluded that Oka and Atkinson's model underestimates the critical velocities whereas

the Wu and Bakar's model overestimates the effect of tunnel width on critical velocity for all fire sizes. They showed that the increase in both tunnel width and height results in a decrease in the critical velocities for small fires. But an increase in the tunnel height causes significant increase in the critical velocity for a large fire. Therefore, a new model was proposed to find the critical velocity as shown below:

$$U_C^* = \begin{cases} 0.81\beta^{-1/12}(Q^*)^{1/3} & for\ Q^* \leq 0.15\beta^{-1/4} \\ 0.43 & for\ Q^* \geq 0.15\beta^{-1/4} \end{cases}$$

where $\beta = W/H$.

As the critical Froude number of 4.5 was widely used to calculate the critical velocity in a ventilated tunnel, Li and Ingason studied the critical Froude number [29], its effectiveness, and original sources of the critical Froude model. They proved that using a Critical Froude number equal to 4.5 leads to lower critical velocities for large fire sizes which is not conservative. According to their investigation, this failure is due to the lack of consideration of the tunnel aspect ratio and tunnel geometry when a constant Froude number is considered. So, the critical Froude number is not only a constant but is also influenced by both the HRR and tunnel aspect ratio. Therefore, it can be concluded from all these evidences that the critical velocity changes by one-third power of HRR for low HRR and is independent of HRR at higher rates. The NFPA 502 – 2020 edition is based on the equations proposed by Li et.al.

2.1.2. Backlayering

Backlayering is the upstream flow of the fire and smoke when the ventilation velocity is lower than the critical velocity. There has been a lot of research and experimental tests in order to understand and develop a relationship between the critical velocity and the backlayering distance. It is important to understand the characteristics of these backlayering plumes, to know how far the hot smoke and gases would travel upstream from the fire source. As mentioned in the section 2.1.1 a theoretical analysis was initially established by Thomas [8]. Thomas proposed a dimensionless relation to estimate the smoke backlayering flow length which is given as:

$$L_b^* = \frac{L_b}{H} \propto \frac{gQ}{\rho_0 C_p T_a V^3 W}$$

where L_b is the backlayering length, ρ_0 is the ambient density, C_P is the specific heat, T_a is the ambient temperature, V is the ventilation velocity, and H is the height of the tunnel. From the above relationship it can be concluded that the backlayering length depends on the HRR, the height and width of the tunnel and the ventilation velocity. However, the equation proposed by Thomas was not backed by the experiments and was applicable only to smaller HRRs. Vantelon [30] after carrying out a few experiments gave his version of the equation for the dimensionless backlayering distance that was based on Richardson's number.

$$\frac{L_b}{H} = (Ri')^{0.3}$$

$$Ri' = \left[\frac{gQ}{\rho_0 C_p T_a V^3 H}\right]$$

According to Vantelon, the backlayering length varied only to first power of height for each value of Q, and the proposed equation cannot correlate all the test results. Hu et al. [31] further, studied the backlayering length and the critical in tunnel fires. They predicted the backlayering length through the temperature rise distribution upstream along the tunnel and its dependence on buoyancy and inertia forces.

$$L_b = \frac{ln[K_2(C_k H/V^2)]}{0.019}$$

With,

$$K_2 = g\gamma\left(\frac{Q^{*2/3}}{Fr^{1/3}}\right)^{\epsilon}$$

Here, the backlayering length increases with the fire size and decreases with tunnel height and ventilation velocity. Hu et.al study showed that the equations developed by Thomas were underestimating the backlayering distance.

Ingason and Li [26] performed experiments using wood cribs where, the number of wood cribs, longitudinal ventilation rate, and the ceiling height were changed to study different HRR, fire growth rate, maximum gas temperature, and temperature distribution produced by smoke flow under the ceiling. They defined a relation between the dimensionless flame length and a dimensionless HRR as:

$$L_b^* = 4.3Q^*$$

They also expressed the dimensionless backlayering length as a function of the dimensionless ventilation velocity:

$$L_b^* = 17.3\ ln\left(\frac{0.4}{V^*}\right)$$

Li and Ingason also conducted experimental tests to study the backlayering length in tunnel fires. They found that the backlayering length varies significantly with the ventilation velocity and the relationship between them is not straightforward. It was clearly demonstrated that the backlayering length increases with HRR when HRR < 6.7 kW but, in cases of large fires, the backlayering length is independent of the dimensionless HRR. Li's study showed that the dimensionless backlayering length can be related to the ratio of longitudinal ventilation velocity and the critical velocity (V^{**}) [25] in the form of an exponential relationship:

$$V^{**} = e^{(-0.054L_b^*)}$$

The final derived formula to predict the dimensionless backlayering length is:

$$L_b^* = \begin{cases} 18.5\ ln\left(\dfrac{0.81Q^{*1/3}}{V^*}\right) & for\ Q^* \le 0.15 \\ 18.5\ ln\left(\dfrac{0.43}{V^*}\right) & for\ Q^* \ge 0.15 \end{cases}$$

These formulations are depicted in the NFPA 502 2020 calculations for the backlayering length. Various experiments were carried out by different researchers Minehero et al., Yao et al., Fan et al. etc. Their major conclusions are summarized [7]:

1. The smoke layering length was longer downstream in comparison to upstream.
2. Increase in the ventilation velocity reduces the backlayering length.
3. The dimensionless backlayering length increased with a higher HRR.
4. An increase in the tunnel cross-sectional area led to greater backlayering length.

2.2. Critical Velocity according to NFPA 502 – 2017 Edition.

In compliance with the NFPA 130, section 7.2, the emergency ventilation system should be designed to "produce sufficient airflow rates within enclosed trainways to meet critical velocity". The methodology to calculate the critical velocity is described in the NFPA 502, Annex D [1], and is shown here below:

$$V_c = K_1 K_g \left(\frac{gHQ}{\rho C_p A T_f} \right)^{1/3}$$

$$T_f = \left(\frac{Q}{\rho C_p A V_c} \right)$$

where: :

V_c = critical velocity (m/s);
g = Acceleration caused by gravity, equal to 9.81 m/s^2;
H = height of tunnel at the fire site;
Q = heat fire is adding directly to air at the fire site;
ρ = average density of the approach (upstream) air (kg/m^3);
C_p = Specific Heat of Air;
A = Area perpendicular to the flow;
T_f = Average Temperature of the fire site gases (K);
T = Temperature of the approach air (K).
K_1 = Froude number factor, calculated according the table below;

Q (MW)	K_1
>100	0.606
90	0.62
70	0.64
50	0.68
30	0.74
<10	0.87

Table 2.1. Froude Number Factor, K_1 [1].

K_g = grade factor, obtained from the graph below;

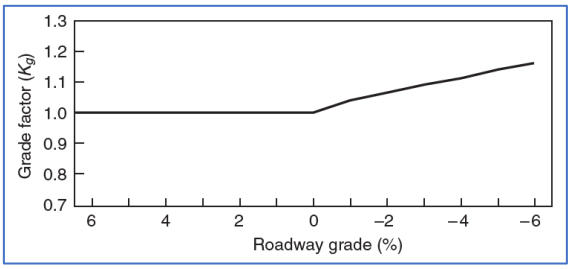

Table 2.2. Grade Factor, K_g [1].

Fire Heat Release – Freight Train – no Hazard Material	X0231-S02-EST-RP-10005-00 Preliminary Design Report - Tunnel MEP Systems	20000	kW
Fire Heat Release - Freight Train – Hazard Material	X0231-S02-EST-RP-10006-AA Tunnel Ventilation Analysis (Freight Only)	250000	kW
Section - Geometrical Data – height With LEP	X0231-KFK-EST-DG-10201-AA KFK Tunnels - Typical Cross Section (CS-1) With Longitudinal Egress Passage - Tangent Track	8	m
Section - Geometrical Data - Area perpendicular to the flow – With LEP	X0231-KFK-EST-DG-10201-AA KFK Tunnels - Typical Cross Section (CS-1) With Longitudinal Egress Passage - Tangent Track	64,45	m^2
Section - Geometrical Data – height Without LEP	X0231-KFK-EST-DG-10202-AA KFK Tunnels - Typical Cross Section (CS-2) Without Longitudinal Egress Passage - Tangent Track	7,8	m
Section - Geometrical Data - Area perpendicular to the flow – Without LEP	X0231-KFK-EST-DG-10202-AA KFK Tunnels - Typical Cross Section (CS-2) Without Longitudinal Egress Passage - Tangent Track	61,15	m2
Trainway Slope - Worst Scenario	X0231-KFK-EST-DG-10200-AA KFK Tunnels TK1 & TK2 - General Layout X0231-KFK-ERA-DG-10002-AA Khor Fakkan Line Plan & Profile Ch. 3+000 to Ch. 6+000 X0231-KFK-ERA-DG-10003-AA Khor Fakkan Line Plan & Profile Ch. 6+000 to Ch. 9+000 X0231-KFK-ERA-DG-10004-AA Khor Fakkan Line Plan & Profile Ch. 9+000 to Ch. 12+000	-0,5	%
Outdoor Temperature	X0231-S23-EAM-FS-00001-00 Technical Specification - MEP Services	46	°C
Fraction of firepower directly to air	*IDA Tunnel* - version 1,2 - Theoretical Reference	0,7	

Table 2.3. Input data for the calculation of Critical Velocity.

2.2.1 Critical Velocity – Cross section with LEP and HRR of 20 MW

The results of the iterative calculations are listed below:

Output Data		
Critical velocity (V_C) =	2,5398	m/sec
Smoke temperature (T_f) =	122,80	°C
Slope Factor (K_g) =	1,02	
Outdoor Density =	1,106	kg/m^3
Air Specific heat (C_p) =	1,007	kJ/kg K

Table 2.4. Results for 20 MW HRR.

With a critical velocity of about 2.54 m/s, the minimum air flow is 164 m^3/s.

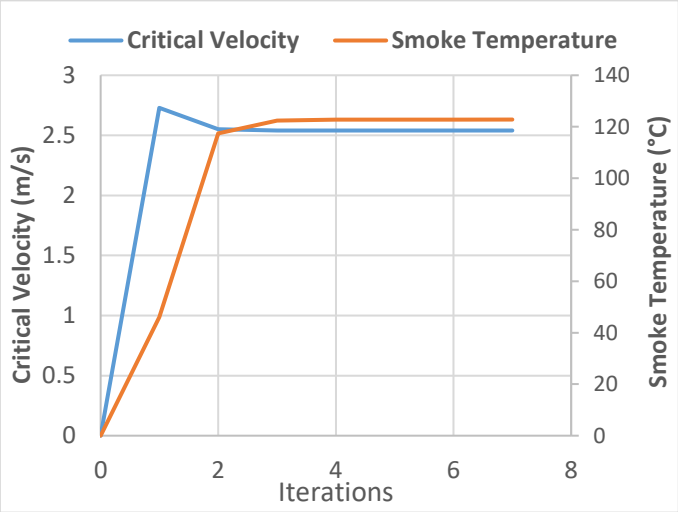

Figure 2.5. Iterative calculations of Critical Velocity for HRR – 20 MW.

2.2.2. Critical Velocity – Cross section with LEP and HRR of 250 MW

The results of the iterative calculations are listed below.

Output Data		
Critical velocity (V_C) =	3,5337	m/sec
Smoke temperature (T_f) =	735,99	°C
Slope Factor (K_g) =	1,02	
Outdoor Density =	1,106	kg/m^3
Air Specific heat (C_p) =	1,007	kJ/kg K

Table 2.5. Results for 250 MW HRR.

With a critical velocity of about 3.54 m/s, the minim air flow is 228 m^3/s.

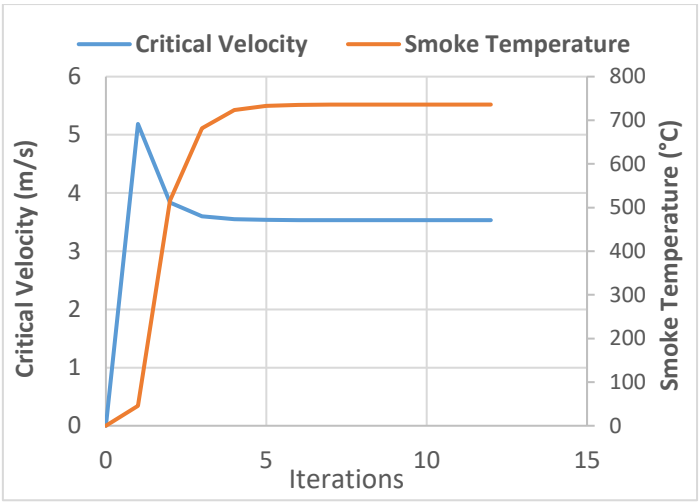

Figure 2.6. Iterative calculations of Critical Velocity for HRR – 250 MW.

2.2.3. Critical Velocity – Cross section without LEP and HRR of 20 MW

The results of the iterative calculations are listed below.

Output Data		
Critical velocity (V_C) =	2,5551	m/sec
Smoke temperature (T_f) =	126,46	°C
Slope Factor (K_g) =	1,02	
Outdoor Density =	1,106	kg/m³
Air Specific heat (C_p) =	1,007	kJ/kg K

Table 2.6. Results for 20 MW HRR.

With a critical velocity of about 2.56 m/s, the minimum air flow is 157 m³/s.

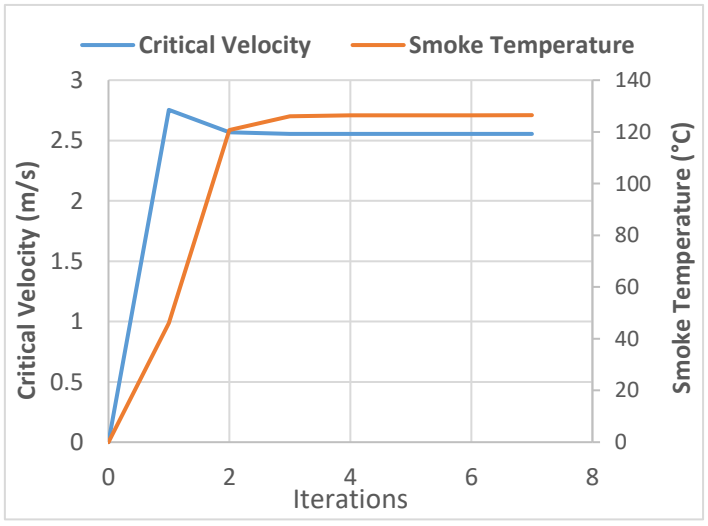

Figure 2.7. Iterative calculations of Critical Velocity for HRR – 20 MW.

2.2.4. Critical Velocity – Cross section without LEP and HRR of 250 MW

The results of the iterative calculations are listed below.

Output Data		
Critical velocity (V_C) =	3,5200	m/sec
Smoke temperature (T_f) =	776,07	°C
Slope Factor (K_g) =	1,02	
Outdoor Density =	1,106	kg/m^3
Air Specific heat (C_p) =	1,007	kJ/kg K

Table 2.7. Results for 250 MW HRR.

With a critical velocity of about 3.52 m/s, the minimum air flow is 216 m^3/s.

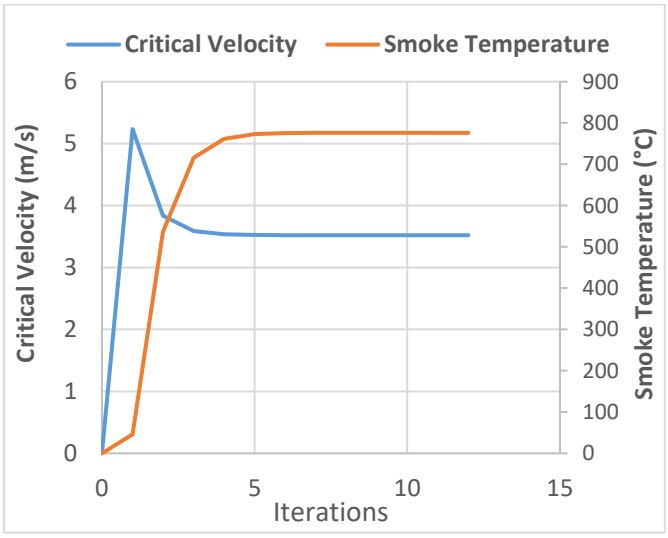

Figure 2.8. Iterative calculations of Critical Velocity for HRR – 250 MW.

2.3. Critical Velocity according to NFPA 502 – 2020 Edition

Following the recent numerical and theoretical works, conducted to investigate the effect of tunnel cross section on critical velocity for smoke control in longitudinally ventilated tunnel fires, a new approach for the calculation of critical velocity has been proposed in the NFPA 502, 2020 Edition [2]. Both theoretical considerations and numerical results show that tunnel height plays a much more important role in critical velocity than tunnel width. For small fires, the critical velocity decreases with both the increasing tunnel height and tunnel width. For large fires, the critical velocity significantly increases with the increasing tunnel height but is closely independent of tunnel width. The following new equations for tunnel have been proposed based on Li et al.'s model [28]:

I. Case 1

$$\frac{\dot{Q}}{\rho_a C_p T_a g^{1/2} H^{5/2}} \leq 0.15 \left(\frac{H}{W}\right)^{-1/4},$$

$$\frac{K_g u}{\sqrt{gH}} = 0.81 \left(\frac{\dot{Q}}{\rho_a C_p T_a g^{1/2} H^{5/2}}\right)^{1/3} * \left(\frac{H}{W}\right)^{1/12} * e^{\left(-\frac{L_b}{18.5H}\right)};$$

II. Case 2

$$\frac{\dot{Q}}{\rho_a C_p T_a g^{1/2} H^{5/2}} > 0.15 \left(\frac{H}{W}\right)^{-1/4},$$

$$\frac{K_g u}{\sqrt{gH}} = 0.43 e^{\left(-\frac{L_b}{18.5H}\right)};$$

Where:

ρ_a = ambient density (kg/m^3);

C_p = heat capacity (kJ/kg K);

H = tunnel height (m);

L_b = back layering length (m), where $L_b = 0$ defines critical velocity (no back layering of smoke), and $L_b \neq 0$ defines confinement velocity (velocity corresponding to the controlled back layering length);

T_a = ambient gas temperature (K);

u = longitudinal velocity (m/s);

$\dot{Q}$ = Total heat release rate (HRR) (kW);

W = tunnel width (m); K_g = grade factor.

Fire Heat Release - Freight Train No Hazard Material	X0231-S02-EST-RP-10005-00 Preliminary Design Report - Tunnel MEP Systems	20000	kW
Fire Heat Release - Freight Train Hazard Material	X0231-S02-EST-RP-10006-AA Tunnel Ventilation Analysis (Freight Only)	250000	kW
Section - Geometrical Data – height With LEP	X0231-KFK-EST-DG-10201-AA KFK Tunnels - Typical Cross Section (CS-1) With Longitudinal Egress Passage - Tangent Track	8	m
Section - Geometrical Data - Area perpendicular to the flow With LEP	X0231-KFK-EST-DG-10201-AA KFK Tunnels - Typical Cross Section (CS-1) With Longitudinal Egress Passage - Tangent Track	64,45	m^2
Section - Geometrical Data – width With LEP	X0231-KFK-EST-DG-10201-AA KFK Tunnels - Typical Cross Section (CS-1) With Longitudinal Egress Passage - Tangent Track	7,2	m
Section - Geometrical Data – height Without LEP	X0231-KFK-EST-DG-10202-AA KFK Tunnels - Typical Cross Section (CS-2) Without Longitudinal Egress Passage - Tangent Track	7,8	m
Section - Geometrical Data - Area perpendicular to the flow Without LEP	X0231-KFK-EST-DG-10202-AA KFK Tunnels - Typical Cross Section (CS-2) Without Longitudinal Egress Passage - Tangent Track	61,15	m^2
Section - Geometrical Data – width Without LEP	X0231-KFK-EST-DG-10202-AA KFK Tunnels - Typical Cross Section (CS-1) With Longitudinal Egress Passage - Tangent Track	7,3	m
Trainway Slope - Worst Scenario	X0231-KFK-EST-DG-10200-AA KFK Tunnels TK1 & TK2 - General Layout X0231-KFK-ERA-DG-10002-AA Khor Fakkan Line Plan & Profile Ch. 3+000 to Ch. 6+000 X0231-KFK-ERA-DG-10003-AA Khor Fakkan Line Plan & Profile Ch. 6+000 to Ch. 9+000 X0231-KFK-ERA-DG-10004-AA Khor Fakkan Line Plan & Profile Ch. 9+000 to Ch. 12+000	-0,5	%
Outdoor Temperature	X0231-S23-EAM-FS-00001-00 Technical Specification - MEP Services	46	°C
Air density at 20 °C and atmosphere pressure	Carrier Psychrometric Diagram	1,204	kg/m^3
Air Specific heat at constant pressure	Carrier Psychrometric Diagram	1,007	kJ/kg*K

Table 2.8. Input data used for the calculation of Critical Velocity.

2.3.1. Critical Velocity – Cross section with LEP, HRR of 20 MW and no back layering

0,15*(H/W)^(-1/4)	0,146	-/-
Air density at 46 °C and Atmospheric Pressure	1,106	kg/m^3
Dimensionless heat release rate	0,099	-/-
Lenght of backlayering	0,000	m
Slope Coefficient	1,013	-/-
Critical Velocity (Vc)	3,394	m/s

Table 2.9. Results of the Iterative calculations – LEP with 20 MW.

With a critical velocity of about 3.40 m/s, the minimum air flow is 219 m^3/s.

2.3.2. Critical Velocity – Cross section with LEP, HRR of 20 MW and back layering

0,15*(H/W)^(-1/4)	0,146	-/-
Air density at 46 °C and Atmospheric Pressure	1,106	kg/m^3
Dimensionless heat release rate	0,099	-/-
Lenght of backlayering	43,000	m
Slope Coefficient	1,013	-/-
Critical Velocity (Vc)	2,538	m/s

Table 2.10. Results of the Iterative calculations – LEP with 20 MW.

With a confinement velocity of about 2.54 m/s, very similar with the value calculated earlier, the minimum air flow is 164 m^3/s, with a back-layering of about 43.0 m.

2.3.3. Critical Velocity – Cross section with LEP, HRR of 250 MW and no back layering

0,15*(H/W)^(-1/4)	0,146	-/-
Air density at 46 °C and Atmospheric Pressure	1,106	kg/m^3
Dimensionless heat release rate	1,241	-/-
Lenght of backlayering	0,000	m
Slope Coefficient	1,013	-/-
Critical Velocity (Vc)	3,857	m/s

Table 2.11. Results of the Iterative calculations – LEP with 250 MW.

With a critical velocity of about 3.9 m/s, the minimum air flow is 249 m^3/s.

2.3.4. Critical Velocity – Cross section with LEP, HRR of 250 MW and back layering

0,15*(H/W)^(-1/4)	0,146	-/-
Air density at 46 °C and Atmospheric Pressure	1,106	kg/m^3
Dimensionless heat release rate	1,241	-/-
Lenght of backlayering	13,000	m
Slope Coefficient	1,013	-/-
Critical Velocity (Vc)	3,533	m/s

Table 2.12. Results of the Iterative calculations – LEP with 250 MW.

With a confinement velocity of about 3.5 m/s, very similar with the value calculated earlier, the minimum air flow is 228 m^3/s, with a back-layering of about 13.0 m.

2.3.5. Critical Velocity – Cross section without LEP, HRR of 20 MW and no back layering

0,15*(H/W)^(-1/4)	0,148	-/-
Air density at 46 °C and Atmospheric Pressure	1,106	kg/m^3
Dimensionless heat release rate	0,106	-/-
Lenght of backlayering	0,000	m
Slope Coefficient	1,013	-/-
Critical Velocity (Vc)	3,411	m/s

Table 2.13. Results of the Iterative calculations – No LEP with 20 MW.

With a critical velocity of about 3.40 m/s, the minimum air flow shall be about 209 m^3/s.

2.3.6. Critical Velocity – Cross section without LEP, HRR of 20 MW and back layering

0,15*(H/W)^(-1/4)	0,148	-/-
Air density at 46 °C and Atmospheric Pressure	1,106	kg/m^3
Dimensionless heat release rate	0,106	-/-
Lenght of backlayering	42,000	m
Slope Coefficient	1,013	-/-
Critical Velocity (Vc)	2,550	m/s

Table 2.14. Results of the Iterative calculations – No LEP with 20 MW.

With a confinement velocity of about 2.55 m/s, very similar with the value calculated earlier, the minimum air flow is 156 m^3/s, with a back-layering of about 42.0 m.

2.3.7. Critical Velocity – Cross section without LEP, HRR of 250 MW and no back layering

0,15*(H/W)^(-1/4)	0,148	-/-
Air density at 46 °C and Atmospheric Pressure	1,106	kg/m^3
Dimensionless heat release rate	1,322	-/-
Lenght of backlayering	0,000	m
Slope Coefficient	1,013	-/-
Critical Velocity (Vc) =	3,808	m/s

Table 2.15. Results of the Iterative calculations – No LEP with 250 MW.

With a critical velocity of about 3.8 m/s, the minimum air flow is 233 m^3/s.

2.3.8. Critical Velocity – Cross section without LEP, HRR of 250 MW and back layering

0,15*(H/W)^(-1/4)	0,148	-/-
Air density at 46 °C and Atmospheric Pressure	1,106	kg/m^3
Dimensionless heat release rate	1,322	-/-
Lenght of backlayering	11,000	m
Slope Coefficient	1,013	-/-
Critical Velocity (Vc) =	3,529	m/s

Table 2.16. Results of the Iterative calculations – No LEP with 250 MW.

With a confinement velocity of about 3.53 m/s, very similar with the value calculated earlier, the minimum air flow is 216 m^3/s, with a back-layering of about 11.0 m.

Table 2.17 summarizes the calculations of the critical velocity for both the cross-sections of the tunnel. For the section with LEP a minimum critical velocity of 3.39 m/sec is needed for the 20 MW fire whereas, 3.86 m/sec is needed for the 250 MW fire. These values were determined using the NFPA 502-2020 formulations and the results show that the previous version of the calculations using the NFPA 502-2017 underestimates the critical ventilation velocity thereby resulting in backlayering for both the fire sizes. The results of the section without LEP follow the similar trend where 3.41 m/sec is required for the 20 MW fire and 3.81 m/sec for the 250 MW fire.

In the next chapter the mono-dimensional analysis is carried out using *IDA Tunnel* where both the fire scenarios, 20 MW and 250 MW is carried out at the most critical sections of the tunnel.

2.4. Critical Velocity – Summary

Case 1 - NFPA 502 - 2017	*Fire Heat Release - Freight Train No Hazard Material*	*20000*	*kW*	*Critical velocity (Vc) =*	2,54	*m/s*	*Length of Back layering*	0,00	*m*	WITH LEP
Case 2 - NFPA 502 - 2020	*Fire Heat Release - Freight Train No Hazard Material*	*20000*	*kW*	*Critical Velocity (Vc) =*	3,39	*m/s*	*Length of Back layering*	0,00	*m*	
Case 3 - NFPA 502 - 2020	*Fire Heat Release - Freight Train No Hazard Material*	*20000*	*kW*	*Critical Velocity (Vc) =*	2,54	*m/s*	*Length of Back layering*	43,00	*m*	
Case 4 - NFPA 502 - 2017	*Fire Heat Release - Freight Train Hazard Material*	*250000*	*kW*	*Critical velocity (VC) =*	3,53	*m/s*	*Length of Back layering*	0,00	*m*	
Case 5 - NFPA 502 - 2020	*Fire Heat Release - Freight Train Hazard Material*	*250000*	*kW*	*Critical Velocity (Vc) =*	3,86	*m/s*	*Length of Back layering*	0,00	*m*	
Case 6 - NFPA 502 - 2020	*Fire Heat Release - Freight Train Hazard Material*	*250000*	*kW*	*Critical Velocity (Vc) =*	3,53	*m/s*	*Length of Back layering*	13,00	*m*	

Case 7 - NFPA 502 - 2017	*Fire Heat Release - Freight Train No Hazard Material*	*20000*	*kW*	*Critical velocity (VC) =*	2,56	*m/s*	*Length of Back layering*	0,00	*m*	WITHOUT LEP
Case 8 - NFPA 502 - 2020	*Fire Heat Release - Freight Train No Hazard Material*	*20000*	*kW*	*Critical Velocity (Vc) =*	3,41	*m/s*	*Length of Back layering*	0,00	*m*	
Case 9 - NFPA 502 - 2020	*Fire Heat Release - Freight Train No Hazard Material*	*20000*	*kW*	*Critical Velocity (Vc) =*	2,55	*m/s*	*Length of Back layering*	42,00	*m*	
Case 10 - NFPA 502 - 2017	*Fire Heat Release - Freight Train Hazard Material*	*250000*	*kW*	*Critical velocity (VC) =*	3,52	*m/s*	*Length of Back layering*	0,00	*m*	
Case 11 - NFPA 502 - 2020	*Fire Heat Release - Freight Train Hazard Material*	*250000*	*kW*	*Critical Velocity (Vc) =*	3,81	*m/s*	*Length of Back layering*	0,00	*m*	
Case 12 - NFPA 502 - 2020	*Fire Heat Release - Freight Train Hazard Material*	*250000*	*kW*	*Critical Velocity (Vc) =*	3,53	*m/s*	*Length of Back layering*	11,00	*m*	

Table 2.17. Critical Velocity summary for LEP and No LEP sections.

Chapter 3

One-Dimensional Modelling

3.1. Introduction

Ensuring an adequate environment in underground facilities like subways, railway stations, tunnels for the moving equipment, etc., is quite a difficult engineering task. Basically, in an underground system ventilation and heat balance is given by complex interactions with the train piston action and heat emission; buoyancy driven low; wind induced and meteorological pressure differences on the portals and openings and also by the mechanical HVAC systems. As stated earlier, the occurrence of a fire in the tunnel has added even more complexity for designing an efficient and a robust strategy to maintain the minimum air quality and control the flow of smoke and hot gases. The most critical scenario is to ensure that the passengers and boarding crew can evacuate from the tunnel and allow the rescue teams access to the tunnels for rescue and fire-fighting operations.

Therefore, studies of the tunnel ventilation flows and fires are fundamental to assess the capabilities of a ventilation system and determines its effectiveness. The solution to this problem can be obtained in different ways using numerical models. '1D models' are typically adopted as a preliminary study as it allows for the complete description of the system involving a wide range of ventilation scenarios, boundary conditions at the portals and the description of fire with different sizes and at different locations. These models are quite compact and provide the means for the assessment of safety strategies of complex tunnels. However, they are not suitable to simulate the fluid behaviour in the regions close to fire or jet fans where there are high temperature and velocity gradients.

In this section the ventilation requirements for Khor Fakkan Tunnel (KFK) are determined to a sufficient level of detail, firstly with a 1D analysis, such that it supplements the Overall Tunnel FLS Strategy. The feasible ventilation strategy will be examined respecting the space proofing constraints. The 1D analysis of the KFK tunnel is carried out using *IDA Tunnel*, developed by *EQUA* in 1995. The IDA 1-D code is used extensively and has been validated for the design of tunnel ventilation systems throughout the world. The features in this model include the geometrical description of the tunnel, i.e. height coordinates and cross-sectional areas along with the length of each tunnel segment. Other input data cover ambient conditions including portal wind pressure, traffic inflow, coefficients of drag and friction, heat release rate (HRR) and thrust provided by fans.

3.2. *IDA Tunnel*

IDA Tunnel is a comprehensive tunnel environment simulation software based on the pre-complied component models, developed by EQUA. The approach of the simulation software is based on these mathematical models which are described in terms of equations in the modelling language 'Modelica'. The detailed explanations of these mathematical models are presented in detail in the Appendix section A.1.

3.3. Input parameters and Boundary Conditions

This section delves into all the input parameters and boundary conditions that have been used in the *IDA Tunnel* software.

3.3.1. Environmental Conditions

The environmental conditions contribute quite significantly in designing the ventilation system of the tunnels. The varying slopes, pressure differences, climatic and wind data are all considered for the zones where the KFK tunnel is located. According to the Climatic Study Report provided by the Client, cod. X0231-S23-GEN-RP-10001-00, the climatic zone related with the tunnels in Hajar area are labelled as the "Mountain Zones". These zones are like inland zones with higher humidity levels and have bigger bands of variation in the mean, low and high temperatures. Five major data sources have been used to describe the different micro-climatic zones along the alignment:

a) Abu Dhabi Area: It represents the Abu Dhabi City which is an example of coastal climate;

b) Dubai Area: It represents Dubai Area, which is located within the typical coastal climate;

c) Al Ain Area: Represented by Al Ain City, which is the only non-coastal major city in the UAE and is an example of inland climate;

d) Fujairah Area: Represented by Fujairah city which is a major city lying on the eastern coast of the UAE;

e) Ras Al Khaimah Area: Represented by Ras Al Khaimah city which is the only major city located in the north of the UAE.

Therefore, the climatic data of Al Ain area has been considered because of the similarity with the inland zones. The typical climatic conditions of Al Ain area are summarized below:

1. Outside Summer dry bulb temperature: 45.9 °C
2. Outside Summer wet bulb temperature: 22.3 °C
3. Outside Winter dry bulb temperature: 11.1 °C
4. Relative Humidity: 11.53%
5. Humidity Ratio: 7.23 g/kg $_{\text{dry air}}$

Also, an extensive study about the directionality and speeds of the wind in different weather conditions have been evaluated in the Al Ain area, of which the details are summarized:

a) Winter:

Pre-dominant direction: North-West;

Wind Speeds: Largely between 0 – 8 m/s (96.3% of the monitoring period).

b) Spring:

Pre-dominant direction: North-West;

Wind Speeds: Largely between 0 – 8 m/s (96.3% of the monitoring period).

c) Summer:

Pre-dominant direction: South & South-East;

Wind Speeds: Largely between 0 – 10 m/s (99.4 % of the monitoring period).

d) Autumn:

Pre-dominant directions: South / South-East and North / North-West.

Wind Speeds: Largely between 0 – 8 m/s (97.9 % of the monitoring period).

Wind Speeds: Largely between 0 – 8 m/s (97.9 % of the monitoring period). The wind rose diagrams for different seasons of the Al Ain area is shown below:

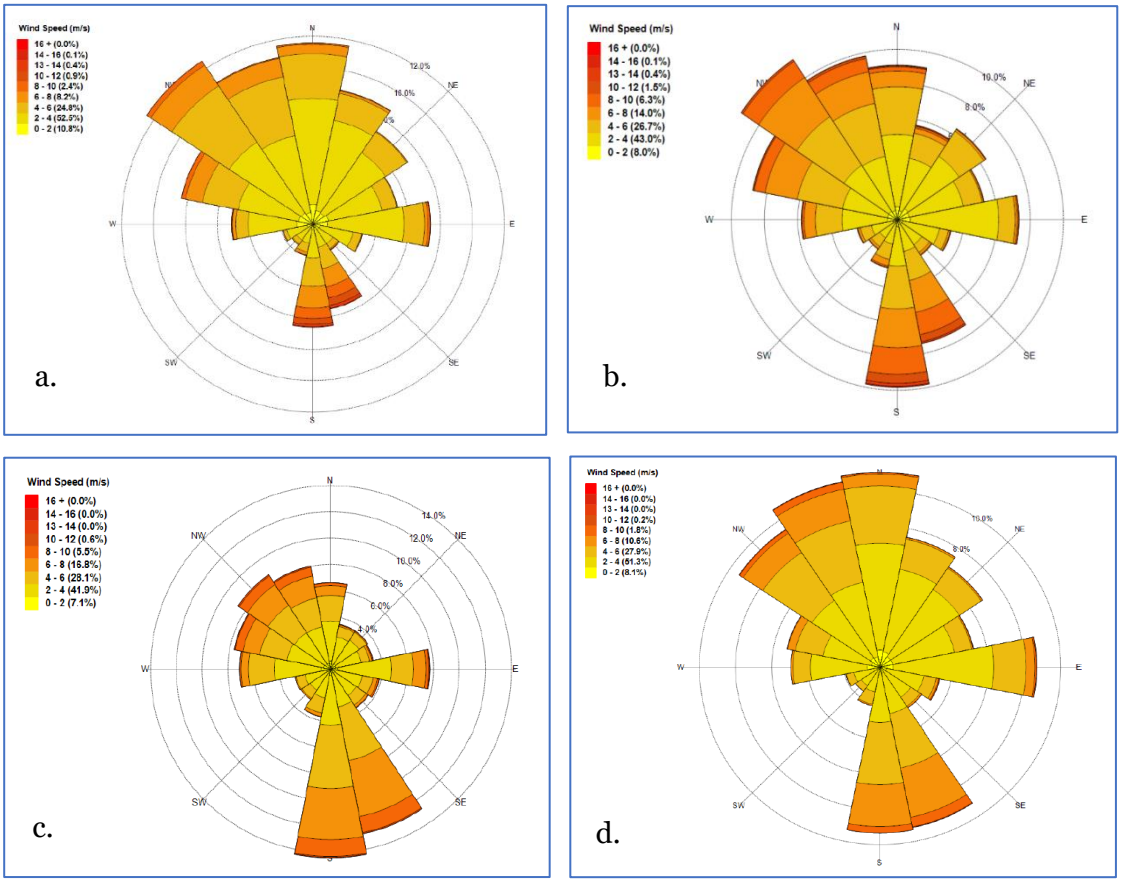

Figure 3.1. Al Ain Winter Wind Rose diagram: a. December to February; b. March to May; c. June to August; d. September to November.

The coefficients of the influence of wind on the longitudinal ventilation of rail tunnel has been evaluated considering the Probabilistic Approach proposed by Werner Blendermann in 1976 in his article "On a probabilistic approach to the influence of wind on the longitudinal ventilation of Road Tunnels" [34]. The "above ground portal" configuration has thus been considered, as showed in the figure below.

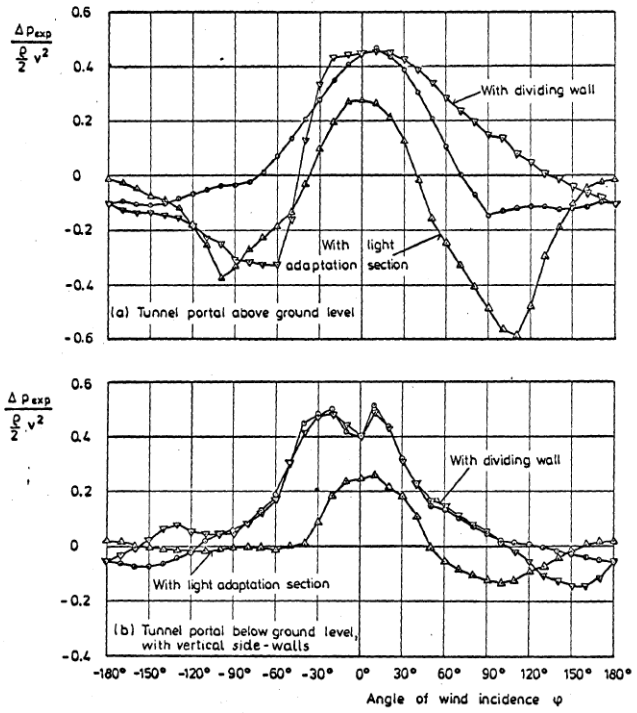

Figure 3.2. Wind pressure differences at a tunnel portal [34].

Based on the consideration above, the following conditions have been determined for the two idealized tunnel fires:

For the fire at chainage 5+100:

a) Maximum wind velocity: 10 m/s;
b) Wind Coefficient at portal n° 1, chainage 3+500: -0.6. The portal pressure is

$$\Delta p = \beta \frac{1}{2} \rho v^2 = +0.6 \frac{1}{2} 1.106 * 10^2 = +33.18\ Pa$$

c) Wind Coefficient at portal n° 2, chainage 9+400: +0.5. The portal pressure is

$$\Delta p = \beta \frac{1}{2} \rho v^2 = -0.5 \frac{1}{2} 1.106 * 10^2 = -27.65\ Pa$$

For the fire at chainage 6+450:

a) Maximum wind velocity: 10 m/s;

b) Wind Coefficient at portal n° 2, chainage 9+400: -0.6. The portal pressure is

$$\Delta p = \beta \frac{1}{2} \rho v^2 = +0.6 \frac{1}{2} 1.106 * 10^2 = +33.18\ Pa$$

c) Wind Coefficient at portal n° 1, chainage 3+500: +0.5. The portal pressure is

$$\Delta p = \beta \tfrac{1}{2} \rho v^2 = -0.5 \tfrac{1}{2} 1.106 * 10^2 = -27.65\ Pa.$$

Ambient Air Properties implemented on IDA Tunnel			
P	101325	Pa	Atmospheric Pressure at ref. level
T	45.9	°C	Ambient Temperature
CO_2*	0	Ppm(vol)	Fraction CO_2 in Ambient Air
Particles*	0	µg/m³	Particle Fraction in Ambient Air
relHum	11.53	%	Relative Humidity
WindDir	0	Deg.	Wind Direction (wind from E - 90 Deg.)
WindVel	10	m/sec	Wind Speed
*The concentrations of air fractions maybe given either as absolute values or relative to their normal levels.			

Figure 3.3. IDA Software ambient boundary conditions.

3.3.2. Tunnel entry and exit – *IDA Tunnel* input

A tunnel entry (K_{entry}) loss of 0.5 and an exit portal loss of (K_{exit}) of 1.0 is considered. These values are consistent with most fluid mechanics textbook and with the recommendation of Permanent International Association of Road Congresses (PIARC) [38]. These values have also been confirmed in the following ASHRAE fitting database:

a) K_{exit}: SD2-1 Abrupt exit (Idelchik 1986, diagram 11-1) [39];

b) K_{entry}: ED1-1 Duct mounted in Wall (Idelchik 1986, diagram 3-1) [39].

The input conditions for rail tunnel entry and exit have been summarized below:

Tunnel Entry Loss Coefficient			
kPos	0.5		Loss Coeff. for flow into tunnel
kNeg	1.0		Loss Coeff. for flow out of tunnel
PWind	33.18	Pa	Wind pressure
Tunnel Exit Loss Coefficient			
kPos	0.5		Loss Coeff. for flow into tunnel
kNeg	1.0		Loss Coeff. for flow out of tunnel
PWind	-27.65	Pa	Wind pressure

Figure 3.4. Tunnel Entry and Exit loss coefficient.

3.3.3. Rail tunnel section boundary conditions

In this section the boundary conditions defined in the rail sections, upstream and downstream of the Tunnel Ventilation Shaft located at chainage 6+150 are summarized.

i. Jet fans

The kinematic envelope of the train determines the allowable area for MEP equipment within the tunnels. It has been considered that placing jet fans along the tunnel crown is not feasible, with plans of an overhead catenary line in the future. Therefore, jet fans are proposed along the tunnel side wall, immediately above the emergency walkway envelope. Fans will be installed in banks of two and spaced approximately 330 - 350 m apart, which is sufficient enough to prevent the high jet flow from one fan affecting the performance of the fans downstream. The 'spacing allowed' guidelines from the fan manufactures recommends that the jet fans are positioned with a minimum, '10 times the tunnel hydraulic diameter' from each other. The details of the jet fans used for this analysis are presented in table below. Fans are assumed to be 100% reversible and therefore the thrust achieved in forward direction is expected to be achieved in reverse direction too.

Parameter	Values
Fan Diameter	1000 mm
Fan External Diameter	1200 mm
Fan Thrust	820 N
Jet Velocity	29.5 m/s
Shaft Power	33.00 kW

Table 3.1. Performance of Jet fans

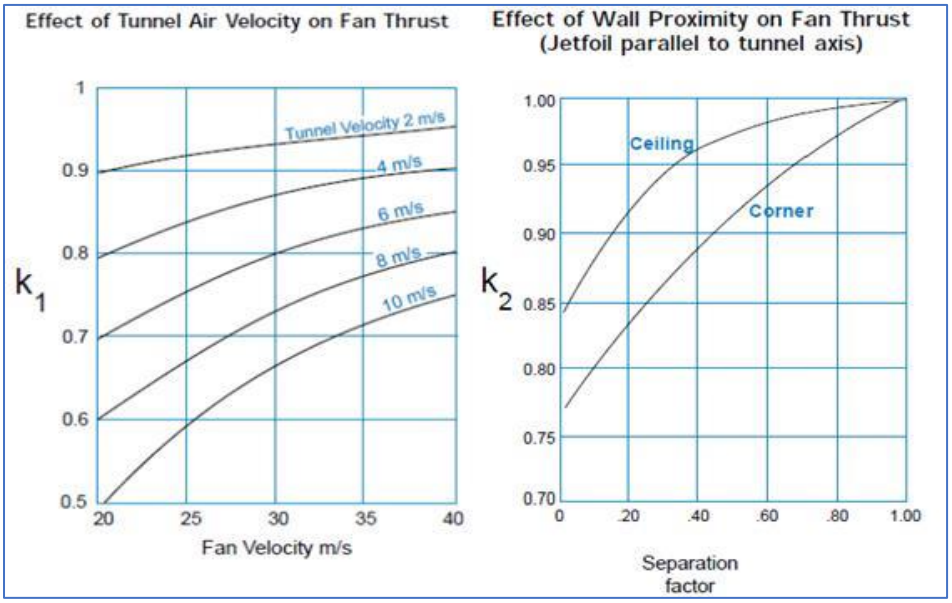

Figure 3.5. Standard correction factors for jet fans [56].

The momentum transfer between the fast-moving jet velocity and the slower moving bulk tunnel air is most efficient when it is unconstrained by localized blockage (cable trays, tunnel MEP equipment's) or wall proximity. The aerodynamic efficiency of jet fans is critical while assessing the system. It is evaluated using standard correction factors accounting for the effect of tunnel air velocity (k_1) and wall proximity (k_2) on fan thrust as shown in Figure 3.5. Thus, the separation factor S_F can be calculated as:

$$S_F = \frac{2z}{D_T - D_F},$$

Where,

z is the distance of jet axis to tunnel wall or ceiling;

D_F is the jetfoil fan diameter;

D_T is the tunnel hydraulic diameter.

Assuming that:

z is 0.15 m;

D_F is 1.0 m;

D_T is 8.53 m for section without LEP and 7.94 m for section with LEP,

Maximum longitudinal velocity is about 4.0 m/s,

The minimum aerodynamic efficiency is:

$$\eta = K_1 K_2 = 0.86 * 0.83 = 0.7138.$$

Considering all the equipment in the tunnel, an installation factor of 0.65 has been assumed which is quite conservative to the design.

The tunnel ventilation system has been designed to maintain its design requirement even when a fan is unavailable due to routine maintenance or failure. For this reason, the following acceptable level of redundancy via stand-by fans have been considered:

- 2 jet fans or 10% of the fans (whichever is greater) have been considered out of service. In the current case study, with a total number of 36 jet fans installed along the tunnel, 4 of them have been considered out of service;
- Due to the effects of fire and in addition to the redundancy assumed for maintenance reason, it has been assumed that the fans within specified distance from the fire source have been destroyed.

Based on the table below, extracted from Standard BD 78/99, the following assumptions have been made:

- HRR of 20 MW – 1 couple, downstream of the fire have been destroyed.
- HRR of 250 MW – 2 couple, downstream of the fire have been destroyed.

Fire Size (MW)	Distance Upstream of Fire (m)	Distance Downstream of Fire (m)
5	-	-
20	10	40
100	30	120
This information is extracted from BD78/99		

Figure 3.6. BD 78/99 Standard. [55]

ii. Change of Tunnel Cross Section

IDA Tunnel can keep into account the changes of cross sections that happen in a tunnel. With reference to the tunnel TK1, there is a change at the chainage 5+400 between the cross sections with and without LEP. Thus, the following coefficients have been considered:

Contraction Loss Coefficient wrt. Minimum Area	0.2	dimensionless*
Extraction Loss Coefficient wrt. Minimum Area	0.2	dimensionless*

Figure 3.7. *IDA Tunnel* - Loss coefficients.

This is conservative enough, if compared with the values according to ASHRAE Duct Fitting, SD4-2 Transition, Rectangular to Round, Idelchik 1986, Diagram 5-27, equal to 0.1 [39].

iii. Fire modelling

For the analysis, four fire scenarios have been considered, in the emergency conditions:

a) Train on fire stopped in an intermediate section of tunnel equipped with LEP, at chainage 5+100, with heat release rate equal to 20 MW;

b) Train on fire stopped in an intermediate section of tunnel equipped with LEP, at chainage 5+100, with heat release rate equal to 250 MW;

c) Train on fire stopped in an intermediate section of tunnel without LEP, at chainage 6+450, with heat release rate equal to 20 MW;

d) Train on fire stopped in an intermediate section of tunnel without LEP, at chainage 6+450, with heat release rate equal to 250 MW;

The basic fire evacuation strategy in a longitudinally ventilated tunnel is to keep the tunnel free of smoke upstream of the fire by using jet fans, which blow the smoke in the opposite direction of evacuation. Trains downstream of the fire are assumed to be able to drive out of the tunnel ahead of the smoke front. The fire position has been selected to provide the 'worst-case scenario' in terms of the thermal stack effect, which is stronger when the fire is closer to the entry portal of downhill part.

The 1D fire model is capable of describing the overall effects of the fire to an accuracy which is acceptable for a typical 'fire security study' in rail tunnels. However, the effects of the fire in the near field are not described in detail. For this reason, the length parameter that should reflect the size of the near field around the fire has been as 20 m (length of single stack container flat). Heat from fire (or heat release rate) is the basic parameter, describing the size of the fire, including both radiated and convected heat. The fire sizes 20 MW and 250 MW has been defined as a function of time by connecting it to an input table. In compliance with NFPA 92 [54], two methodologies have been selected:

1) HRR equal to 20 MW – fire class "Fast".

$$q = at^2,$$

where,

q = rate of heat release (kW);
a = constant governing the speed of growth;
t = time (s).

The constant a can be calculated in compliance with table B.7.1 – NFPA 92 [54]:

$$a = \frac{1055.06\ kW}{150^2\ s^2} = 0.047\ \frac{kW}{s^2}.$$

2) HRR equal to 250 MW – fire class "Ultra-fast".

The constant a can be calculated in compliance with table B.7.1 – NFPA 92 [54]:

$$a = \frac{1055.062\ kW}{75^2\ s^2} = 0.19\ \frac{kW}{s^2},$$

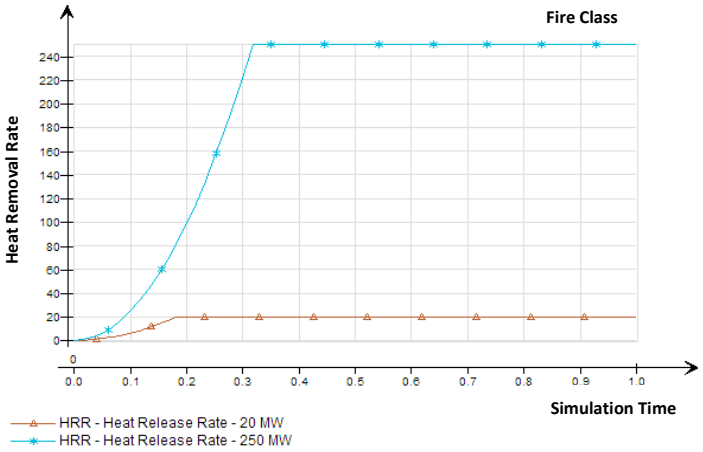

Figure 3.8. Set up of Fire on IDA Software for both curves.

A tunnel fire will result in a so-called throttling effect, i.e. the fire plume will act as an obstacle to flow over the fire region. This effect is difficult to estimate in a 1D model and typically a parameter, fire pressure drop is required as an input to account for this pressure drop.

A reasonable default value, extracted from *IDA Manual* – Theoretical Reference, of 0.1 Pa/MW has been considered. By default, the fire power is limited by available oxygen, i.e. if the air flow through the tunnel is not enough for maintaining a fire of the specified size (HRR), the heat release rate is reduced accordingly.

If the air (momentarily) will be standing still, the heat release rate is further reduced (by default by 90%) for reasons of numerical stability. To complete the fire modeling the following global parameters have been considered:

a) Heat of combustion, H: 25.4 MJ/kg;

b) Soot Yield, Y_s: 0.13 kg/kg;

c) Mass Extinction Coefficient, K: 8700 m^2/kg;

d) Combustion Efficiency, k_{ic}: 70%.

The above values have been extracted from the experimental data proposed in different scientific articles [33], [35], [36], [37] . The parameters listed above relate the amount and optical density of produced smoke to the heat release rate. In *IDA Tunnel*, the parameter *fire2air* determines the amount of fire-heat that impacts directly to heat the tunnel air, and (1 - *fire2air*) will radiate from the flame to the surrounding tunnel wall. This empirical parameter has been assumed to be around 70%. It has been observed that the results in the far field are not as sensitive to this input, since radiated heat will heat the wall which then, in turn, will heat the air by convection.

Accurate computation of the air temperature, and thereby density, downstream of the fire is naturally critical to predict the stack effect. To resolve the exponentially decaying temperature, an automatic refinement of the grid around the fire is provided. The following parameters have been considered to control the automatic grid refinement around a fire:

a) *dxFire0:* it gives the cell size next to the fire cell, where the gradient is the steepest and has been considered as 0.2 m.

b) *dxFireFactor:* it determines how much big the next cell is and has been considered as 1.05.

c) *dxFireExtent:* it specifies the total extent in all directions that should get a refined grid, and is equal to 1000 m.

The grid refinement algorithm of IDA Software refines the grid in all directions around a fire, i.e. it has no notion of the direction fire gases will take or the distance it will take for gases to cool. When a branch or plenum component is encountered in a possible air path, the refinement will continue in all connecting branches.

iv. Central Ventilation Station

In compliance with NFPA 130, section 7.2.5, [3] due to the potential for a valid incident ventilation response to move smoke past (and engulf) a non-incident train, the best protection to passengers is to allow no more than one train in a ventilation zone. The Operational plan of railway line, together with signaling schematic plan with moving block, permits that no more than one train could be in tunnel TK1 in case of a train on fire stopped in station. For this reason, the ventilation system has been designed to ensure the division in two ventilation zones so that the signaling system will allow only one train in each zone and the smoke cannot engulf the non-incident train:

a) Ventilation zone n° 1 – from ch. 3+500 to ch. 6+150.

b) Ventilation zone n° 2 – from ch. 6+150 to ch. 9+400.

The aim has been achieved with the design of a ventilation station located at ch. 6+150, connected with the tunnel through a structure shaft-plenum. The ventilation station consists of three axial fans with motorized dampers with a nominal air flow of 180 m^3/s for each fan.

Monodimensional ventilation scheme

In the picture below the 1D model is shown, compliant with the boundary conditions listed in the previous sections. The maximum discretization step is 50 m and the equipment has been simulated considering the positions listed in the table below.

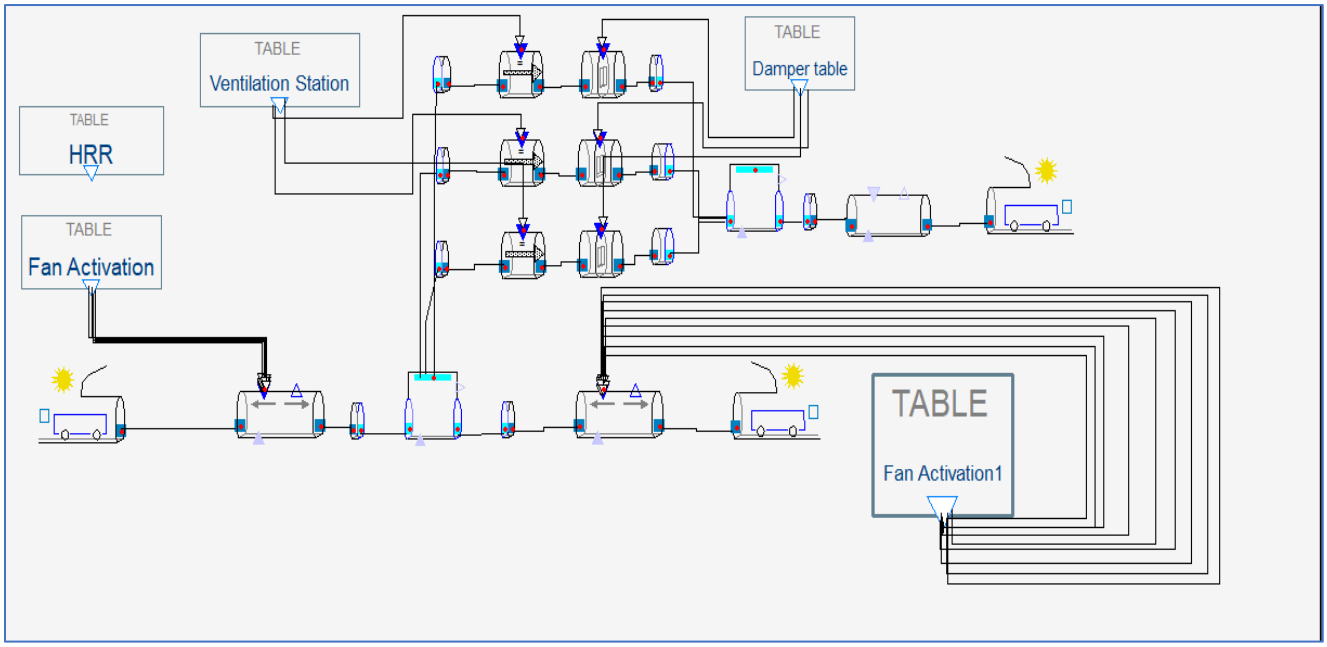

Figure 3.9. Tunnel Ventilation Scheme on *IDA Tunnel* Software.

Object	Chainage
Right Portal	3+500
Jet fan – couple 1	3+652
Jet fan – couple 2	3+987
Jet fan – couple 3	4+322
Jet fan – couple 4	4+657
Jet fan – couple 5	4+992
Sensor 1	5+000
Sensor 2	5+050
Fire for scenarios a) and b) section 5.3.3	5+100
Sensor 3	5+150
Sensor 4	5+200
Jet fan – couple 6	5+327
Change of cross section area (LEP to NO LEP)	5+400
Jet fan – couple 7	5+662
Jet fan – couple 8	5+997
Plenum for ventilation central	6+150
Jet fan – couple 9	6+322
Sensor 5	6+350
Sensor 6	6+400
Fire for scenarios c) and d) section 5.3.3	6+450
Sensor 7	6+500
Sensor 8	6+550
Jet fan – couple 10	6+647
Jet fan – couple 11	6+972
Jet fan – couple 12	7+297
Jet fan – couple 13	7+622
Top elevation of tunnel	7+825
Jet fan – couple 14	7+947
Jet fan – couple 15	8+272
Jet fan – couple 16	8+597
Jet fan – couple 17	8+922
Jet fan – couple 18	9+247
Left Portal	9+400

The points mentioned as 'Sensors' are sections where the following properties are recorded:

- Air temperature
- Air velocity
- Total pressure w.r.t. ambient
- Static pressure w.r.t. ambient
- Wall temperature
- Extinction coefficient

Table 3.2. Configuration of the KFK Tunnel.

3.4. Results - 1D Simulation

3.4.1. Scenario 1: Train on fire stopped in the tunnel at ch. 5+100 with HRR of 20 MW

The Scenario n° 1 is compliant with the following input:

a) HRR of 20 MW and growing according to the fast curve, as per NFPA 92 [54];
b) Direction of wind effect from entry portal at ch. 3+500 to exit portal at ch. 9+400;
c) Egress travel direction from ch. 5+100 to ch. 6+150;
d) Jet fan activation time: 180 s after receiving the fire alarm in the Control Centre;
e) Time to reach to nominal air flow for jet fans and main axial fans: 60 s;
f) The following jet fans have been assumed out of service:
   - Couple n° 5: destroyed by fire;
   - Couple n° 8: under maintenance;
   - Couple n° 18: under maintenance.
g) Main ventilation station at ch. 6+150: only 1 fan has been activated with variable frequency driver at 15 Hz (about 30% of the nominal flow).

a) Velocity of Air (m/s)

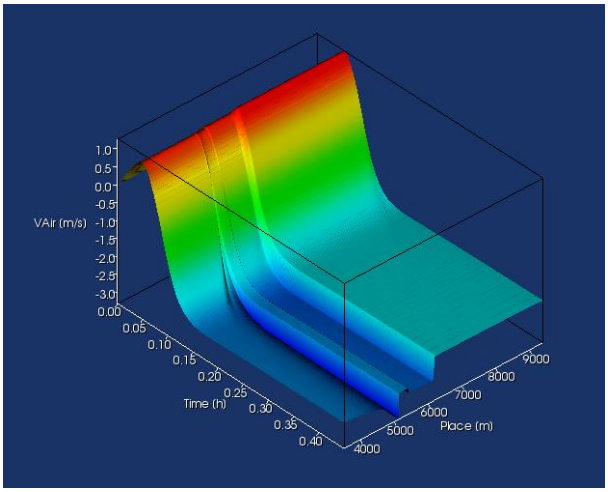

Figure 3.10. Velocity of the Air for 20 MW fire at chainage 5+100.

- From 0.00 h up to 0.05 h the velocity is positive (i.e. from left to right), with a maximum value of 1.3 m/s, due to wind and stack effects that are predominant over the ventilation thrust. Following from 0.5 h to 1 h, a stationary scenario is reached, where there is negligible change in the air velocity.
- At the end of simulation, 1:00 h, the velocity is about -2.1 m/s (i.e. from right to left) up to ch. 6+170 m. Then, the longitudinal velocity increases up to -2.7 m/s due to the additional air flow generated by the main ventilation station at chainage 6+150. The velocity is -2.55 m/s upstream of the fire, due to the discontinuity between tunnel cross section with and without LEP. Close to the fire, at ch. 5+100, due to the decreasing air density generated by the HRR of 20 MW and in compliance with the

principle of conservation mass, the velocity increases up to -3.31 m/s. Close to the access portal, at ch. 3+500, after the cooling effect, the velocity becomes -2.6 m/s.

b) Air Volume flow (m³/s)

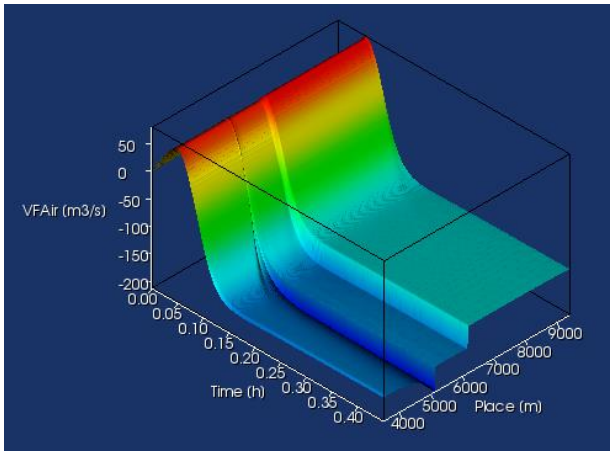

Figure 3.11. Air Volume flow for the 20 MW fire at chainage 5+100.

- From 0.00 h up to 0.05 h the air flow is positive (i.e. from left to right), with a maximum value of 80.0 m^3/s, due to wind and stack effects that are predominant over the ventilation thrust. Then from 0.5 h to 1 h, a stationary scenario is reached, where there is negligible change in the air volume flow.
- At the end of simulation, 1:00 h, the air flow is about -126 m^3/s (i.e. from right to left) up to ch. 6+170 m. Then the longitudinal air flow increases up to -166 m^3/s due to the additional air flow generated by the main ventilation station at chainage 6+150. The air flow is about -165 m^3/s upstream of the fire due to the discontinuity between tunnel cross section with and without LEP. Close to the fire, at ch. 5+100, due to the decreasing air density generated by the HRR of 20 MW, in compliance with the principle of conservation mass, the air flow increases up to -213 m^3/s.

c) Air Temperature (°C)

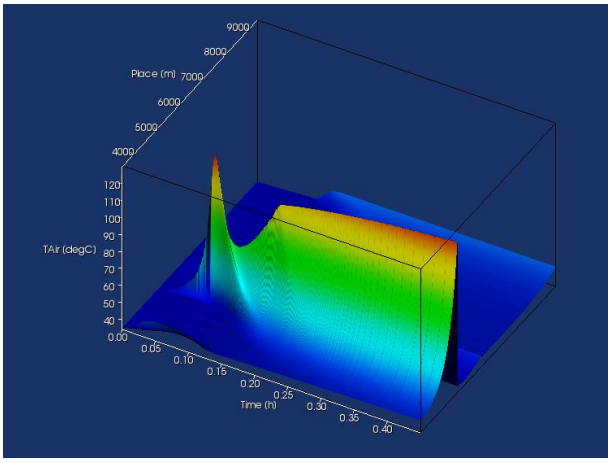

Figure 3.12. Air temperature for the 20 MW fire at chainage 5+100.

- The temperature starts to increase since time 0.00 h because the fire scenario is growing in compliance with the fast curve (NFPA 92). The greatest temperature fluctuation starts at 0.078 h because, simultaneously with the increasing of the HRR, the air flow starts to decrease due to the ventilation thrust contrasting the wind and stack effects.
- In the time period between 0.085 h and 0.118 h, the reduction of the air flow will be lower the HRR due to the lack of oxygen and the air temperature starts to decrease up to 75.3 °C. Following from 0.5 h to 1 h, a stationary scenario is reached, where there is negligible change in the value.
- With the ventilation thrust prevailing over the wind and stack effects, the air flow exceeds the value necessary to restart the growing of the HRR (the level of oxygen brings back above the stoichiometric value) and the air temperature increases up to 130 °C.

d) Extinction coefficient (1/m)

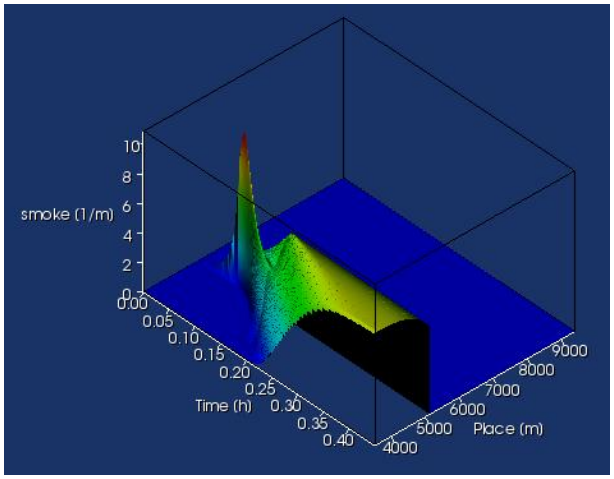

Figure 3.13. Extinction coefficient for the 20 MW fire at chainage 5+100.

The extinction coefficient is a measure of the visibility due to the fire-smoke. It describes the per meter drop of light. The extinction coefficient of the smoke is calculated using the following equation:

$$K = \frac{1}{L} ln \frac{I_0}{I} = 2.3 D_0,$$

Where,

$$D_0 = \frac{D}{L} \; or \; D_0 = \frac{1}{L} log_{10} \frac{I_0}{I},$$

With,

D_0 is the optical density for a path length of 1 m (bel(m)) [50],
L is the path length (m),
I_0 is the light intensity measured in absence of smoke (transmittance 100%),
I is the light intensity measured with smoke.

Visibility is not a parameter that is directly measured. It is calculated or estimated using models taking optical density or smoke concentration as inputs. Jin [42] claims that for people unfamiliar with the escape route an extinction coefficient limit of 0.15 m^{-1} (D_0=0.06 bel/m) and for regular people 0.5 m^{-1} (D_0=0.2 bel/m); while Rasbash [43] gives a visibility limit of 10 m, equivalent to an optical density of 0.08 bel/m (k=0.19 m^{-1}). For Babraukas [44], the extinction coefficient should be higher than 1.2m^{-1} (D0=0.5 bel/m). Finally, for safety reasons, the visibility limits are obtained for extinction coefficients in the range (0.15 ÷ 0.20) m^{-1}.

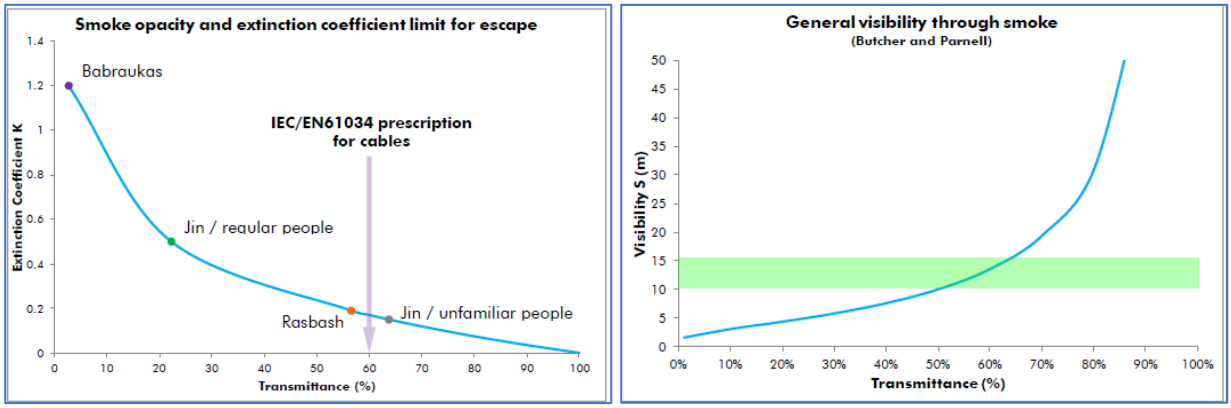

Figure 3.14. Visibility models from Literature [45].

- Up to 0.1 h, i.e. during the transient period when the ventilation system activation is in progress, combined with the growing of the HRR, the wind and stack effects, the extinction coefficient is above 0.3 m^{-1} between the ch. 5+100 and 5+300.
- Starting from 0.1 h, upstream the fire at ch. 5+100, the extinction coefficient is always less than 0.3 m^{-1}, ensuring a safe evacuation path to the passengers (From 0.5 h a stationary scenario is reached, where there is negligible change in the extinction coefficient). It is relevant to note that 1D simulations are not able to take in account the boundary cross section effects and, therefore, a 3D analysis has been performed to evaluate if, in compliance with NFPA 502-2020 edition, a back layering length is possible even if the final longitudinal velocity is above the minimum value calculated with "Kennedy methodology".

3.4.2. Scenario 2: Train on fire stopped in the tunnel at chainage 5+100 with HRR of 250 MW

The Scenario n° 2 is compliant with the following input:

a) Heat release rate of 250 MW, growing according "super-fast curve", as per NFPA 92;
b) Direction of wind effect from entry portal at chainage 3+500 to exit portal at chainage 9+400;
c) Egress travel direction from chainage 5+100 to chainage 6+150;
d) Jet fan activation time: 180 s after receiving the fire alarm in the Control Centre;
e) Time to reach to nominal air flow for jet fans and main axial fans: 60 s;

f) The following jet fans have been assumed out of service:

- Couple n° 4: destroyed by fire;
- Couple n° 5: destroyed by fire;
- Couple n° 8: under maintenance;
- Couple n° 18: under maintenance.

g) Main ventilation station at chainage 6+150: 2 fans have been activated with variable frequency driver at 50 Hz (100% of the nominal flow).

a. Velocity of Air (m/s)

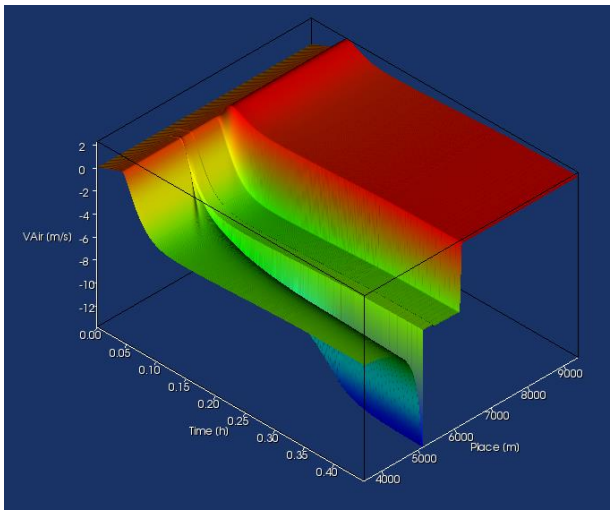

Figure 3.15. Velocity of the Air for 250 MW fire at chainage 5+100.

- From 0.00 h up to 0.05 h the velocity is positive (i.e. from left to right) in the tunnel, with a maximum value of 0.9 m/s, due to wind and stack effects. Then until 0.05 h the ventilation system, jet fans and main axial fans, are switched off and the resistant action to the longitudinal flow is operated by the throttling effect of the fire plume.
- After 0.05 h, the velocity becomes negative (i.e. the direction of the longitudinal flow is from right to left) from chainage 3+500 to ch. 6+150 due to the ventilation thrust operated by the jet fan couples and the central main ventilation station.
- Instead from ch. 6+150 to ch. 9+400, the velocity is still positive because the thrust operated by the central ventilation station is higher compared with that one created by the jet fan couples in tunnel sector 2, the jet fans in sector 2 can only generate a throttling effect, maximizing the amount of air from the central station to the entry portal at ch. 3+500.
- Following from 0.5 h to 1 h, a stationary scenario is reached, where there is negligible change in the air velocity.
- At the end of simulation, 1:00 h, the velocity is about +2.2 m/s (i.e. from left to right) close to the portal at ch. 6+170 m. Due to the cooling effect of tunnel wall, and the consequent increasing of air density, the velocity decreases up to 2.16 m/s close to the exit portal at ch. 9+400. Instead, the longitudinal velocity increases up to -3.7 m/s close to the plenum at ch. 6+150, due to the additional air flow generated by the main ventilation station.

- The discontinuity between tunnel cross section with and without LEP, stabilizes the velocity at -3.5 m/s immediately upstream the train of fire (stopped at ch. 5+100).
- Close to the fire, at ch. 5+100, due the decreasing air density generated by the HRR of 250 MW, in compliance with the principle of conservation mass, the velocity increases up to -13.9 m/s. Close to the access portal, at ch. 3+500, after the cooling effect of tunnel wall, the velocity becomes -3.8 m/s.

b. Air Volume flow (m^3/s)

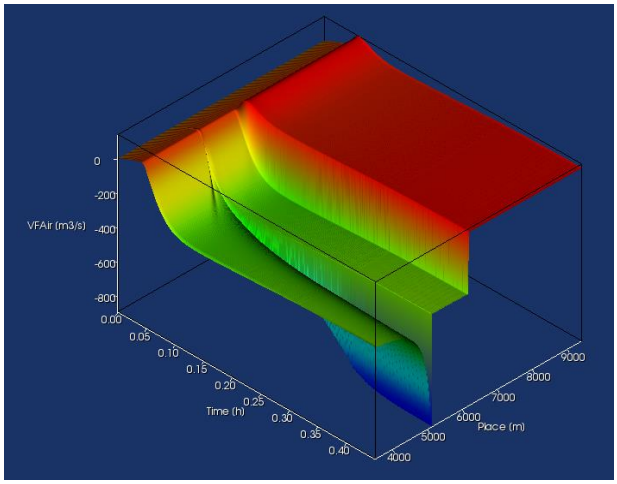

Figure 3.16. Air Volume flow for the 250 MW fire at chainage 5+100.

- From 0.00 h up to 0.05 h the air flow is positive (i.e. from left to right) in all the tunnel. For the reasons already explained in the previous section, the following maximum values have been calculated:
  - ✓ 53.6 m^3/s in tunnel sector 1 (from ch. 3+500 to ch. 6+150).
  - ✓ 136.0 m^3/s in tunnel sector 2 (from ch. 6+170 to 9+400). This peak value is measured at 0.062 h.
- Then from 0.5 h to 1 h, a stationary scenario is reached, where there is negligible change in the air volume flow. At the end of simulation, 1:00 h, the air flow is about +132 m^3/s (i.e. from left to right) close to the exit portal at ch. 9+400. The longitudinal air flow is about -225 m^3/s at ch. 6+150, due to the additional air flow generated by the main ventilation station. Immediately upstream of the fire, at chainage 5+120, the air flow decreases up to -221 m^3/s due to the discontinuity between tunnel cross section with and without LEP.
- Close to the fire, at ch. 5+100, due to the decreasing air density generated by the HRR of 250 MW, in compliance with the principle of conservation mass, the air flow increases up to -892 m^3/s.
- Close to the access portal, at ch. 3+500, after the wall cooling effect, the air flow becomes -225.5 m^3/s.

c. Air Temperature (°C)

- The temperature does not increase significantly up to 0.05 h, even if the HRR should grow according the super-fast curve described in the NFPA 92: this phenomenon is explained because the air flow generated by the wind is not enough to provide the amount of oxygen necessary to develop the combustion. The maximum temperature registered in the preliminary phase is 147 °C.
- In the time period between 0.06 h and 0.08 h, the reduction of the air flow lowers the HRR due to lack of oxygen and the air temperature starts to decrease up to 84.5 °C.

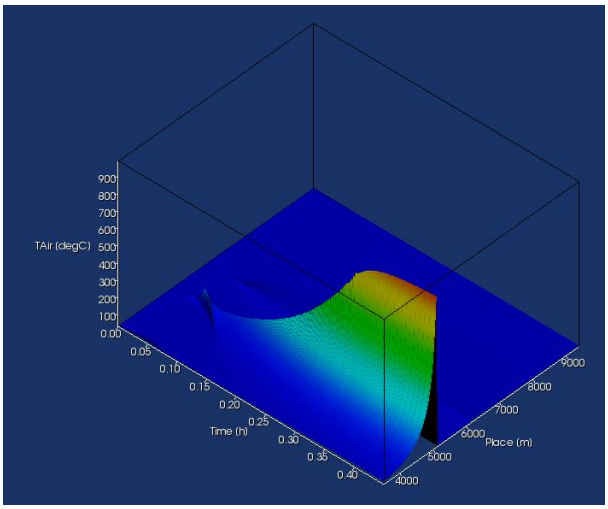

Figure 3.17. Air Temperature for the 250 MW fire at chainage 5+100.

- With the ventilation thrust prevailing over the wind and stack effects, the air flow exceeds the value necessary to restart the growing of the HRR (the level of oxygen will be greater than the stoichiometric value) and the air temperature increases up to 988 °C.
- Following from 0.5 h to 1 h, a stationary scenario is reached, where there is negligible change in the value.
- It is interesting to note that, close to the ch. 6+150, where the central ventilation station is blowing air into the tunnel, a limited temperatures increase is registered (about 45 °C): it arises mainly because the outdoor air temperature is greater than tunnel air temperature and heated by fan motors. This peak is easily managed through the cooling process of tunnel wall.

d. Extinction coefficient (1/m)

- Up to 0.1 h, i.e. during the transient period when the ventilation system activation is in progress, combined with the growing of the HRR, the wind and stack effects, the extinction coefficient is above 0.3 m^{-1} between the ch. 5+100 and 5+200.

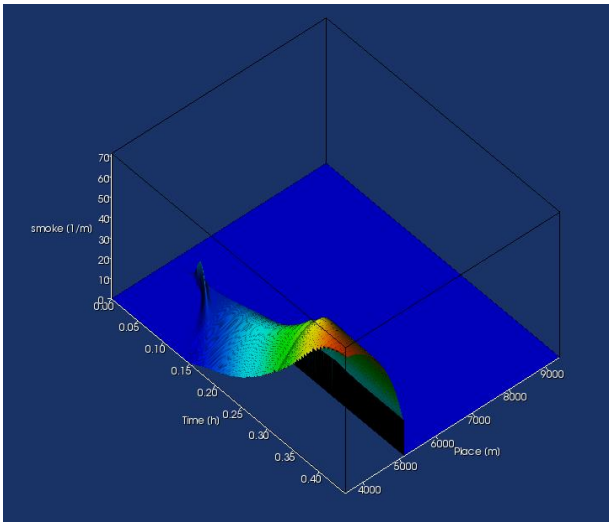

Figure 3.18. Extinction coefficient for the 250 MW fire at chainage 5+100.

- Starting from 0.1 h, upstream the fire at ch. 5+100, the extinction coefficient is always less than 0.3 m^{-1}, ensuring a safe evacuation path to the passengers (From 0.5 h a stationary scenario is reached, where there is negligible change in the extinction coefficient).
- It is relevant to note that, as per the previous case, 1D simulations are not able to take in account the boundary cross section effects and, therefore, a 3D analysis has been performed to evaluate if, in compliance with NFPA 502-2020 edition, a back layering length is possible even if the final longitudinal velocity is above the minimum value calculated with "Kennedy methodology".

3.4.3. Scenario 3: Train on fire stopped in tunnel at chainage 6+450 with HRR of 20 MW.

The Scenario n° 3 is compliant with the following input:

a) Heat release of 20 MW, growing according fast curve, as per NFPA 92;
b) Direction of wind effect from entry portal at chainage 9+400 to exit portal at chainage 3+500;
c) Egress travel direction from chainage 6+450 to chainage 6+150;
d) Jet fan activation time: 180 s after receiving the fire alarm in the Control Centre;
e) Time to reach to nominal air flow for jet fans and main axial fans: 60 s;
f) The following jet fans have been assumed out of service:
    - Couple n° 10: destroyed by fire;
    - Couple n° 8: under maintenance;
    - Couple n° 18: under maintenance.
g) Main ventilation station at chainage 6+150: completely switched off.

a. Velocity of Air (m/s)

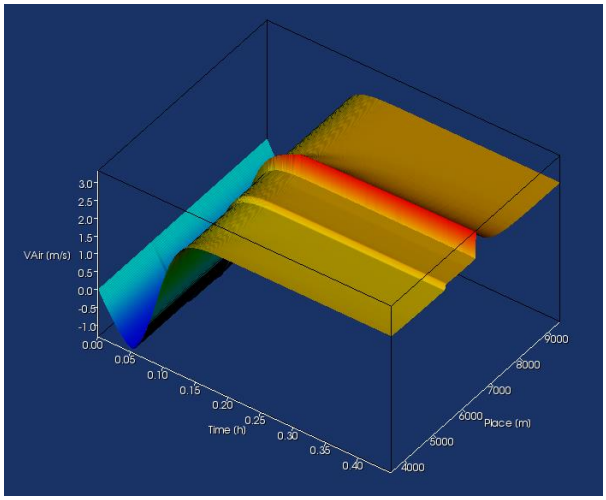

Figure 3.19. Velocity of the Air for 20 MW fire at chainage 6+450.

- Minimum value generated by wind effect during switching on of tunnel ventilation system is -1.34 m/s at 0.05 h. Following from 0.5 h to 1 h, a stationary scenario is reached, where there is negligible change in the air velocity.
- At the end of simulation, time step 1:00 h, the following values have been registered:
  - At exit portal, ch. 9+400, longitudinal velocity is +2.56 m/s;
  - Immediately upstream of train on fire, stopped at ch. 6+450, velocity is +2.55 m/s;
  - At chainage 6+450, where fire is positioned with an assumed length of 20 m, due to decreasing density, the velocity rises up to 3.30 m/s;
  - Upstream the ch. 5+400, where the LEP starts, due to the slight cross section increase, the velocity decrease to +2.4 m/s;
  - Close to the entry portal, at chainage 3+500, the velocity is +2.5 m/s because the air outdoor temperature is higher than the one inside the tunnel, where the wall is operating a cooling action.

b. Air Volume flow (m^3/s)

- Minimum value generated by wind effect during switching on of tunnel ventilation system is -81.6 m^3/s at 0.05 h.
- Then from 0.5 h to 1 h, a stationary scenario is reached, where there is negligible change in the air volume flow. At the end of simulation, time step 1:00 h, the following values have been registered:
  - At exit portal, ch. 9+400, air flow is +160 m^3/s.
  - Immediately upstream of train on fire, stopped at ch. 6+450, air flow is +156 m^3/s.
  - At chainage 6+450, where fire is positioned with an assumed length of 20 m, due to decreasing density, the air flow rises up to ≈+204 m^3/s.

- Upstream the ch. 5+400, where the LEP starts, due to the slight cross section increase and the almost constant temperature, the air flow is almost constant and equal to +157 m^3/s.

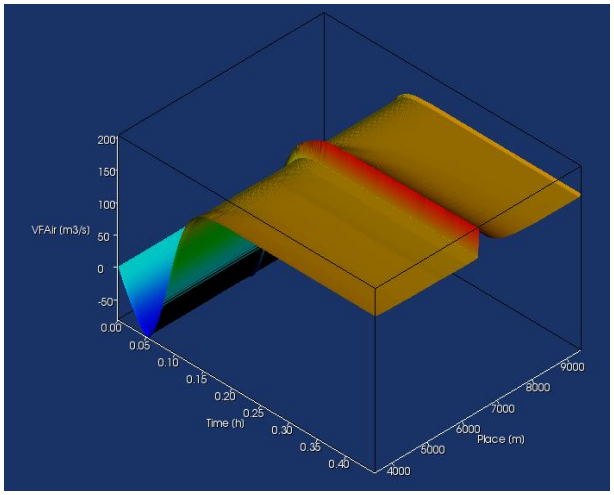

Figure 3.20. Air Volume flow for 20 MW fire at chainage 6+450.

- Close to the entry portal, at chainage 3+500, the air flow is +160 m^3/s because the air outdoor temperature is higher than the one inside the tunnel, where the wall is operating a cooling action.

c. Air Temperature (°C)

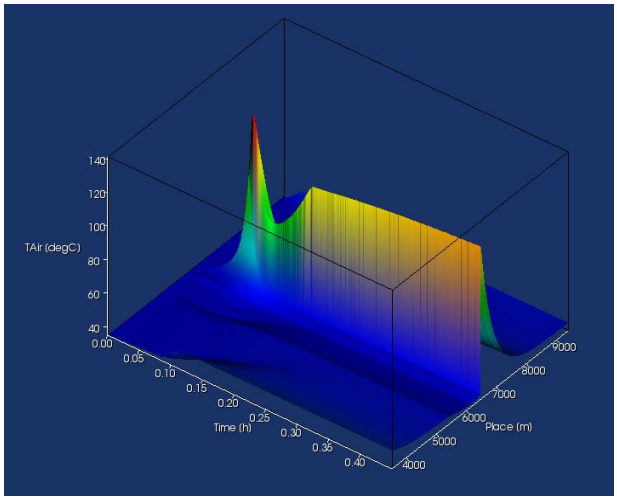

Figure 3.21. Air Temperature for 20 MW fire at chainage 6+450.

- Close to ch. 6+450, where the fire is positioned, starting from step 0.00 h, the temperature quickly starts to increase up to 141 °C (0.09 H), following the HRR fast curve: initially the amount of oxygen is ensured by the air flow generated by the wind effect (direction: from portal at 9+400 to portal at ch. 3+500). After the peak, the temperature starts to decrease up to 82 °C (0.12 h), because the ventilation system is

activated at time 0.03 h and, after 60 s, its action is prevalent on the wind effect: the air flow starts to decrease and the level of oxygen is not sufficient to sustain the combustion. Nevertheless, at time step 0.125 h, the temperature starts to increase again following the constant growth of the air flow (with reverse direction due to the thrust of jet fans, from ch. 3+500 to ch. 9+400), with a maximum temperature of 133 °C after 1:00 h of simulation. Following from 0.5 h to 1 h, a stationary scenario is reached, where there is negligible change in the value.

- At the end of simulation, the following data have been registered:
  - ✓ Temperature at entry portal, ch. 3+500: 45.6 °C - very close to the outdoor temperature.
  - ✓ Temperature upstream the fire, at ch. 6+400: 38.0 °C, due to the tunnel cooling effect.
  - ✓ Temperature at exit portal, at ch. 9+400: 39.5 °C, due to the heat exchanged with tunnel wall through radiative and convective transmission.

d. Extinction coefficient (1/m)

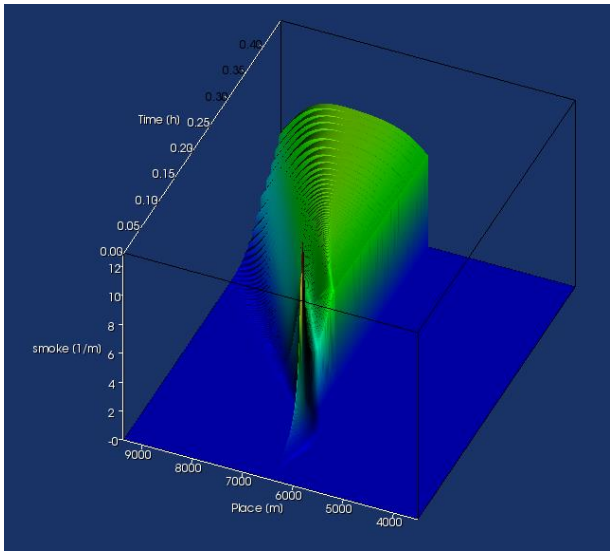

Figure 3.22. Extinction coefficient for 20 MW fire at chainage 6+450.

- In the time range between 0.00 h and 0.13 h there is a back-layering of smoke in the direction of evacuation path: this is the consequence of wind effect, not fully compensated by the ventilation system due to the delay in the activation (180 s) and the starting time constant (60 s) to reach the nominal thrust. The back-layering reaches the maximum value at 0.09 h, affecting the tunnel up to ch. 6+050.
- The peak value of extinction coefficient is 12.7 m^{-1}, at ch. 6+500, at time 0.10 h, with a moderate timing difference with the time step where the peak temperature generated by the train on fire is reached (0.09 h).
- After time step 0.13 h, and up to the end of simulation (1:00 h), the extinction coefficient is always less than 0.3 m^{-1} in the direction of the evacuation path, ensuring a safe evacuation (From 0.5 h a stationary scenario is reached, where there is

negligible change in the extinction coefficient). At the end of simulation (1:00 h), no back-layering is registered above the ch. 6+450, in contrast with the methodology proposed in the NFPA 502-2020 edition: this data will be checked with the CFD analysis in the next chapter, to evaluate the 3D effects of tunnel cross section on the back-layering. The maximum value at the end of simulation, close to portal at chainage 9+400, is about 8 m^{-1}, making impossible any chance of evacuation by passengers or access by the fire brigades.

3.4.4. Scenario 4: Train on fire stopped in tunnel at chainage 6+450 with HRR of 250 MW.

The Scenario n° 4 is compliant with the following input:

a) Heat release rate equal to 250 MW, growing according "super-fast curve", as per NFPA 92;
b) Direction of wind effect from exit portal at chainage 9+400 to entrance portal at chainage 3+500;
c) Egress travel direction from chainage 6+450 to chainage 6+150 (i.e. from right to left);
d) Jet fan and central ventilation station activation time: 180 s after receiving the fire alarm in the Control Centre;
e) Time to reach to nominal air flow for jet fans and main axial fans: 60 s;
f) The following jet fans have been assumed out of service:
    - Couple n° 10: destroyed by fire;
    - Couple n° 11: destroyed by fire;
    - Couple n° 8: under maintenance;
    - Couple n° 18: under maintenance.
g) Main ventilation station at chainage 6+150: 2 fans have been activated with variable frequency driver at 50 Hz (100% of the nominal flow).

a. Velocity of Air (m/s)

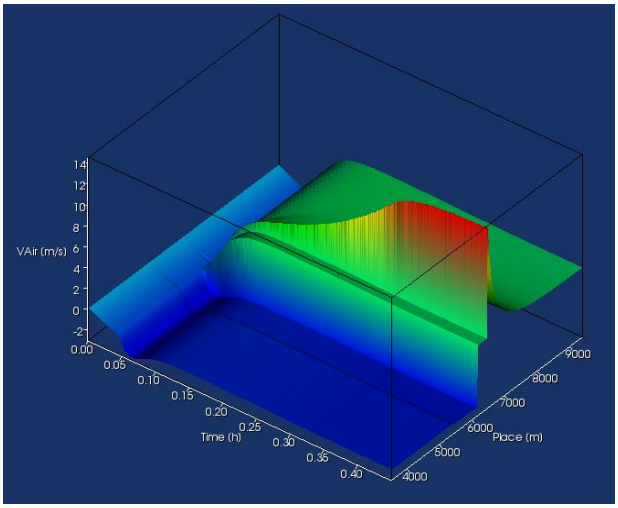

Figure 3.23. Velocity of the Air for 250 MW fire at chainage 6+450.

- Due to the initial wind effect, the longitudinal velocity is negative (i.e. the direction of the flow is from right to left) in all the tunnel from 0.00 h up to +0.056 h. The minimum value reached in the tunnel sector 2, from ch. 6+150 up to ch. 9+400, is -1,32 m/s at time 0.042 h.
- In the sector 1, from ch. 3+500 up to ch. 6+150, the minimum velocity is -2.85 m/s (time 0.064 h), generated by the simultaneous effect of wind pressure and mechanical ventilation of main axial fans at ch. 6+150.
- At the end of simulation, the direction of longitudinal flow in sector 1 is still negative (i.e. from right to left) but the final velocity at the entry portal has been reduced up to -2.15 m/s due to the braking action operated by the jet fans (direction of thrust from ch. 3+500 to ch. 6+150, i.e. from the left to right). Following from 0.5 h to 1 h, a stationary scenario is reached, where there is negligible change in the air velocity.
- Finally, at the end of simulation (time 1:00 h), the following main data has been recorded:
    - Entry portal, at ch. 3+500, velocity is -2.15 m/s;
    - Downstream of ch. 5+400, where the Longitudinal Evacuation Passage is interrupted, the cross section decreases and, as consequence, the velocity increases up to -2.26 m/s;
    - Downstream of ch. 6+150, due to the air flow supply by the central ventilation station, the longitudinal velocity increases up to +3.6 m/s;
    - Downstream of ch. 6+450, where the train on fire is stopped, due to the HRR of 250 MW and the high reduction of density, in compliance with continuity equation, the velocity increases up to +14.5 m/s;
    - At exit portal, ch. 9+400, due to the cooling effect of tunnel wall (radiative and convective heat exchanged), the increase of air density is balanced by a decrease of air velocity up to +3.5 m/s.

b. Air Volume flow (m³/s)

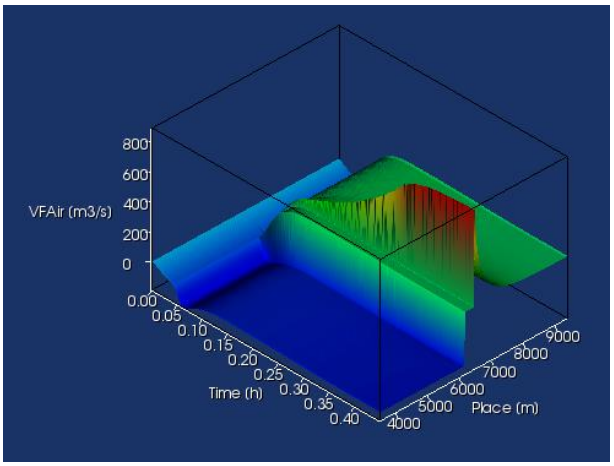

Figure 3.24. Air Volume flow for 250 MW fire at chainage 6+450.

The diagrams are consistent with velocity output and the following data have been recorded:

- Minimum air flow in tunnel sector 2: -75 m^3/s at 0,042 s;
- Minimum air flow in tunnel sector 1: -189 m^3/s at 0.065 s;
- Air Flow at entrance portal at ch. 3+500: -141 m^3/s at the end of simulation;
- Air Flow downstream ch. 6+150: +219 m^3/s at the end of simulation;
- Air Flow downstream ch. 6+450: +887 m^3/s at the end of simulation;
- Air Flow at exit portal at ch. 9+400: 219 m^3/s at the end of simulation.

c. Air Temperature (°C)

- The temperature does not increase significantly up to 0.06 h, even if the HRR should grow according the super-fast curve described in the NFPA 92: this phenomenon is explained because the air flow generated by the wind is not enough to provide the amount of oxygen necessary to develop the combustion. The maximum temperature registered in the preliminary phase is 186 °C.

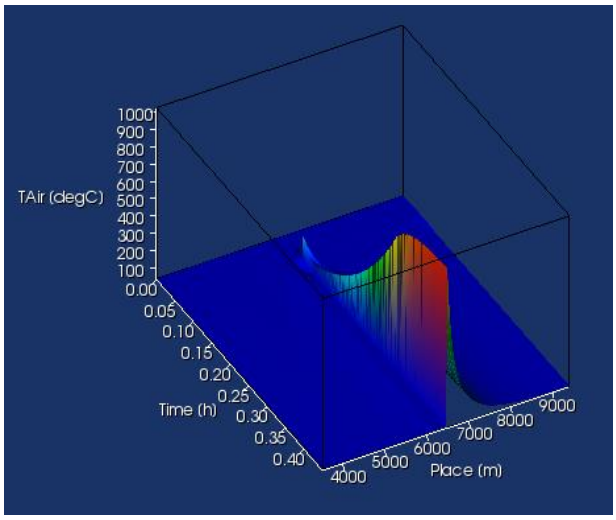

Figure 3.25. Air Temperature for 250MW fire at chainage 6+450.

- In the time period between 0.06 h and 0.09 h, the reduction of the air flow lowers the HRR due to the lack of oxygen and the air temperature starts to decrease up to 100.5 °C.
- With the ventilation thrust prevailing over the wind and stack effects, the air flow exceeds the value necessary to restart the growing of the HRR (the level of oxygen will be greater than the stoichiometric value) and the air temperature increases up to 1018 °C. Following from 0.5 h to 1 h, a stationary scenario is reached, where there is negligible change in the value.
- At the of simulation (1:00 h), the following values have been recorded:
    - Entry portal, ch. 3+500: 39.5 °C;
    - Ventilation shaft, ch. 6+150: 46 °C. The temperature increasing can be explained considering that, where the central ventilation station is blowing air into the tunnel, the outdoor air temperature is greater than tunnel air

temperature and, additionally, it is heated by axial fan motors. This peak is easily managed through the cooling process of tunnel wall.

- Train on fire stopped in tunnel, ch. 6+450 – ch. 6+460: 1018.5 °C;
- Exit portal, ch. 9+400: 42 °C.

d. Extinction coefficient (1/m)

- Up to 0.1 h, i.e. during the transient period when the ventilation system activation is in progress, combined with the growing of the HRR, the wind and stack effects, the extinction coefficient is above 0.3 m^{-1} between the ch. 6+350 and 6+570.

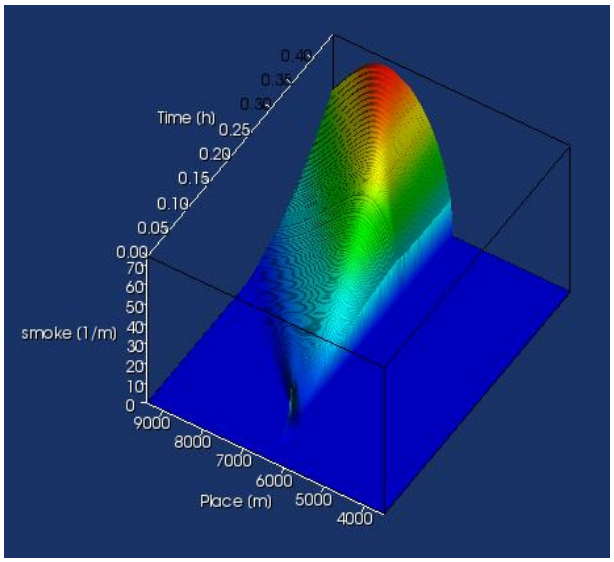

Figure 3.26. Extinction coefficient for 250MW fire at chainage 6+450.

- Starting from 0.1 h, downstream to the fire at ch. 6+450, the extinction coefficient is always less than 0.3 m^{-1}, ensuring a safe evacuation path to the passengers (From 0.5 h a stationary scenario is reached, where there is negligible change in the extinction coefficient).
- After time step 0.1 h, and up to the end of simulation (1:00 h), no back-layering is registered above the ch. 6+450, in contrast with the methodology proposed in the NFPA 502-2020 edition: this data will be checked with the CFD analysis in the next chapter, to evaluate the 3D effects of tunnel cross section on the back-layering
- The maximum value at the end of simulation, close to portal at chainage 9+400, is about 74 m^{-1}, making impossible any chance of evacuation by passengers or access by the fire brigades from the exit portal.

Chapter 4

Three-Dimensional Modelling

4.1. Introduction

Computational fluid dynamics is a powerful tool that is used to solve the equations of motion of the fluid in order to produce quantitative predictions of the fluid flow phenomenon. It is widely adopted across different branches of engineering and over the last few decades has gained considerable popularity in the field of fire-safety engineering due to its advantages over full-scale fire tests. The advantages of using CFD methods is that they are economical (as they don't need any prototypes or testing facilities); have lower lead times than other conventional methods; offer better visualization in areas that are hard to see; and allow testing of different configurations and various possible scenarios. CFD simulations provide considerable information of the fire behaviour. They provide a deeper insight of the flow field generated by the action of ventilation devices, the change in behaviour of the fluidic medium in the presence of an obstruction inside an enclosure and also predict the smoke spread phenomenon. However, the main disadvantage of the CFD method is that certain physical phenomenon cannot be modelled mathematically, therefore, adding uncertainty to the solution produced.

Basically, three-dimensional CFD simulations are calculated as functions of time and space using partial differential equations keeping in mind the conservation of mass, momentum, and energy. These equations are solved continuously leading to detailed predictions of velocity and temperature fields, species concentration, heat fluxes and so on. These calculations are performed by enforcing the laws of conservation on a high number of control volumes that are generated by the discretization of the computational domain. That is, it involves discretizing the spatial domain into fine number of elements (meshing) and carrying out the numerical solution, forward, in discrete time steps. The two dominant approaches used in CFD are the finite-difference formulation and the finite-volume formulation [6]. Basically, in the finite difference formulation the individual derivative terms in the equations of motion are written in terms of 'field-value differences' determined at or between the grid of mesh points and the resulting algebraic equations are solved numerically. Whereas, for the case of a finite-volume approach, the equations of motion are solved within small elements, usually cell centroids, that cover the spatial domain with similar conditions between elements leading to a system of algebraic equations and are solved numerically. Different approaches to discretization and time marching can be preferred depending on the flow conditions and the physics of the system.

However, severe limitation to the full numerical solution of governing equations is induced due to the impossibility of resolving the entire range of spatial and time scales that are involved in case of a turbulent flow like in the case of a ventilation system or a potential fire scenario in a tunnel. This issue can be resolved by modifying the governing equations in order to model the unresolvable turbulent transport phenomena. Therefore, two main approaches can be used, the first one is based on 'Time-Averaging' of the Navier-Stokes equations (RANS) whereas the second one uses 'Spatial-Averaging' using specific filter functions and is known generally as Large Eddy Simulation (LES). Apart from the uncertainty related to the turbulence modelling considerable difficulties are also introduced by the description of turbulent combustion chemistry; buoyancy; and radiation heat transfer. Also,

a great amount of uncertainty is introduced by the definition of boundary conditions; due to unknown meteorological conditions at the portals; fire dimensions; roughness of the walls; presence of any vehicles or obstructions; etc. In addition to this, further complexity is introduced by the numerical solution of the final set of partial differential equations where the quality of the CFD solution is influenced by the choice of numerical schemes and accuracy of the grid [6].

There are different CFD packages that are used in order to simulate a tunnel fire scenario, for example, Fire Dynamic Simulator (FDS) from NIST (US), Flow3D, STAR-CD, ANSYS CFX, *ANSYS Fluent*, etc... Here, in this project work, *ANSYS Fluent* is used for simulating the tunnel ventilation flow on the onset of a fire. *ANSYS Fluent*, has broad physical modelling capabilities that helps in modelling the fluid-flow phenomenon, turbulence phenomenon, heat transfer phenomenon and other reactions for various industrial applications. The preliminary monodimensional analysis is carried out using *IDA Tunnel* software and the results are discussed in Chapter 3. The analysis performed on the Monodimensional software is carried for the entire length of the Tunnel Section 1 (TK1) of the KFK tunnel. This is one big advantage that a monodimensional software has over the 3D CFD analysis, that is, it allows for a complete and compact description of the Tunnel Ventilation System with all suitable constants and variables. However, its intrinsic limit is that the flow in each cross-section is assumed to be homogeneous, thereby making these models inappropriate to simulate the fluid-flow behaviour in regions that are characterized by high temperature, pressure, or velocity gradients. These gradients are mostly encountered near the occurrence of a fire and around the presence of ventilation devices.

Four different cases of fire scenario are studied using the *IDA Tunnel* software. These simulations are carried out for one hour following the rate of fire growth idealized from the curves of the 'Fire Class' – 'Fast' for the 20MW fire and 'Ultra-Fast' for the 250MW fire. The results of the analyses reveal significant information about the thermal conditions inside the tunnel providing user with potential locations of varying temperature and pressure gradients, direction of air circulation and also establish an evacuation guideway for stranded passengers. In this chapter, the aforementioned four cases of the fire scenario are simulated using *ANSYS Fluent* in order to predict if a backlayering phenomenon occurs within the tunnel. In order to reduce the complexity of the model only the most critical sections of the tunnel have been modelled on *Fluent*. Also, auxiliary devices like jet fans, sensors, other MEP systems, etc., are neglected in order to reduce the complexity of the model.

Figure 4.1. KFK Tunnel TK1 Configuration.

4.2. Governing Equations

Fluid flow of both gases and liquids is transient or unsteady in nature. *ANSYS Fluent* models the fluid phenomena by solving the governing equations of conservation of mass, momentum, energy, and chemical species. These equations are shown below [6]:

Conservation of Mass:

$$\frac{\partial \rho}{\partial t} + \frac{\partial (\rho u_i)}{\partial x_i} = 0$$

Conservation of Momentum:

$$\frac{\partial (\rho u_i)}{\partial t} + \frac{\partial (\rho u_i u_j)}{\partial x_i} = -\frac{\partial \rho}{\partial x_i} + \frac{\partial (\rho \tau_{ij})}{\partial x_j} + \sum S_{u_i}$$

Conservation of Energy:

$$\frac{\partial (\rho h)}{\partial t} + \frac{\partial (\rho u_i h)}{\partial x_i} = \frac{\partial}{\partial x_i}\left(k \frac{\partial T}{\partial x_i}\right) - \frac{\partial}{\partial x_i} \sum_{j'} h_{j'} J_{j'} + \frac{\partial P}{\partial t} + u_i \frac{\partial P}{\partial x_i} + \tau_{ij} \frac{\partial (u_i)}{\partial x_j} + S_h$$

Conservation of Species:

$$\frac{\partial (\rho m_{i'})}{\partial t} + \frac{\partial (\rho u_i m_{i'})}{\partial x_i} = \frac{\partial \left(J_{i',i}\right)}{\partial x_i} + S_{i'}$$

Where ρ is the fluid density; u_i and x_i are the velocity and coordinate axis in the i^{th} direction; τ_{ij} is the stress tensor acting in the i^{th} face in the j^{th} direction; g is the gravitational acceleration and $\sum S_{u_i}$ a vector containing the momentum source terms per unit volume in the i^{th} direction; h and k are the static enthalpy and the thermal conductivity; P is the pressure; $J_{i',i}$ is the diffusive mass flux for species i' in the i^{th} direction, $m_{i'}$ is the mass fraction of the species i ', and $S_{i'}$ and S_h are the source terms for the mass production of species i' and enthalpy.

ANSYS Fluent is like an advanced spreadsheet where the operator feeds in the equations and the solver simply executes them. It is basically a CFD machine that knows only to solve the mathematical equations and does not understand if the equations translate properly into expected real-world problems. Navier-Stokes equations are the equations of motion of a fluid that describe the fluid flow assuming that the fluid behaves as a continuum rather than discrete particles. Each of these equations can be obtained for fluid particles of volume *dx·dy·dz. Fluent* basically uses a finite volume method wherein the entire domain is discretized into a finer grid of a number of cells, that could be either prisms, tetrahedral or polyhedral. These flow variables are usually stored in cell centroids and are assumed to be varying linearly. The CFD software solves for the values of velocity, temperature, chemical species concentration, and any other variable of interest at every grid point in the

computational domain. *Fluent* uses either SIMPLE or SIMPLEC algorithms to solve the equations. The tunnel ventilation flows and fires are typically characterized by turbulent regimes where flow variables fluctuate in a chaotic and random manner both in time and space. Therefore, these flow variables can be described by decomposing them into a steady value and a fluctuating value. This is called Reynolds decomposition and using this technique the characteristics of the flow variables can be pictured in terms of mean values along with their fluctuating components which are averaged. For example, if we calculate the velocity at a particular point in the turbulent fluid flow, the instantaneous velocity (U) would be like in Figure 4.2, with $U = \overline{U} + u'$ at any point of time.

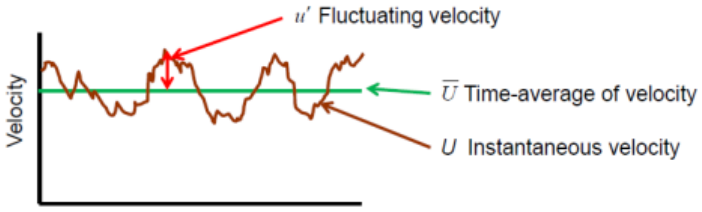

Figure 4.2. Mean and Fluctuating components [46].

Turbulence being a three-dimensional phenomenon is visualized by a series of vortices called eddies. These eddies affect the flow pattern and induce shear stresses in the fluid that are called as Reynolds stresses (functions of the velocity fluctuations). As a result, the heat, mass, and momentum transfers are highly enhanced and since most of the industrial applications are turbulent it is not necessary to resolve all these turbulent fluctuations. Thus, it is easier to analyse time-averaged quantities. After applying the concept of averaging in the governing equations Reynolds Averaged Navier Stokes (RANS) equations are obtained, with the assumption that the time averaged values of the fluctuating components are zero. With this the RANS equations become [6]:

$$\frac{\partial \rho}{\partial t} + \frac{\partial (\rho u_i)}{\partial x_i} = 0$$

$$\frac{\partial (\rho u_i)}{\partial t} + \frac{\partial (\rho u_i u_j)}{\partial x_i} = -\frac{\partial \rho}{\partial x_i} + \frac{\partial}{\partial x_j}\left[\mu\left(\frac{\partial u_i}{\partial x_j} + \frac{\partial u_j}{\partial x_i} - \frac{2}{3}\delta_{ij}\frac{\partial u_l}{\partial x_l}\right)\right] + \frac{\partial}{\partial x_j}\left(-\rho\overline{u_i' u_j'}\right)$$

As mentioned before the additional term $-\rho\overline{u_i' u_j'}$ called Reynolds stresses is introduced and has to be modelled in order to close the equations. A common closure method uses the Boussinesq hypothesis to model the Reynolds stresses which are related to the mean velocity gradients as shown in equation [6]:

$$-\rho\overline{u'_i u'_j} = \mu_t\left(\frac{\partial u_i}{\partial x_j} + \frac{\partial u_j}{\partial x_i}\right) - \frac{2}{3}\left(\rho k + \mu_t \frac{\partial u_k}{\partial x_k}\right)\delta_{ij}$$

Where, k is the turbulent kinetic energy per unit mass and μ_t is the turbulent viscosity (eddy viscosity). This hypothesis is used in various turbulence models like the k-ε and k-ω SST models. Thus, the averaging process introduces additional unknown terms into the transport equations, like Reynolds Stresses and Fluxes, that need to be solved by selecting suitable turbulence closures. In this project work the Realizable k-ε model with suitable wall function and k-ω SST model are tested for both the configurations of the fire scenarios. However, the analysis carried out in this project work utilizes the Academic version of the software, wherein the mesh limitation is applied with a maximum number of cells being 512,000. Therefore, a suitable mesh for different tunnel profiles is developed and results are compared. Turbulence modelling also introduces additional dependent variables. For the case of the k-ε model we have the kinetic energy of turbulence "k" and turbulence dissipation "ε" and the turbulence kinetic energy "k" and specific dissipation rate "ω" when k-ω SST is used. The transport equations for k and ε for the realizable k-ε model is [4]:

$$\frac{\partial(\rho k)}{\partial t} + \frac{\partial\left(\rho k u_j\right)}{\partial x_j} = \frac{\partial}{\partial x_j}\left[\left(\mu + \frac{\mu_t}{\sigma_k}\right)\frac{\partial k}{\partial x_j}\right] + G_k + G_b - \rho\varepsilon - Y_M + S_k$$

$$\frac{\partial(\rho \varepsilon)}{\partial t} + \frac{\partial\left(\rho \varepsilon u_j\right)}{\partial x_j} = \frac{\partial}{\partial x_j}\left[\left(\mu + \frac{\mu_t}{\sigma_\varepsilon}\right)\frac{\partial \varepsilon}{\partial x_j}\right] + \rho C_1 S\varepsilon - \rho C_2 \frac{\varepsilon^2}{k + \sqrt{\nu\varepsilon}} + C_{1\varepsilon}\frac{\varepsilon}{k}C_{3\varepsilon}G_b + S_\varepsilon$$

In the above equations G_k represents the generation of turbulence kinetic energy due to mean velocity gradients; G_b is the generation of turbulence kinetic energy due to buoyancy; Y_M represents the contribution of the fluctuating dilatation in compressible turbulence to the overall dissipation rate; C_2 and $C_{1\varepsilon}$ are constants; σ_k and σ_ε are the turbulent Prandtl numbers for k and ε; S_k and S_ε are the source terms. This model has been extensively validated for a wide range of flows for example channel, boundary layer flows and separated flows. The performance of this model has been found to be substantially better than the standard k-ε model. Similar to the other models the eddy viscosity, μ_t is formulated as [4]:

$$\mu_t = \rho C_\mu \frac{k^2}{\varepsilon}$$

The only difference being that C_μ is not constant and is calculated as []:

$$C_\mu = \frac{1}{A_0 + A_s \frac{kU^*}{\varepsilon}}$$

C_μ is a function of the mean strain and rotation rates, angular velocity of the system rotation and the turbulence fields. The model constants are $C_{1\varepsilon}$ = 1.44; C_2 = 1.9; σ_k = 1.0; σ_ε = 1.2. More detailed explanation on the constants and the empirical relationships can be found in the *ANSYS Fluent* guide section 4.4 [4].

The k-ω SST model is also run for the same scenarios of fire. This model is blend of the standard k-ε model in the far field region and the k-ω model in the near wall region. The

Shear-stress transport model is similar to the standard *k-ω* model but includes a blending function that helps is switching the models in the near-wall region and away from the surface. However, this model requires a suitable refinement of the grid near the walls of the tunnel with a high mesh density. This was not able to achieve using the academic versions of the software and proved to be a constraint in the application of the model. In the following sections of the results the simulations using the SST model are also shown where a stationary Backlayering phenomenon can be seen but the accuracy of the length of Backlayering is questionable due to mentioned mesh constraints.

4.3. Geometry and Mesh requirements

4.3.1. Geometrical Profile of the KFK Tunnel – Section TK1

For the KFK Tunnel Section TK1 which runs 5900m two critical sections have been considered: one with train on fire, stopped inside the tunnel at chainage 5+100 and the other one with train on fire stopped inside the tunnel at chainage 6+450. Rather than the entire section of tunnel, sub-sections spanning 200m and 100m covering the critical sections are profiled. The first section lies in the LEP section which consists of an egress pathway for evacuation purposes, whereas the second section does not have the egress pathway. The geometrical profiles have been modelled considering these changes in cross-sections. Also, the MEP and other components are neglected to simplify the geometry. The two geometrical profiles used are shown below:

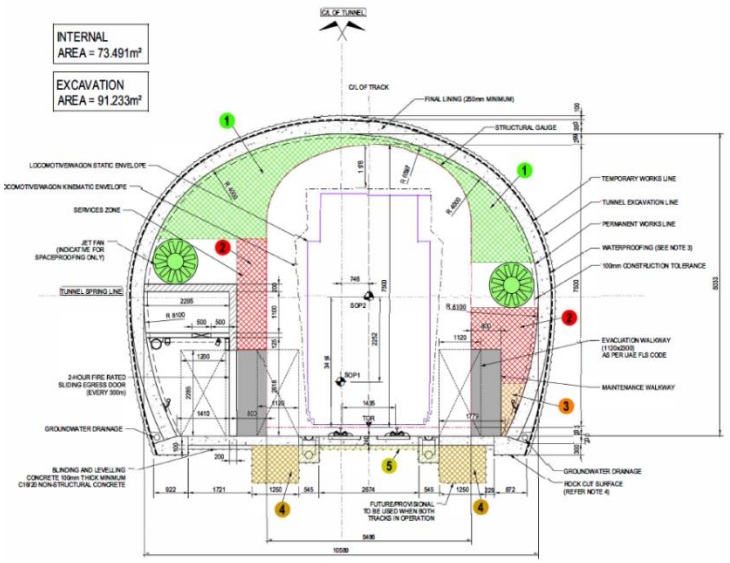

Figure 4.3. Cross-section (CS-1) with LEP until chainage 5+400.

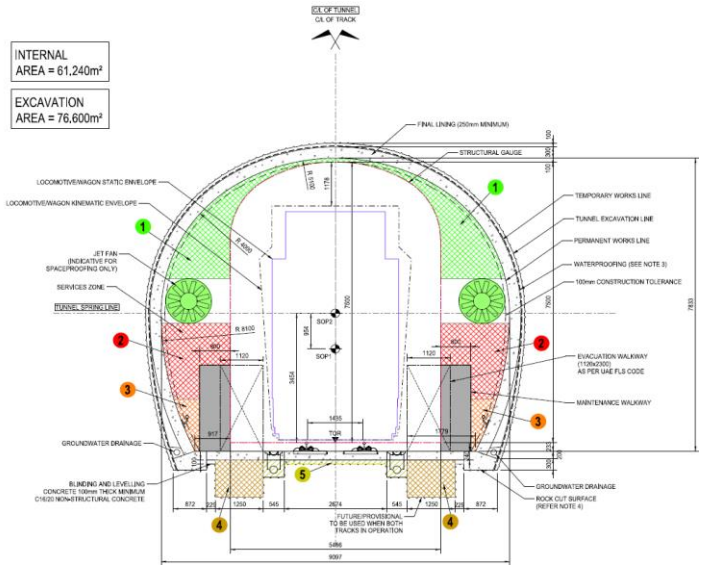

Figure 4.4. Cross-section (CS-2) without LEP from chainage 5+400.

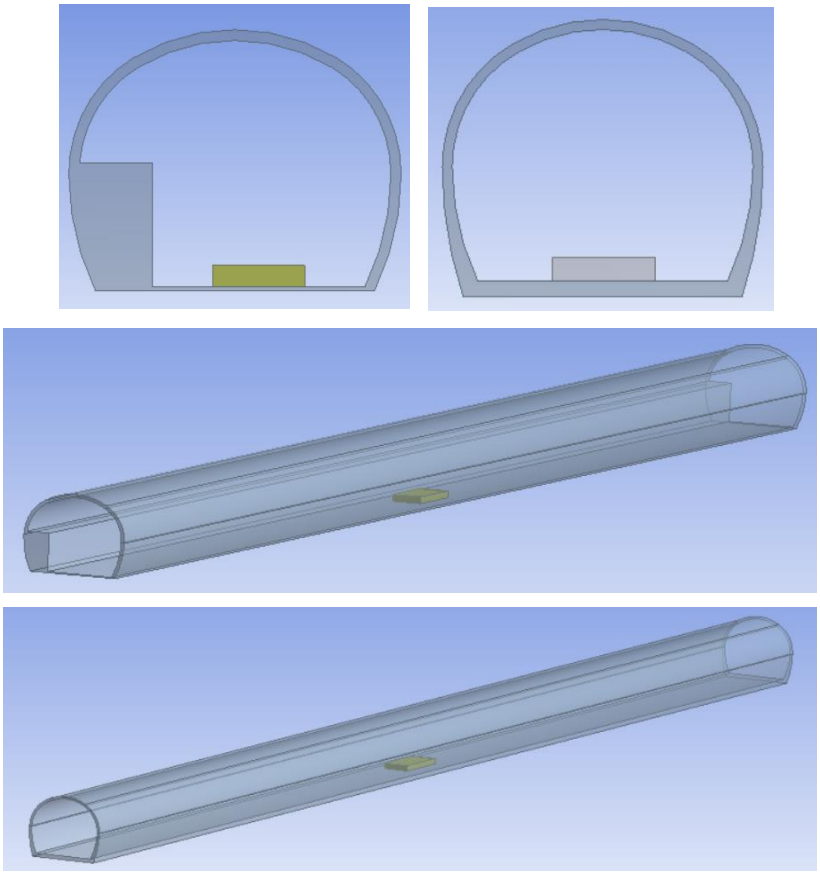

Figure 4.5. Tunnel profile at chainage 5+100 (With LEP) and 6+450 (No LEP) for HRR 20 MW.

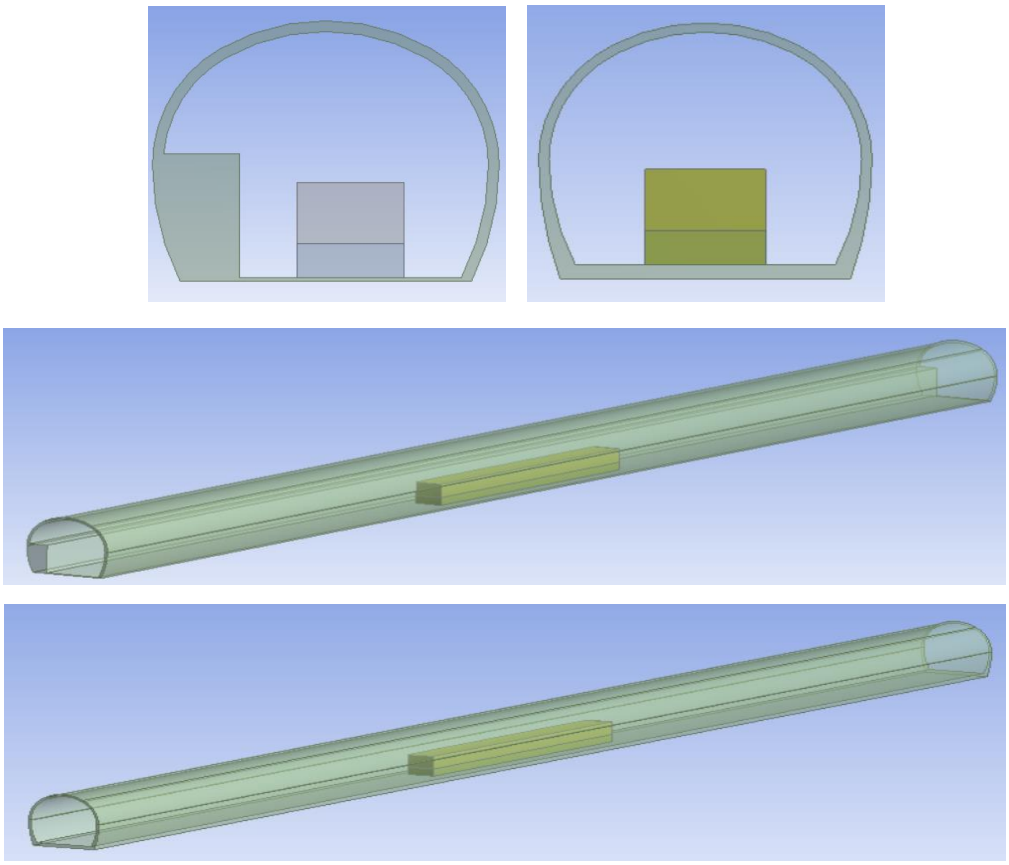

Figure 4.6. Tunnel profile at chainage 5+100 (With LEP) and 6+450 (No LEP) for HRR 250 MW.

The cuboids inside the tunnel are idealized as fire source with HRR of 20 and 250 MW. For the section with the Longitudinal Egress Passage the geometrical profile is altered in such a way that the passage area is subtracted/removed from the internal profile of the tunnel section. The next step is to generate the mesh of the domain.

4.3.2. Mesh

Discretization of the computational domain is the most critical activity in numerical modelling. The process comprises of dividing the analysed geometry into numerous small control volumes and is commonly called as "meshing". As mentioned earlier about *Fluent* using a Finite volume approach for solving the equations, the purpose of meshing is to solve these equations that located at the cell/nodal locations. Usually the information is stored in the cell centroids and the information varies linearly amongst the neighbouring cells. In the present analysis the simulation is carried out with a limitation in the number of mesh cells the maximum being 512,000. As a result, different elements were considered before applying the mesh Hexahedral, Tetrahedral and Polyhedral.

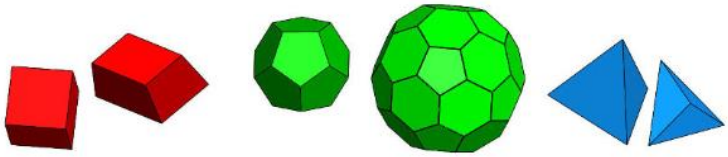

Figure 4.7. Hexahedral (red); Polyhedral (green) and Tetrahedral (blue) [40].

Generally, for most of the applications it is desirable to divide the domain into hexahedral (HEX) control volumes as the resulting mesh is characterized by low numerical diffusion particularly in case of flow perpendicular to the faces of control volumes. Unfortunately, it not always possible to construct a structured HEX mesh for complex geometries and also it can be time-consuming. Thus, tetrahedral (TET) mesh generation algorithms come into picture. TETs are the simplest volume elements built out of four faces. The unquestionable advantage of TET mesh is the ease of generation even in case of complicated geometry. But TETs cannot be stretched excessively and thus, a large number of elements has to be used in comparison to the HEX mesh in order to achieve a reasonable accuracy. Moreover, TETs have only four neighbours, therefore computing gradients can be problematic due to spatial position of the neighbour nodes. Also, low quality TETs result in convergence errors and significantly reduce the accuracy of the solution.

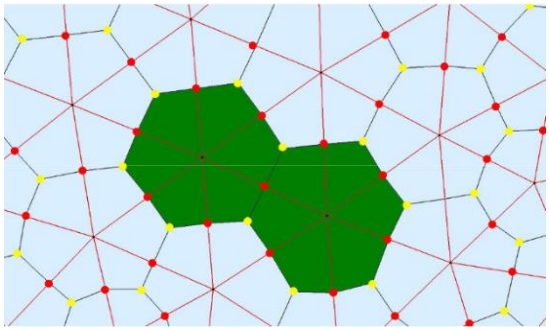

Figure 4.8. Generation of Polyhedral cell [40].

The polyhedral (POLY) mesh was introduced in STAR-CCM+ solver and ANSYS *Fluent* in order to combine the advantages of HEX (low numerical diffusion resulting in accurate solution) and TET mesh (rapid semi-automatic generation) as well as to overcome the disadvantages of both the mentioned type of control volumes. The biggest advantage is that every individual cell has many adjacent neighbours, as a result the gradients can be much better approximated in comparison to the TETs [40]. POLYs are also less sensitive to stretching than TETs which results in better numerical stability of the model. In some cases, they can even achieve better accuracy than HEXs due to larger number of neighbouring elements. They allow the exchange of mass over a larger number of faces thereby, reducing numerical diffusion effects caused by flows not perpendicular to any of the cell's faces. This proves to be and leads to a more accurate solution achieved with a lower cell count. POLY mesh generation in *ANSYS Fluent* consists in simple conversion of TET elements to POLYs by decomposition of cell into multiple sub-volumes. In order to do so, new edges are created on

each face between the face centroid (yellow dots in Figure 4.8) and the centroids of the edges of that face (red dots in Figure 4.8). Subsequently new faces are created within the cell by connecting the cell centroid to the new edges on each face. The newly created faces may be adjusted and merged with neighbouring faces during the agglomeration process in order to minimize the number of faces on the resultant polyhedral cell. For the tunnel profiles a mesh using polyhedral cells is idealized, but before this conversion an appropriate local mesh is obtained with the regular TETS. The flowchart below explains the process of meshing carried out on *Fluent*. The geometrical profile is first imported on the mesh module of ANSYS. Initially a rough mesh generation is applied which is created automatically when clicked on the 'Generate Mesh' icon. This mesh is very coarse and have roughly a few thousand cells with a minimum element size being 5m. By default, TETS are generated non-uniformly throughout the entire span of the domain.

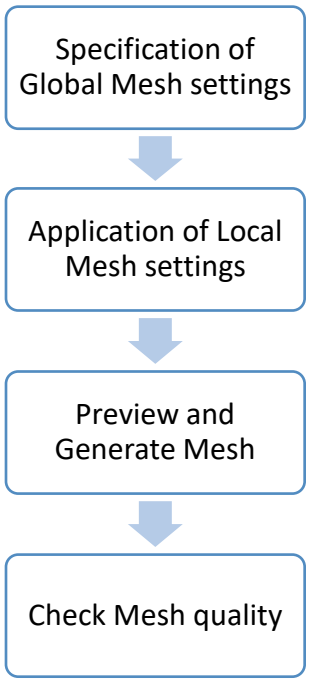

Figure 4.9. Meshing Process on *ANSYS Fluent*.

Keeping in mind the limitations, before applying the mesh controls, the mesh size calculator for determining the cell size on FDS is used and as a thumb rule a rough size of the cells to be discretized is obtained. The cell sizes are determined using the characteristic fire diameter and cell size ratio that accurately resolves the fire based on the total heat release rate. The FDS User Guide [47] used a D^*/dx ratio between 4 and 16 to accurately resolve fires in various scenarios. From the FDS User Guide: "These values were used to adequately resolve plume dynamics, along with other geometrical characteristics of the models as well. This range does not indicate what values to use for all models, only what values worked well for that particular set of models". The cell size (dx) can be related to the characteristic fire diameter (D^*), i.e., the smaller the characteristic fire diameter, the smaller the cell size should be in order to adequately resolve the fluid flow and fire dynamics.

The characteristic fire diameter (D^*) is [47]:

$$D^* = \left(\frac{\dot{Q}}{\rho_\infty c_p T_\infty \sqrt{g}}\right)^{\frac{2}{5}}$$

Where, Q is the heat release rate (kW); ρ_∞ is the density of the fluid medium (kg/m^3); c_p is the specific heat (k-J/kg K) at ambient temperature T_∞ (k) and g (m/sec^2) the gravitational constant. Therefore, using this calculator, the characteristic fire diameter for the 20 MW fire is 2.877. Upon varying the *D*/dx* ratio (4 for coarse mesh, 10 for moderate mesh and 16 for finer mesh), the minimum size of the cells were found to be 0.719m for the coarser one; 0.288m for the moderate one and 0.18m for the finer one. Similarly, for the 250 MW fire the characteristic fire diameter is 7.902 and the minimum size of the cells were found to be 1.975m for the coarser one; 0.79m for the moderate one and 0.494m for the finer one. Usually moderate size is chosen for the simulations carried out on FDS in order to reduce the computational burden. These calculations are performed merely to understand what possible cell size could be used for region with the fire source. However, a grid independency test is recommended for finding out the best mesh size for the entire domain.

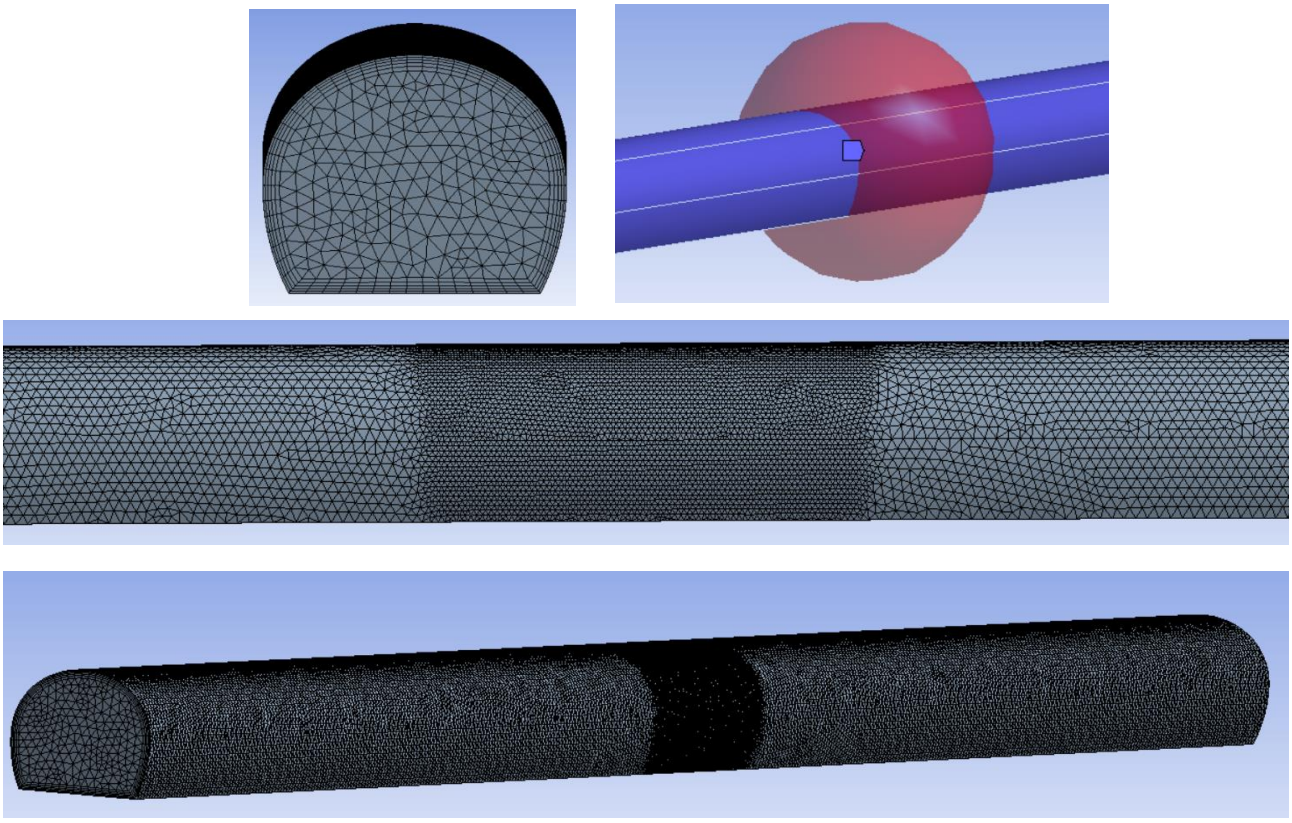

Figure 4.10. Mesh generated on *ANSYS Fluent*.

Keeping this information in mind the meshing strategy was applied step by step, refining the regions of interest (fire zone). The element size (0.5m) was set in the global mesh settings. In the local mesh settings, the area around the fire was further refined using the operations 'Body sizing' (0.25m), where the mesh is refined by constructing a 'Sphere of Influence', and 'Face size' for the faces of the cuboidal body which emits the hot combustion products. Around the walls 'Inflation' layers was also applied to discretize the domain around the walls, sufficiently enough, with the available computational power. Figure 4.10. shows the mesh profile generated on *ANSYS Fluent*. By default, the elements generated are Tetrahedral. The last step of checking the quality of mesh is performed and two parameters the Orthogonal quality and Skewness is monitored for the different meshes that were generated. Typically, low Orthogonal Quality or high skewness values are not recommended. The main sources of errors are meshes being too coarse, high skewness and large jumps between adjacent cells. The figure below shows the acceptable spectrum of the mesh quality.

Skewness mesh metrics spectrum

Excellent	Very good	Good	Acceptable	Bad	Unacceptable
0-0.25	0.25-0.50	0.50-0.80	0.80-0.94	0.95-0.97	0.98-1.00

Orthogonal Quality mesh metrics spectrum

Unacceptable	Bad	Acceptable	Good	Very good	Excellent
0-0.001	0.001-0.14	0.15-0.20	0.20-0.69	0.70-0.95	0.95-1.00

Figure 4.11. Mesh Quality Spectrum [41].

For the case of the tunnel geometries the skewness and orthogonal quality was continuously monitored, and sufficient mesh quality was obtained. For example, for the case of the tunnel section without LEP the skewness was found to be: *Minimum - 2.5594e-004; Maximum - 0.87832 and Average - 0.1949* and the orthogonal quality: *Minimum - 0.12168; Maximum - 0.99453 and Average - 0.8037.* On this module of ANSYS the sections are also labelled, like the inlet-outlet section, fire inlet-outlet section, tunnel walls, etc. The next step is applying the solver controls.

4.4. Boundary Conditions

This section explores all the boundary conditions that have been applied for the different fire scenarios in the set-up module on *Fluent*. Previously, the mesh was generated with the elements being TETS and the first step is to convert the elements into polyhedral elements with advantages as mentioned earlier. The conversion resulted in 349769 polyhedral cells.

The following figure shows the generated polyhedral mesh on *Fluent*:

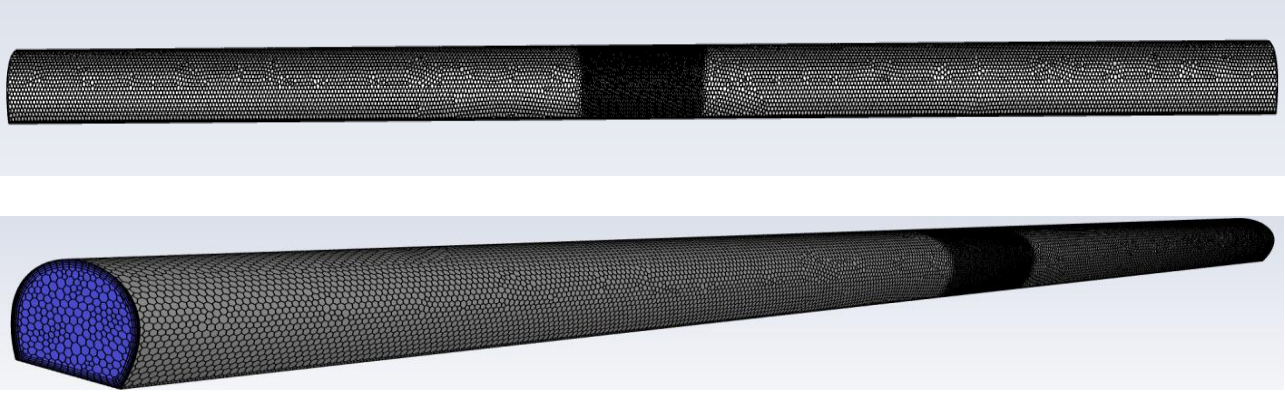

Figure 4.12. Polyhedral Mesh on *Fluent*.

4.4.1. Solver set up

The pressure-based solver is selected, and the gravitational body forces are included in the momentum equations, thereby defining buoyancy terms function of the temperature variations according to the Boussinesq approach. The 'Energy model' is turned on, the turbulence model was selected, and the species transport was also checked which is used to simulate the HRR from the fire source. Realizable *k-ε* model was selected with the standard wall function. Usually, for turbulent flows, the first cell from the wall is preferred to lie within the viscous sub-layer. Though this is possible for certain scenarios, it cannot be fulfilled for complex flows as would require a very fine mesh resolution near the wall also increasing the computational burden. As a result, a wall function is selected that allows the use of a "relatively" larger mesh near the vicinity of the wall. The different regions of the turbulent boundary layers based on y^+ are the laminar sub-layer ($y^+ < 5$), the transition layer ($5 < y^+ < 30$) and the turbulent or log-layer ($y^+ > 30$) region respectively. It is important that the first cell adjacent to the wall not lie in the buffer zone. A standard wall function is selected as they provide accurate predictions for wall-bounded flows with a y^+ value between 30 and 300 [4].

The pressure-velocity linkage has been adopted by the 'SIMPLE' scheme proposed by Patankar and Spading (1972). As for the discretization schemes the following options are chosen:

- *Second order* for pressure,
- *SIMPLE* for velocity-pressure coupling,
- *2nd order upwind* for momentum, turbulence, and species,
- *2nd* order upwind for energy,
- *2nd order implicit* for time dependent terms.

The default under relaxation factors are considered. The convergence of the solution is judged monitoring residual quantities and also monitoring quantities like the mass flow rates and other values like temperature, velocity at the portals. The simulations are said to be converged when the residuals are lower than 10^{-3} for the continuity, turbulence, species, and velocity terms and 10^{-6} for the energy equation. This is basically the solver control setup.

For setting up the boundary conditions at the portals of the tunnel the following conditions are imposed:

- Tunnel Inlet – *Velocity Inlet* boundary conditions are used where the inlet velocity is specified with the values obtained from *IDA Tunnel* simulation at the end of 1 hour. The temperature and the concentration of species are also entered. This is applied for all the cases of the fire scenarios.

- Tunnel Outlet – *Pressure outlet* boundary conditions are used and the option for preventing reverse flow is checked.

- No slip wall condition is applied for the tunnel walls and roughness of 0.002 was considered.

The values for the velocities and temperatures at the portals are carefully entered from the results obtained using *IDA Tunnel* software at the end of 1hour. A simulation of 2 minutes from this interval is performed on *ANSYS Fluent*.

4.4.2. Fire Representation

Modelling fire on *ANSYS Fluent* is quite challenging and in this project work the fire is modelled as a volumetric source of energy, i.e. as a heat sink which emits hot combustion products from the top surface, rather than using a combustion model as it avoids the complexity of determining and balancing the right species required to emulate the fire. The HRR from the fire source is visualized as being released from the top surface of a slab. And the mass conservation principle where the injected stream is balanced by air that is removed across the walls of the slab. The dimensions of the slab are calculated by relating heat release rate with the heat of combustion per square meters. For example, the calculation of the slab dimensions and the concentration of the species based on conservation mass for the case of a 20 MW fire with No LEP section is shown in Figure 4.13.c. The value of energy developed per kg consumption of oxygen is taken based on Thornton's rule (1917) [48] whereas the carbon monoxide concentration is taken from the analysis of Ying Zhen Li et.al. that is based on Influence of fire suppression on combustion products in tunnel fires. Therefore, species that are being released through the top of the slab surface are carbon monoxide, carbon di-oxide, nitrogen (residual air) and soot. In this project work the soot is represented in the form air considering the complexity of modelling of the soot particles. The temperature of the combustion products at the periphery of the slab for the 20 MW fire is 2271.34 K, which is roughly the adiabatic temperature of methane. 7.7 kg/sec of combustion products are being released from the top surface and is balanced by the air insertion through the sidewalls of 6.6 kg/sec.

The surface area needed to obtain an HRR of 20 MW is calculated and as a result a combustion surface of atleast 25 m^2 is required, whereas for the 250 MW, a minimum of 312.5 m^2 combustible surface area is needed. Modelling the 20 MW surface is simple but for the 250 MW considering the huge area needed for visualizing the fire, two slabs were used

wherein the top one is used for releasing the hot stream and the bottom one for entrainment of air.

a.

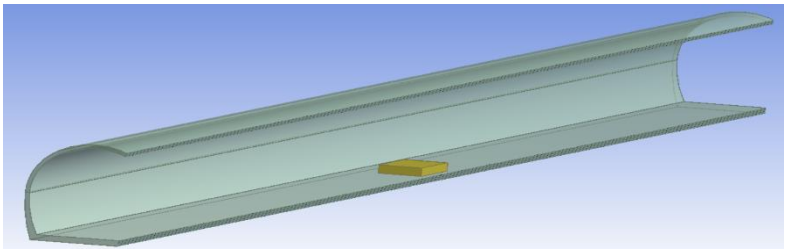

b.

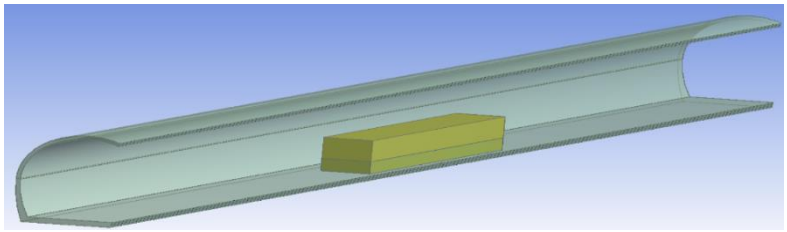

c.

Heat of combustion	H	25.4	MJ/kg
Heat Release Rate	Q	20	MW
Soot Yield	Y_s	0.13	kg_s/kg_f
Combustion efficiency	K_{ic}	70.00%	-
Energy developed per consumed kg of O_2	E_{O2}	13.1	MJ/kg_{O2}
Mass of O_2 per kg of air	M_{O2}	23.14%	kg_{O2}/kg_{AIR}
CO Yield	Y_s	0.031	kg_{CO}/kg_f
Supply Temperature (from IDA Tunnel Simulation)	T_{air}	37.699	°C
Heat of combustion for sqm	H_{sqm}	800	kW/m^2

Fuel mass loss rate	q_c	1.12	kg/s
Soot mass production rate	$\dot{m}_s$	0.15	kg/s
Combustion air mass loss rate	$\dot{m}_{air}$	6.6	kg/s
Total combustion mass rate	$\dot{m}_{combustion}$	7.7	kg/s
CO mass production rate	$\dot{m}_{CO}$	0.03	kg/s
Combustion mixture Temperature (K)	T_g	2271.43	K
Combustion Surface	Ac	25.00	m^2
Side surfaces for combustion air	A_A	7.92	m2
CO_2 mass production rate	$\dot{m}_{air}$	2.4	kg/s
Residual air rate (N_2, i.e.)	$\dot{m}_{N2}$	5.2	kg/s
Specific heat mixture	C_p	1.321	kJ/kgK

Figure 4.13. Cuboids representing fire sources (a.) 20 MW and (b.) 250MW (Top); Sample Calculation for the Surface area needed (Below (c.)).

This approach of representing fire is made sure is valid using the dependency of fire Froude number Q^* that links the HRR with the size of the source. If the surface is very small, then it would bring unrealistic air behaviour due to an excessively high velocity for the hot gases and lead to a wrong balance of momentum and buoyancy of the fire source. It would simple

become a high-momentum jet fire which is wrong. The non-dimensional heat release rate or Froude number, Q^* is given as [49]:

$$Q^* = \frac{Q}{\rho_a c_p T_a D^2 \sqrt{gD}}$$

Where, Q is the heat release of the fire and D is the Characteristic fuel dimension of the fire source, here it is the hydraulic diameter of the top slab surface. Typically, values of Q^* over 2.5 are considered unrealistic for a diffusion flame. Therefore, the dimensions of the slabs are calculated using a value of 1. The species transport module on *ANSYS Fluent* is set up in such a way that the mixture template with all the species are selected. A mass flow inlet/outlet boundary condition is imposed of the faces of the slab. The concentrations of the species in the form of mass fractions is entered along with the temperature of the species. With this the entire set-up of the model is complete and the final step is to initialize the simulation. All the simulations are run for 2 minutes with the available computation power. A time step of 0.1 second (thumb rule wherein the time step is a function of the smallest mesh size, the freestream velocity, and the courant number (unity for explicit formulations; however for an implicit formulation this dependency is not valid as the courant number is pretty high). The total number of timesteps is 1200 and the number of iterations per timestep is taken as 50. All the scenarios are run using the strategy as shown in Figure 4.14.

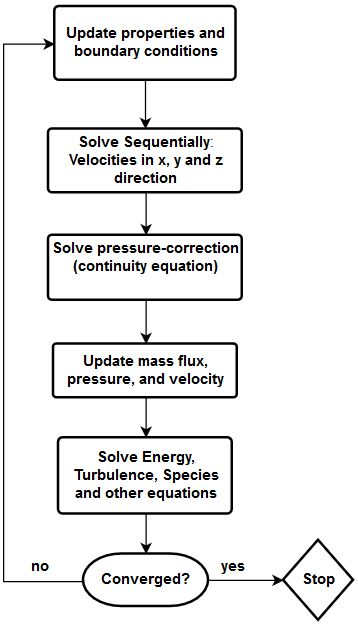

Figure 4.14. Strategy used on *ANSYS Fluent* [4].

The results of the simulation are discussed in the following section for all the cases – 20 MW and 250 MW with and without LEP.

4.5. Results – 3D Simulations

4.5.1. Scenario 1: Train on fire stopped in the tunnel at ch. 5+100 with HRR of 20 MW

For this scenario, the train on fire stopped inside the tunnel at the chainage 5+100 is represented by a slab emitting hot combustion products equivalent to the heat release rate of 20 MW. The ventilation system initially acts into the tunnel from the left to right direction due to the effect of wind and stack. This is overcome by a ventilation thrust which pushes the stream of hot gases and eventually also the hot plume outside the entry portal. The simulations performed on *Fluent* uses the reference values for the portals of the tunnel (at chainages 5+000 and 5+200) taken from the results of the mono-dimensional analysis at the end of the one-hour simulation. The inlet velocity imposed in the 'Velocity-Inlet' boundary condition is -2.5528 m/sec with the temperature at this section (chainage 5+200) taken as 37.699 °C. The simulation is carried out for two minutes.

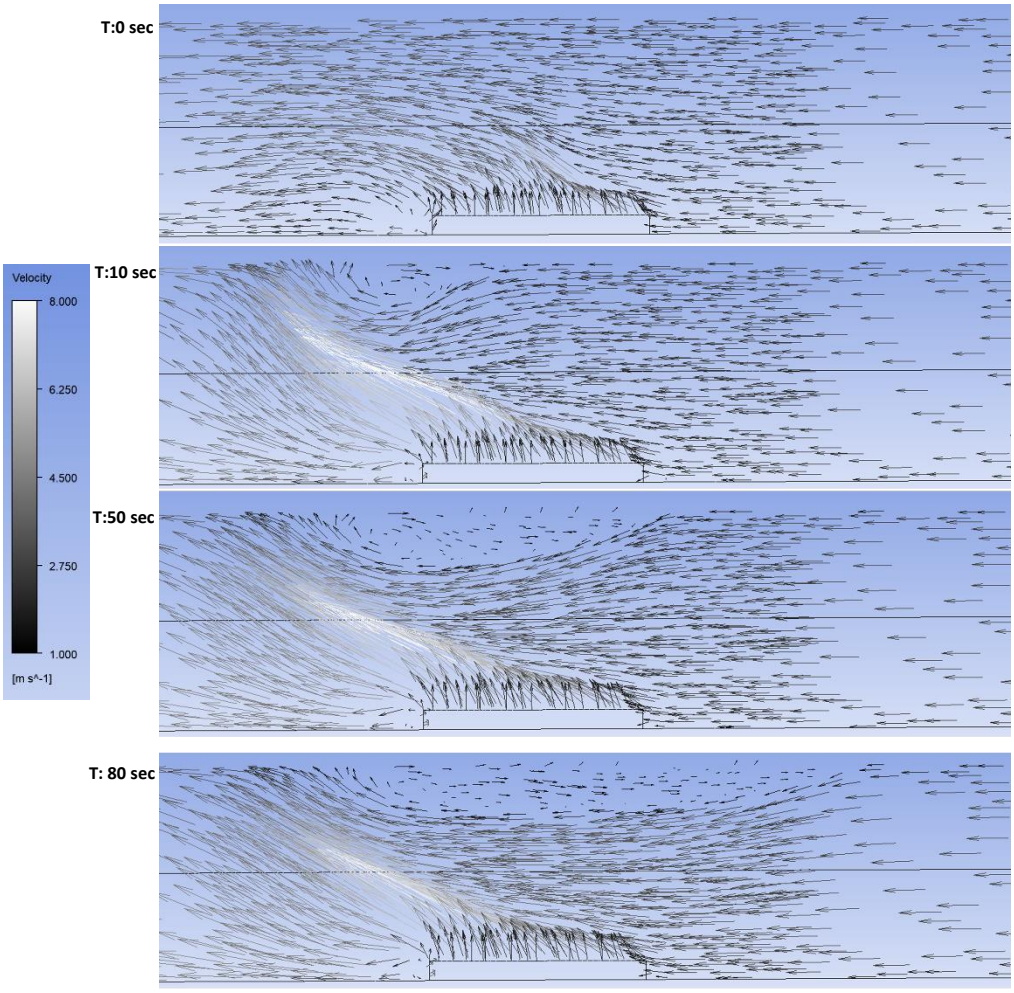

Figure 4.15. Velocity Contours at specific instants of the simulation showing the reverse flow of the hot gases -Backlayering.

Figure 4.15. clearly shows the behavior of the smoke movement which confirms the presence of a Backlayering phenomenon. The calculations based on the NFPA 502-2017 showed the

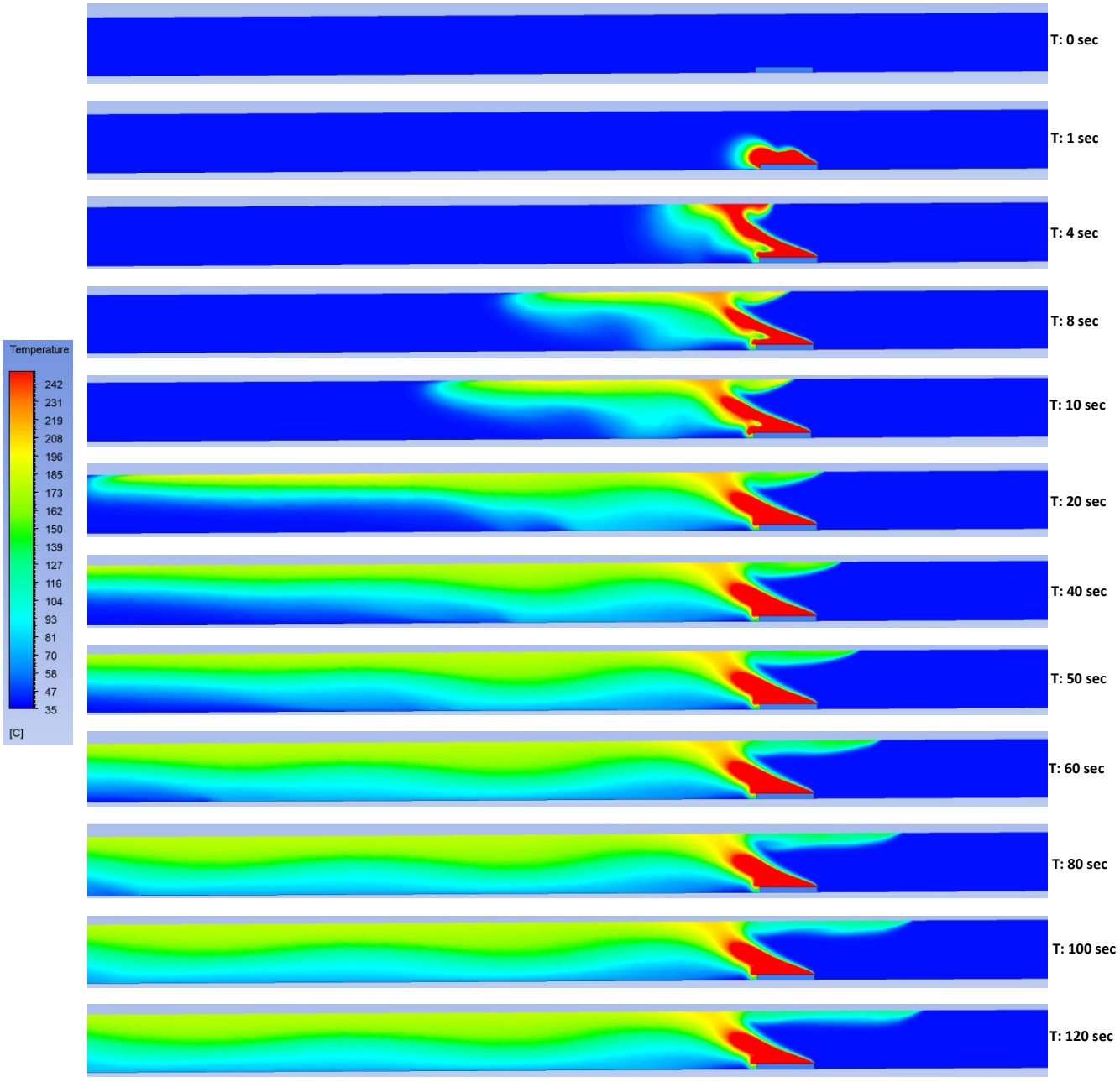

Figure 4.16. Temperature Contours for 20 MW fire at chainage 5+100.

fact that a ventilation velocity of about 2.54 m/sec would be ideal enough to eradicate this behavior, however, the calculations on the NFPA 502 -2020 standard show that a backlayering is evident with a length of approximately 43 meters. Figure 4.16 also confirms the fact of occurring of this phenomenon. The temperature contours show the variation of the temperature inside the tunnel. These contours have been obtained for the temperature

range of 35-250 °C to clearly show the reverse flow. The contours show that on the onset of fire the surrounding medium, air, and smoke, gets heated up and reaches the ceiling of the tunnel. Due to the thrust of the ventilation medium, backlayering is initially stationary downstream from the fire location. But after a few seconds it overcomes the thrust and slowly starts moving upstream. The average temperature of the section at the entry portal, chainage 5+000, is 116.182 °C. Around the vicinity of the fire source the average temperatures range around 130 °C. The average velocity of the stream at the portal is 3.2701 m/sec. The net mass flow rate is also checked at the portals and is 1.12 kg/sec. On the other hand, Figure 4.17 shows the fluid flow when the inlet velocity is equal to the one calculated from NFPA 502-2020. There is no backlayering!

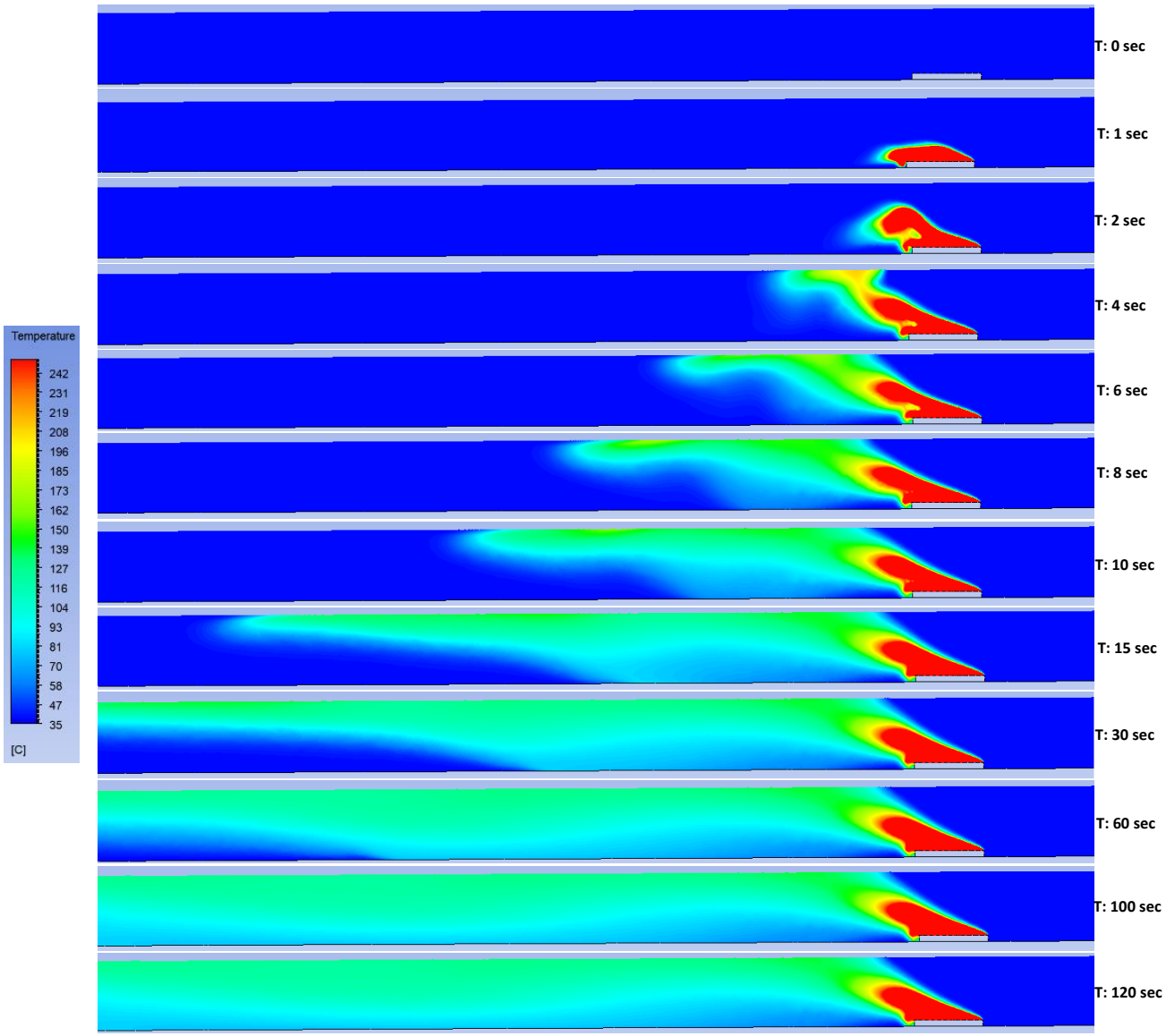

Figure 4.17. Temperature Contours for 20 MW with Critical Velocity equal to 3.39 m/sec (from NFPA 502-2020) – NO BACKLAYERING.

4.5.2. Scenario 2: Train on fire stopped in the tunnel at ch. 5+100 with HRR of 250 MW

For this scenario, the train on fire stopped inside the tunnel at the chainage 5+100 is represented by the top slab emitting hot combustion products equivalent to the heat release rate of 250 MW. Similarly, the ventilation system initially acts into the tunnel from left to right direction because of wind and stack. This is then overcome by the ventilation thrust provided by the jet fans and the central ventilation station which pushes the stream of hot gases outside through the entry portal. The simulations performed on *Fluent* uses the reference values for portals of the tunnel (at chainages 5+000 and 5+200) taken from the results of mono-dimensional analysis at the end of the one-hour simulation. The inlet velocity (at chainage 5+200) imposed in the 'velocity-Inlet' boundary condition is -3.4295 m/sec with the temperature at this section being 39.612 °C. The simulation is carried out again for two minutes.

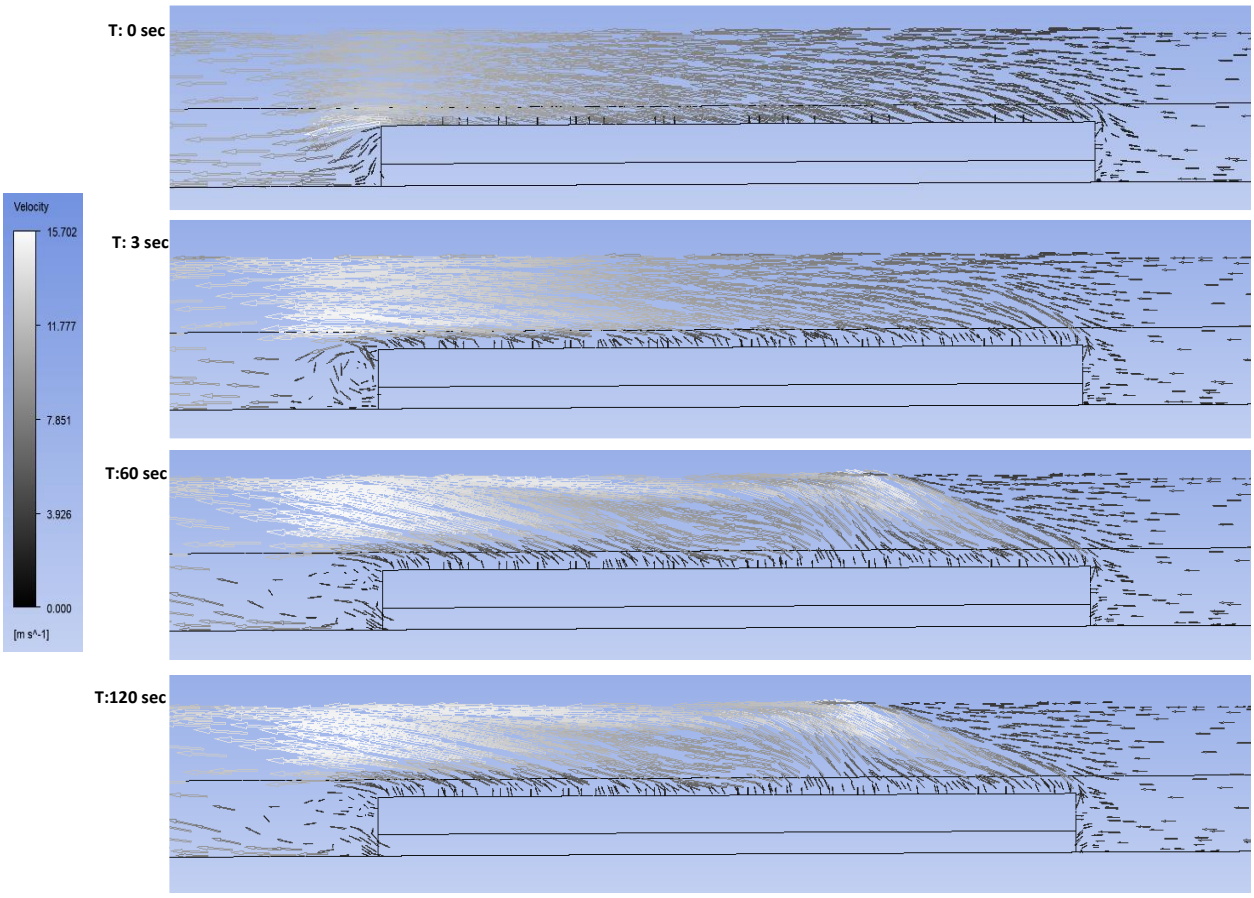

Figure 4.18. Velocity Contours at specific instants of the simulation, No significant reverse flow.

Figure 4.18 shows the velocity contours of the flow inside the tunnel for an HRR of 250 MW. What is interesting, is the fact. that in order to replicate the fire size of 250 MW a surface area of 312.5 m^2 is needed. This is done by constructing a rectangular slab and dividing it

into two parts where the top slab is assigned the emission of combustion products and the bottom slab with injection of air so that the principle of conservation of mass is adhered to. There is no backlayering seen from the contours above. However, the NFPA 502-2020 calculation estimates a minimum backlayering length of 13 meters. The reason for not visualizing the backlayering is due to the presence of a sufficient blockage caused by the presence of slabs with a height of 3.2 meters (roughly around 40%).

Oka and Atkinson [51] studied the effects of blockage on the critical velocity and found a noticeable decrease in the critical velocity value when a solid blockage was placed in the tunnel. According to their experiment when a vehicle occupies 32% of the tunnel cross-section area there is 40–45% reduction of the critical velocity.

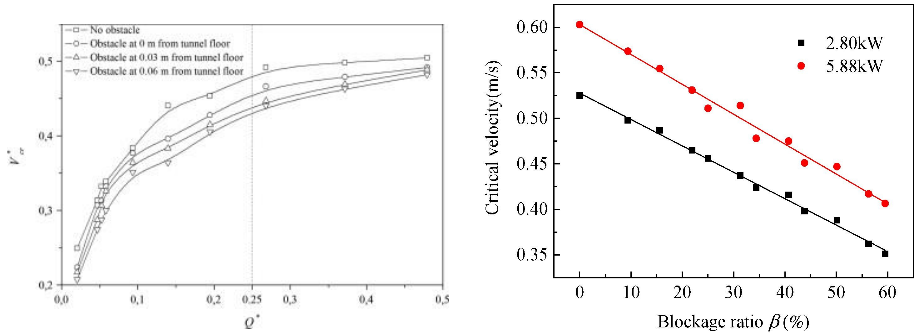

Figure 4.19. Effect of Blockage ratio on Critical Velocity from experiments [51].

This is due to the decrease of air entertainment to the fire size. The hot stream does not have the ability to fully develop like in the previous case. Also, the local velocities at the position of the slab is around 14 m/sec which is quite high and sufficient enough to push the hot stream of gas and smoke through the entry portal.

Figure 4.20 shows the distribution of the temperature inside the tunnel. During the simulation it took less 2 seconds for the plume to reach the ceiling. The average velocity measured along the different sections of the slab ranged from 8-14 m/sec. The average temperature at the entry portal, chainage 5+000, is 737 °C and the at the vicinity of the fire is 810 °C. The average velocity at the chainage is 10.1089 m/sec. The net mass flow rates are also checked to ensure the conservation principles are respected and they are found to be 14.001kg/sec.

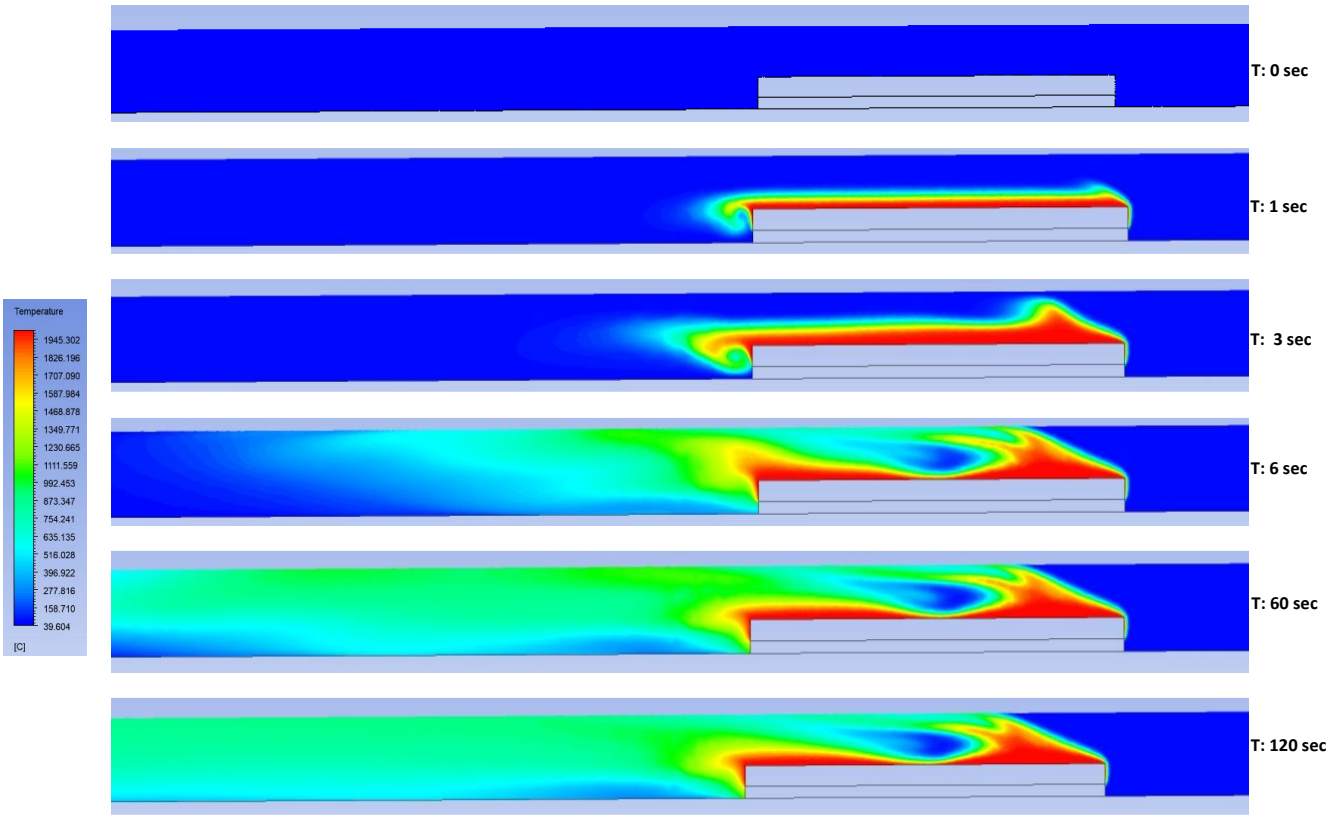

Figure 4.20. Temperature Contours for the 250 MW fire at chainage 5+100.

4.5.3. Scenario 3: Train on fire stopped in the tunnel at ch. 6+450 with HRR of 20 MW

For the case without LEP, the train on fire stopped inside the tunnel at the chainage 6+450 is represented by a slab emitting hot combustion products equivalent to the heat release rate of 20 MW. The ventilation initially is initially negative due to the effect of wind during the activation of the tunnel ventilation system and is overcome by the ventilation thrust with values of 2.56 m/sec therefore helping the flow to move from left to right direction eventually leading to disposal at the chainage 9+400. The simulations performed on *Fluent* uses the reference values for the portals of the tunnel (at chainages 6+350 and 6+550) taken from the results of the mono-dimensional analysis at the end of the one-hour simulation. The inlet velocity imposed in the 'velocity-Inlet' boundary condition is 2.5465 m/sec with the temperature at this section (chainage 6+350) taken as 37.49 °C. The simulation is carried out for two minutes.

The occurrence of the backlayering phenomenon can be pictured by the reverse flow that develops around the ceiling slightly upstream of the fire source, Figure 4.21. This stream slowly develops and moves in a direction opposite to that of the applied thrust.

The NFPA 502 2020 standard throws light on the fact that a length of roughly 42 m is built across the ceiling which the previous standard underestimates and deemed that a velocity of 2.55 m/sec sufficient enough for clearing the smoke content. The fire source representation is well close to the bottom of the tunnel allowing the flame to spread and eventually reach the ceiling where it then splits into two streams.

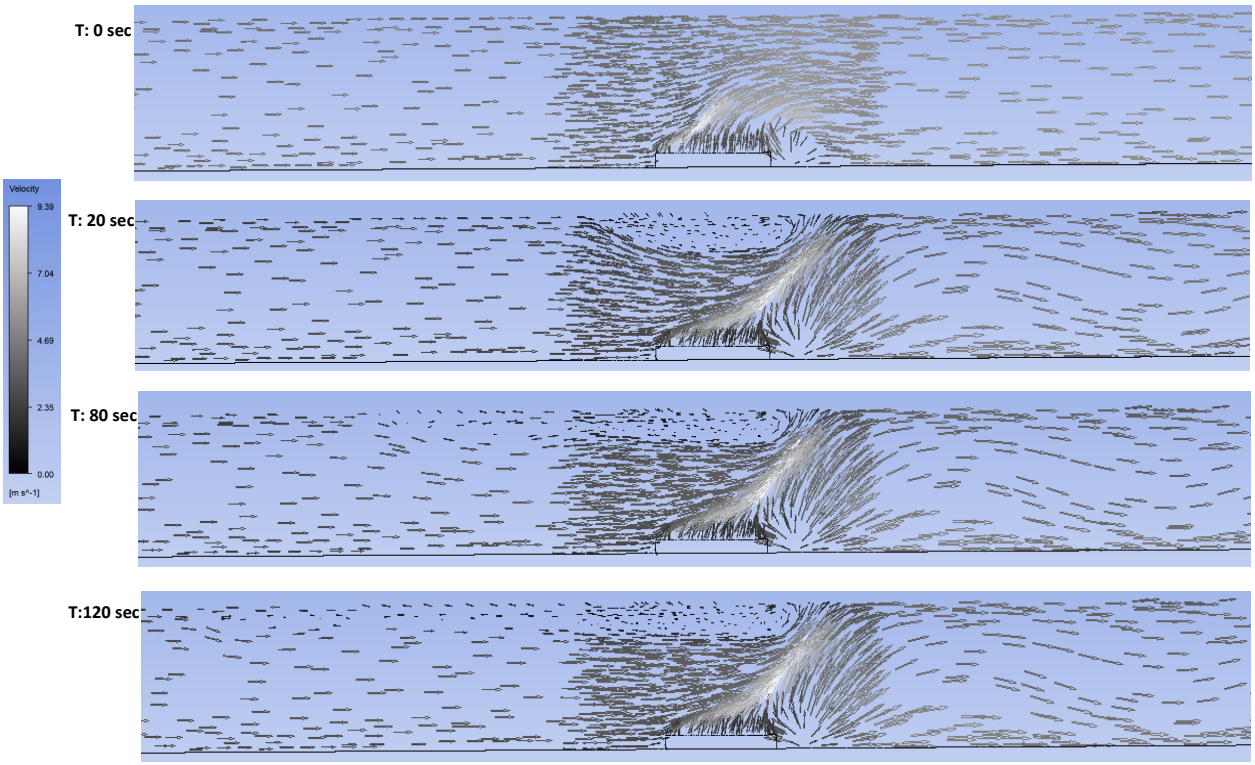

Figure 4.21. Velocity Contours at specific instants of the simulation showing the reverse flow of the hot gases -Backlayering.

The temperature contours, from the Figure 4.22, also gives a visual understanding of how the temperature variation spreads inside the tunnel. Initially, there is the presence of stationary backlayering, seen after the hot stream strikes the ceiling, wherein there is counteracting relationship between the stream and the ventilation thrust. After a few seconds, upstream from the fire, a thin layer of a high temperature stream flow breaks free independent of the thrust. The egress travel direction is from chainage 6+450 to 6+150, right to the left side of the tunnel as the environment downstream from the fire is not tenable for a safer exit. The average velocity at the outlet portal is 3 m/sec whereas around the vicinity of the fire source the average velocity is 3.28 m/sec.

The average temperature at the tunnel portal, chainage 6+450, is 119.72 °C. The temperature around the vicinity of the fire is around 140 °C. The principle of conservation of mass is also ensured by measuring the net mass flow rates at the inlet and outlet sections, 1.11 m/sec. These contours were obtained by the application of the *k-epsilon* model with the standard wall function that allows us to use a coarser mesh and predict the behavior near the walls.

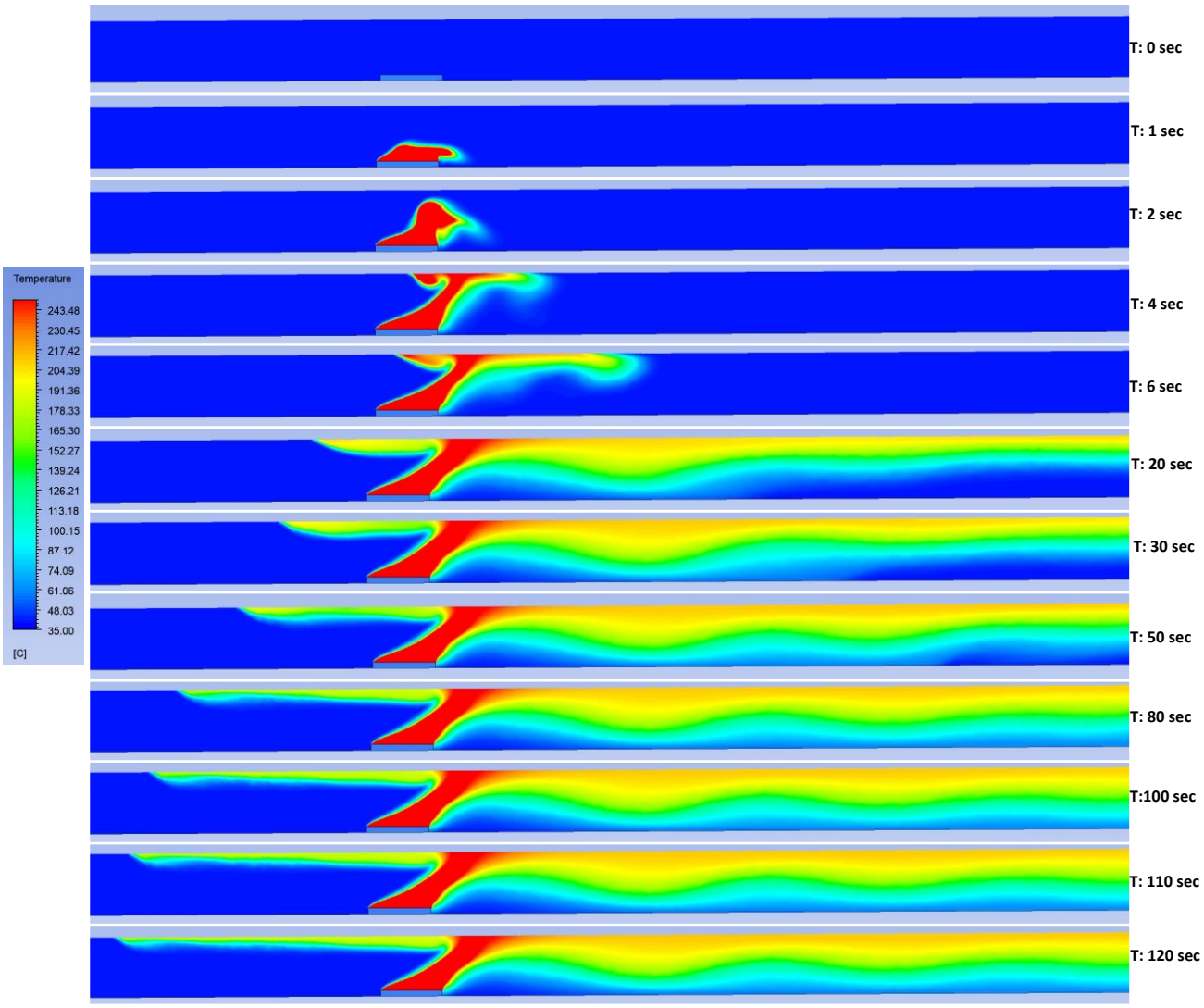

Figure 4.22. Temperature contours for 20 MW fire at chainage 6+450.

Figure 4.23 portrays the spread of the HRR from the fire source of 20 MW, with an inlet velocity of 3.41 m/sec that is determined from the NFPA 502-2020 calculations. It is evident that the ventilation velocity is sufficient enough to push the hot stream and avoids any occurrence of the reverse flow at the ceiling. This points to the fact that the critical velocity predicted by the 2017 edition underestimates the value.

Initially, the backlayering is slightly upstream that takes place near the ceiling. This stagnation of reverse flow is overcome as the thrust gets stronger. The complete eradication of the reverse flow also increases the efficiency of evacuation of passengers and improves access to the location of fire.

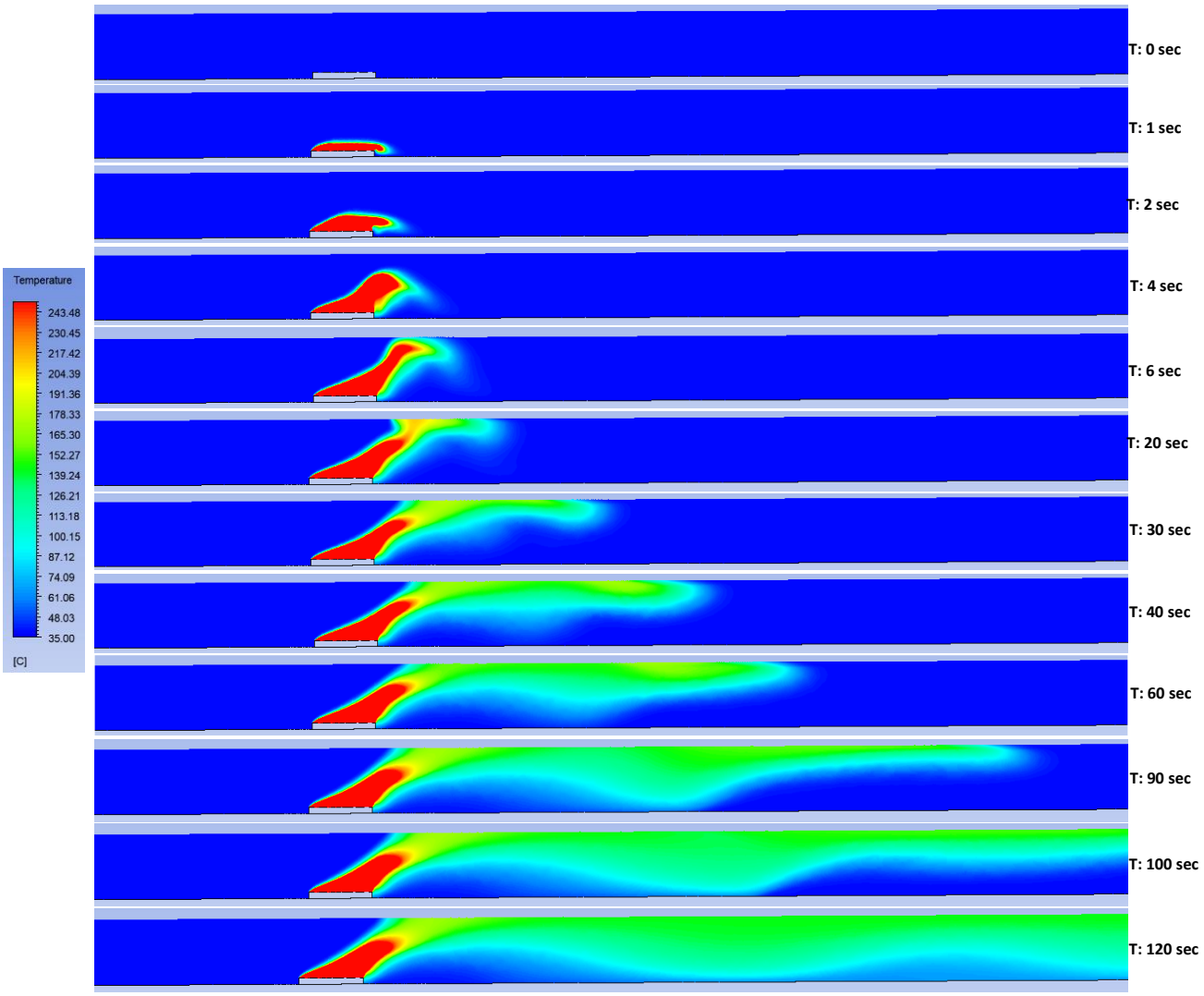

Figure 4.23. Temperature Contours for 20 MW with Critical Velocity equal to 3.41 m/sec (from NFPA 502-2020) – NO BACKLAYERING.

4.5.4. Scenario 4: Train on fire stopped in the tunnel at ch. 6+450 with HRR of 250 MW

Again, for this scenario, the train on fire stopped inside the tunnel at the chainage 6+450 is represented by the slab emitting hot combustion products equivalent to the heat release rate of 250 MW. Initially, the ventilation is negative due to the effect of wind. This is then overcome by the ventilation thrust provided by the jet fans and the central ventilation station which pushes the stream of hot gases and the plume outside the exit portal at chainage 9+400. The ventilation station is present at chainage 6+150 along the tunnel. Along the Sector 1, the flow is from right side towards the entry portal of the tunnel. The simulations performed on *Fluent* uses the reference values for the portals of the tunnel (at chainages 6+350 and 6+550) taken from the results of the mono-dimensional analysis at the end of the

one-hour simulation. The inlet velocity (at chainage 6+350) imposed in the 'velocity-Inlet' boundary condition is 3.673 m/sec with the temperature at this section being 44.653 °C. The simulation is carried out again for two minutes.

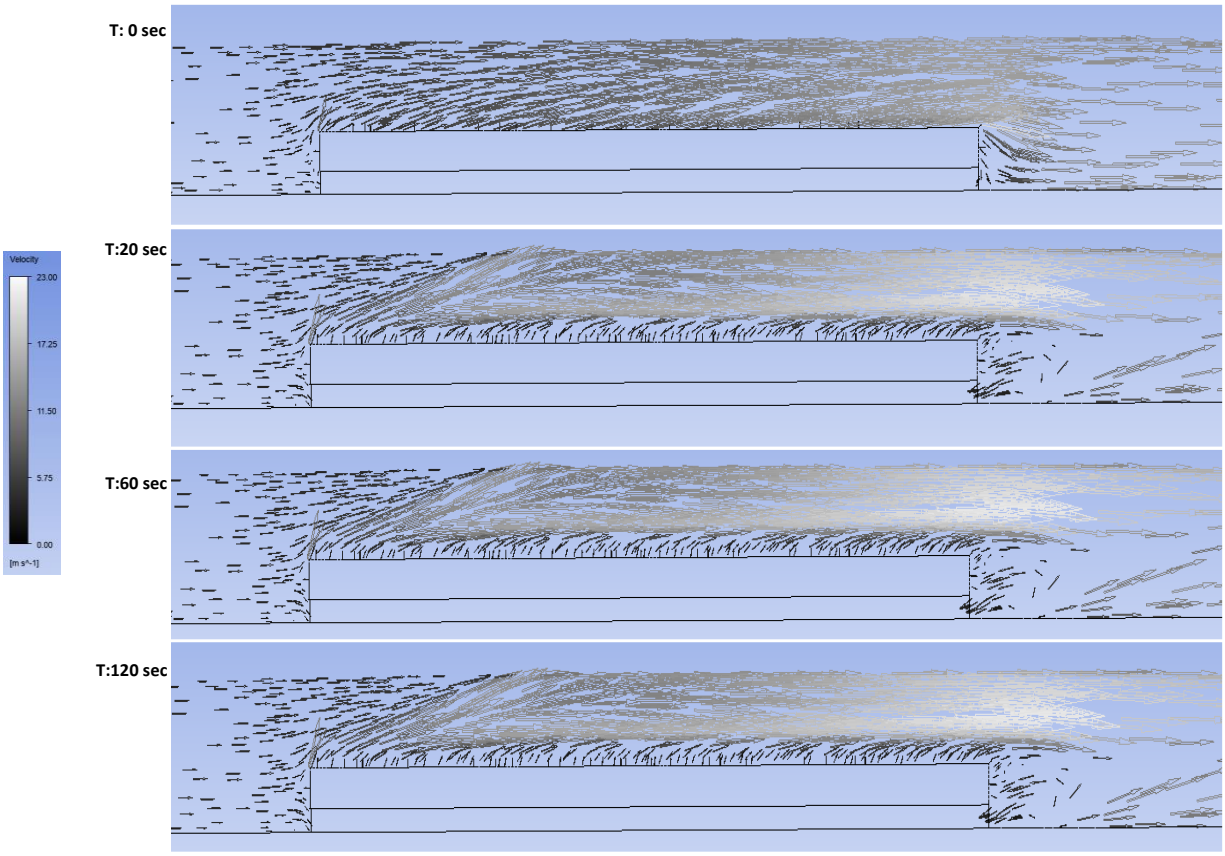

Figure 4.24. Velocity Contours at specific instants of the simulation. No significant reverse flow.

The velocity contours for no LEP section are shown in the Figure 4.24. Clearly there is not much evidence of a backlayering phenomenon occurring here due to the reason as mentioned in the previous section with LEP. The local gradients of velocity are higher near the vicinity of the fire and the fire source is elevated 3 meters from the ground level. The average velocity near the vicinity of the fire at chainage 6+450 is 13.64 m/sec. The average velocity at the outlet chainage 6+550 is 12.3187 m/sec.

The effect of the obstruction inside the tunnel clearly portrays its effect on any development of the reverse flow. The temperature contours also support this statement as shown in the Figure 4.25. The temperature contours show the behaviour of the HRR from the 250 MW source of fire. The average temperature of the stream at the outlet section, chainage 6+550, is 780 °C whereas, near the vicinity of the fire the average temperature is about 995 °C. The net mass flow rate at the section portals is about 13.98 kg/sec.

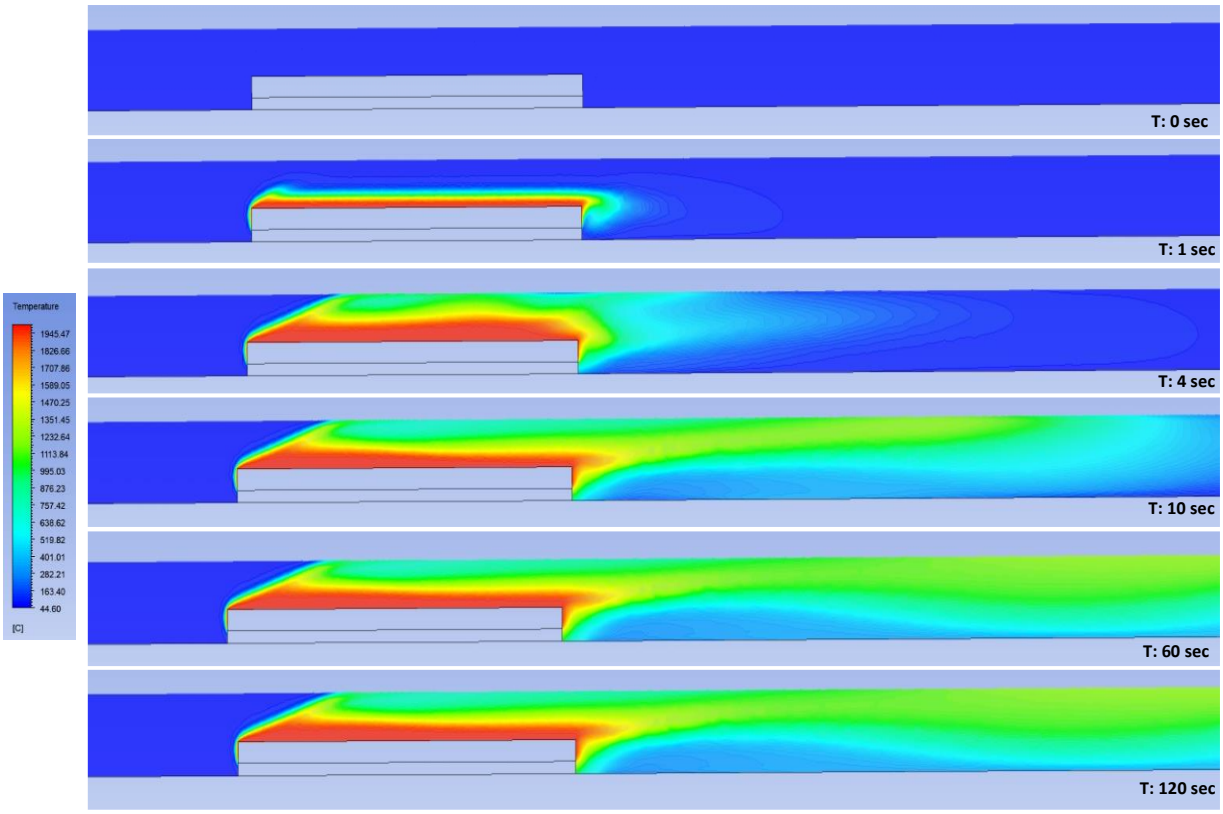

Figure 4.25. Temperature contours for the 250 MW fire at chainage 6+450.

The last step to check the occurrence of the backlayering phenomenon for all the aforementioned fire scenarios was carried out on *ANSYS Fluent*. For the case of train on fire stopped inside the tunnel at chainage 5+100 with an HRR of 20 MW the calculated critical velocity using the NFPA 502-2017 proved to be insufficient thereby producing a reverse flow of the smoke. However, the calculations using NFPA 502-2020 showed significant occurrence of a backlayering which is confirmed by the 3D simulations. For the case train on fire stopped in tunnel at chainage 6+450 with an HRR of 20 MW the 3D simulations again show evidence of a backlayering phenomenon agreeing with the prediction revealed by NFPA 502-2020 standards. However, for the case of the 250 MW fire, a larger surface area representation of the fire added the additional constraint of an obstruction inside the tunnel where the critical velocity is inversely related to the obstruction height. Both the simulations for the 250 MW showed no backlayering. Thus, the 3D simulations provide a visual aid to see the spread of the heat source inside the tunnel. The simulations on Fluent were run by constantly monitoring the residuals and the physical properties of the flow to ensure reliability of the simulations.

Conclusions

The current technological advancements are capable of analysing and evaluating all unique conditions in order to provide proper ventilation for both the normal operating conditions and for the pre-identified emergency conditions. The advantages of a ventilation system during a potential fire scenario will not be completely available until it is operated and reaches its full capacity. During this time period between the initiation of a fire and enactment of the ventilation system to its full capacity, the smoke can spread out polluting the tenable environment and also sabotage the escape pathway for the evacuation of people and restrict access to rescue teams. Thus, the ventilation system should have the sufficient capacity so as to counteract the smoke spread phenomenon. The designed ventilation system should, therefore, assist in the containment and elimination of hazardous gases and also ensure a tenable environment is maintained adhering strictly to all the norms and standards.

The ventilation requirements for the Khor Fakkan Tunnel was carried out to a sufficient level of detail such that it supplements the Overall Tunnel FLS Strategy. The location of the tunnel makes the study even more interesting with the tunnel passing through the Hajar mountains and the ambient temperature of the exterior environment being around 46 °C. The ventilation for the tunnel is provided by a series of jet fans, 36 in total (installed in pairs), and also with the help of a central ventilation station consisting of three axial fans. The analysis is carried out for the critical section of the tunnel, Section TK1, taking into account wind and thermal stack effects with a potential fire scenario at ch. 5+100 and ch. 6+450 with HRR equal to 20 and 250 MW (considered based on the NFPA 130 standard). The performance of the ventilation system was evaluated using different numerical methods by replicating the tunnel environment with all suitable assumptions and hypotheses.

Initially, preliminary calculations based on the NFPA 502-2017 and NFPA 502-2020 were carried out to determine the minimum velocity needed to avoid the reverse flow of the smoke. The calculations show that 2017 edition underpredicts the critical velocity in comparison to that proposed by the 2020 edition, with the presence of a significant backlayering in case of the breakout of a fire. The latest edition of the calculations is based on the Li and Ingason model where the tunnel aspect ratio, in other terms the cross-section of the tunnel – both height and width, influences the variation in calculations. For the case of the 20 MW fire scenario the 2017 edition of the calculations propose a minimum velocity of 2.54 m/sec, however using the 2020 edition the minimum critical velocity needed to avoid the reversal of the smoke is atleast 3.39 m/sec. Upon the application of the 2.54 m/sec as the ventilation velocity, backlayering of the smoke of length equal to 43m is expected. The calculations for the other cases are shown in detail in chapter 2.

The calculations give the basic ideology of the minimum ventilation requirement within the tunnel to maintain a tenable environment. This was followed by the study of the effectiveness of the ventilation system using different numerical methods, which in this project work are – *IDA Tunnel* and *ANSYS Fluent*. The mono-dimensional analysis was carried out for all the cases with the inclusion of a fire and the variation of properties like air temperature, air flow characteristics both the volume of air and the velocity of air, pressure and extinction coefficient for visibility were studied along the tunnel cross-section at different intervals of time. The simulations were run for a minimum of 1 hour wherein the fire is generated following a 'fire class' with a steep increase in the HRR until a period of time and then being constant at the 'design fire size' for the remaining time interval. Such a set-

up was maintained so as to evaluate the efficiency and effectiveness of the ventilation system in case of a worst-case scenario. The results of the simulations are explained in detail in Chapter 3 for both the sections of the tunnel with and without the linear egress passage. The analysis is carried in a very conservative approach as mentioned earlier to procrastinate the effects of a terrible situation. One such assumption was the reduction of the active number of jet fans which are assumed to be destroyed due to the tunnel fire and breakdown due to repair.

Based on the results obtained the extinction coefficient along the egress pathways for all the cases is found be less than 0.3 m^{-1} after 0.1 hours of simulation, thereby ensuring a safe evacuation path to the passengers. The value of the extinction coefficient is deemed optimal guaranteeing sufficient visibility for evacuation along the egress route. The distribution of temperature inside the tunnel was also evaluated, cross referencing to the minimum tenable temperature according to NFPA 130. The objective of checking the potential backlayering is further carried out using CFD on *ANSYS Fluent* to visualize the gradients of the flow of the heat and smoke from the fire source. The model on *Fluent* was constructed by replicating the cross-section of the tunnel geometry at different sections, mainly at chainages 5+100 and 6+450, with the fire source represented based on the principal of conservation of mass.

The results show the proof of the production of a reverse flow phenomenon along the tunnel ceiling when the ventilation velocities are lower than the critical velocities. Again, the average temperatures at section planes perpendicular along the egress pathway are checked and are found to be less than 45 °C, which is less than the maximum air temperature along the egress routes for tenable conditions being 50 °C (that can be considered a tenable environment for approximately 19 mins (18.8 mins according NFPA 130 – table B.2.1.1)). The CFD simulations provide a mere understanding of the fluid flow phenomenon and distribution of heat and smoke. The results of the simulations were validated only after carrying out a grid independency test wherein the Grid Convergence Index(GCI) was found for different mesh sizes. The computational time is a severe constraint when a CFD approach is adopted to analyze performance of the ventilation systems or deal with a fire scenario. The analysis performed on *Fluent* takes into account only a small domain of the entire section of the tunnel with appropriate boundary conditions applied at the tunnel portals.

The future work could possibly be to analyze the performance of the ventilation system with the installation of jet fans along the tunnel sidewalls and other active ventilation systems thereby capturing the real life working of the ventilation scheme. The analysis can also be carried out by increasing the length of the tunnel section by incorporating the varying sloped sections to observe the backlayering phenomenon.

Bibliography

[1] NFPA, 'NFPA 502: Standard for Road Tunnels, Bridges, and Other Limited Access Highways 2017 Edition,' 2017.

[2] NFPA, 'NFPA 502: Standard for Road Tunnels, Bridges, and Other Limited Access Highways 2020 Edition,' 2020.

[3] NFPA 130 – Standard for Fixed Guideway Transit and Passenger Rail Systems – 2017 Edition.

[4] *Fluent* Inc. *FLUENT* 6.2 User's Guide. 2005.

[5] Carvel, Richard & Beard, Alan, The Handbook of Tunnel Fire Safety, 2005.

[6] Francesco Colella, Multiscale Modelling of Tunnel Ventilation Flows and Fires, Doctoral Thesis, Politecnico di Torino, Dipartimento di Energetica, May 2010.

[7] R.K. Haddad, C. Maluk, E. Reda and Z. Harun, Critical Velocity and Backlayering Conditions in Rail Tunnel Fires: State of the Art Review, Hindwai Journal of Combustion, Volume 2019.

[8] P. Thomas, The movement of smoke in horizontal passages against an air flow, Fire Safety Science, vol. 723, 1968.

[9] Woodburn P.J., Britter R.E., CFD simulation of tunnel fire – part I. Fire Safety Journal 26, 1996.

[10] Woodburn P.J., Britter R.E. CFD simulation of tunnel fire – part II. Fire Safety Journal 26, 1996.

[11] Wu Y., Bakar MZA., Control of smoke flow in tunnel fires using longitudinal ventilation systems - a study of the critical velocity. Fire Safety Journal 35, 2000.

[12] Karki K.C., Patankar S.V., CFD model for jet fan ventilation systems. Proceedings of Aerodynamics and Ventilation of vehicle tunnels conference, 2000.

[13] Haukur Ingason, Fredric Seco, Numerical simulation of a model scale tunnel fire test, SP Fire Technology SP REPORT 2005:47.

[14] C. C. Hwang and J. C. Edwards, CFD modelling of smoke reversal, NIOSH/ Pittsburgh Research Laboratory, Pittsburgh, PA 15236.

[15] Abanto J. Reggio, M. Barrero, D. Petro, "Prediction of fire and smoke propagation in an underwater tunnel", Tunnelling and Underground Space Technology 22, 2006

[16] Ballesteros-Tajadura R., Santolaria-Morros C., Blanco-Marigorta E., "Influence of the slope in the ventilation semi-transversal system of an urban tunnel", Tunnelling and Underground Space Technology 21, 2006.

[17] Galdo Vega, M., Maria Arguelles Diaz, K. Fernandez Oro, J.M. Ballesteros Tajadura R., Santolaria Morros C., Numerical 3D simulation of a longitudinal ventilation system: Memorial Tunnel case, Tunnelling and Underground Space Technology, 2007.

[18] Eduardo Blanco, Raúl Barrio, Dpto. Energía, Universidad de Oviedo; Joaquín Fernández, Alfonso Marcos, Dpto. IMEM Universidad de Extremadura, Numerical simulation of the backlayering effect in the memorial tunnel tests. Selected Proceedings from the 14th International Congress on Project Engineering", 2010.

[19] Aleksander Król, and Małgorzata Król, Study on Hot Gases Flow in Case of Fire in a Road Tunnel, mdpi, Energies, 11, 290; doi:10.3390/en11030590, 2018.

[20] Helmut Steiner, Michael Beyer, Peter-Johann Sturm, Requirements for escape doors in the tunnels of the Koralm railway line – special focus on thermal loads during fire, 9th International Conference 'Tunnel Safety and Ventilation', 2018.
[21] P. Hinkley, The flow of hot gases along an enclosed shopping mall a tentative theory, Fire Safety Science, vol. 807, 1970.
[22] N. Danziger, "Longtitudinal ventilation analysis for the glenwood canyon tunnels," in Proceedings of the 4th International Symposium on Aerodynamics & Ventilation of Vehicle Tunnels, 1982.
[23] Y. Oka and G. T. Atkinson, Control of smoke flow in tunnel fires, Fire Safety Journal, vol. 25, pp. 305–322, 1995.
[24] G. T. Atkinson and Y. Wu, Smoke control in sloping tunnels, Fire Safety Journal, vol. 27, pp. 335–341, 1996.
[25] Y. Z. Li, B. Lei, and H. Ingason, Study of critical velocity and backlayering length in longitudinally ventilated tunnel fires, Fire Safety Journal, vol. 45, pp. 361–370, 2010.
[26] H. Ingason and Y. Z. Li, Model scale tunnel fire tests with longitudinal ventilation, Fire Safety Journal, vol. 45, pp. 371–384, 2010.
[27] Y. Z. Li, B. Lei, and H. Ingason, The maximum temperature of buoyancy-driven smoke flow beneath the ceiling in tunnel fires, Fire Safety Journal, vol. 46, pp. 204–210, 2011.
[28] Y. Z. Li and H. Ingason, Effect of cross section on critical velocity in longitudinally ventilated tunnel fires, Fire Safety Journal, vol. 91, pp. 303–311, 2017.
[29] Y. Z. Li and H. Ingason, Discussions on critical velocity and critical Froude number for smoke control in tunnels with longitudinal ventilation, Fire Safety Journal, vol. 99, pp. 22–26, 2018.
[30] J. Vantelon, A. Guelzim, D. Quach, D. Son, D. Gabay, and D. Dallest, "Investigation of fire-induced smoke movement in tunnels and stations: an application to the paris metro," Fire Safety Science, vol. 3, pp. 907–918, 1991.
[31] L.H.Hu, R.Huo, andW.K. Chow, "Studies on buoyancy-driven back-layering flow in tunnel fires," Experimental Thermal and Fluid Science, vol. 32, no. 8, pp. 1468–1483, 2008.
[32] H. Ingason and A. Lönnermark, Heat release rates from heavy goods vehicle trailer fires in tunnels, Fire Safety Journal, Volume 40, Issue 7, October 2005, Pages 646-668.
[33] Ying Zhen Li, and Haukur Ingason, The Fire Growth Rate in a Ventilated Tunnel Fire, SP Technical Research Institute of Sweden, 2011
[34] Werner Blendermann, On a probabilistic approach to the influence of wind on the longitudinal ventilation of Road Tunnels,1976.
[35] Haukur Ingason, Fire Development in Large Tunnel Fires, Fire Technology, SP Technical Research Institute of Sweden, 2005.
[36] Andres Lönnermark, On the Characteristics of Fires in Tunnels, Doctoral Thesis, Department of Fire Safety Engineering, Lund Institute of Technology, Lund University, 2005.
[37] H Weiping, L Yi, L Xin, J Lishuai, L Wanfu, Xu Zhisheng, Y Dongxing, TLiwei, Z Xianzhong, X Jianjun, H Guang, W Jianqiang, Design and heat release rate test of freight carriage model, Tianjin Fire Research Institute of MPS, Tianjin University of Commerce, Central South University, 2018.
[38] PIARC 1999. Fire and Smoke Control in Tunnel Fires (PIARC committee on road tunnels (C5) 05.05.B). P. I: PIARC.

[39] Idelchik, I.E., Handbook of hydraulic resistance, 1986.
[40] Marcin Sosnowski1, Jaroslaw Krzywanski, and Renata Gnatowska, Polyhedral meshing as an innovative approach to computational domain discretization of a cyclone in a fluidized bed CLC unit E3S Web of Conferences, 14, 2016.
[41] Ahmed Nagib Elmekawy, Module 3: Global Mesh Controls, Introduction to ANSYS Meshing, ANSYS.
[42] Jin T., Journal of Fire and Flammability, vol. 12, p. 130, 1981.
[43] Rabash D.J, Relevance of firepoint theory to the assessment of fire behaviour of combustible material, 1975.
[44] Babrauskas, V., Full-Scale Burning Behaviour of Upholstered Chairs, Gaithersburg MD, 1979.
[45] Franck GYPPAZ Nexans Research Center, Smoke and Safety in case of fire, 2014.
[46] André Bakker, Presentation on theme: "Lecture 8 - Turbulence Applied Computational Fluid Dynamics", 2005.
[47] FDS User Guide (Verification and Validation of Selected Fire Models for Nuclear Power Plant Applications. NUREG 1824, United States Nuclear Regulatory Commission, 2007.
[48] W.M. Thornton D.Sc. D.Eng., XV. The relation of oxygen to the heat of combustion of organic compounds, The London, Edinburgh, and Dublin Philosophical Magazine and Journal of Science, 1917.
[49] SFPE Handbook of Fire Protection Engineering, Third Edition, in association with NFPA, 2002.
[50] Bjarne Paulsen Husted, Danish Institute of Fire and Security Technology, Optimal Smoke units and Smoke potential of different products. 2004.
[51] Xuepeng Jiang, Hongxin Zhang, An Jinga, Effect of blockage ratio on critical velocity in tunnel model fire tests, Tunnelling and Underground Space Technology, 2018.
[52] Hue X., Ho J.C., Cheng Y.M., Comparison of different combustion models in enclosure fire simulation, Fire Safety Journal, 2001.
[53] *IDA Tunnel*, Version: 1.2, Theoretical Reference, EQUA Simulation, Stockholm, Sweden, January 2017.
[54] NFPA 92– Standard for Smoke Control Systems – 2015 Edition.
[55] Standard BD 78/99 – Design of Road Tunnels, National Roads Authority Design Manual for Roads and Bridges Addendum, Volume 2 Part 9 BD 78/99, 1999.
[56] Fans & Ventilation, A Practical Guide, WTW Bill Cory 2005 Edition.

Appendix

A.1. Mathematical Models used in *IDA Tunnel*

The results of the simulations obtained on *IDA Tunnel* are obtained with the help of a pre-compiled set of equations like mass balances, energy balances, etc. The thesis work carried out analyses the situation wherein there is a fire outbreak inside a tunnel and the ventilation system is used to eliminate the hot flow of gases and smoke. Here in this section the mathematical models used by the software to calculate the Air flow and Heat flow are illustrated. These sections are taken from the theoretical reference manual of *IDA Tunnel* [53].

A.1.1. Calculation of Air Flow:

The calculations of the airflow in any section of a tunnel is obtained from the air mass flow balance and the total pressure for the whole tunnel. The Loss coefficients are in calculated by the program but can also be implemented by the user. The present lack of detailed knowledge for some of the airflow configurations has been overcome by continuity assumptions and comparisons to measurements of loss coefficients.

A.1.1.1. Rail Tunnel Section

Basically, in the tunnel section module the length of the tunnel is divided into smaller segments and each of this segment has a constant cross-sectional area and hydraulic diameter. The equations for the different pressure contributions are however the same as those used in the SES program [SES User's Manual 1997]. Here, an important assumption is that the effect of vehicles running side by side is neglected in the computation of the pressure changes due to friction and piston action.

The mathematical model is described below with all the components:

$$\Delta \boldsymbol{p_{frict}} = -\sum_i \frac{\rho_i}{2}\frac{\lambda_{Ti}}{d_i}\left[\left(l_i - \sum_j l_{V\_ij}\right) v_i|v_i| - \sum_j \frac{l_{V\_ij}}{\left(1 - A_{V\_j}/A_i\right)^3}\left(\frac{A_{V\_j}}{A_i}v_{V\_ij} - v_i\right)\left|\frac{A_{V\_j}}{A_i}v_{V\_ij} - v_i\right|\right]$$

Where,

Δp_{frict} – Pressure change due to friction against walls (Pa); dPFrict

λ_{Ti} – Darcy friction factor for tunnel wall in segment *I;* lambda

ρ_i – Mean density of air in tunnel segment *i* (kg/m^3); Rho

d_i – hydraulic diameter of tunnel segment *i* (m); dTun

l_i – length of tunnel segment *i* (m); lTun

l_{V_ij} – Length of vehicles of type *j* in tunnel segment *i* (m); lBody

v_i – Mean air velocity in segment *i*, positive from left to right(m/s); VAir

v_{V_ij} – Velocity of vehicle *j* in segment *i*, positive from left to right (m/s);speed

A_{V_j} – Cross section area of vehicle type *j* (m^2); frontArea

A_i – Tunnel area of segment *i* (m^2); aTun

$$\boldsymbol{\Delta p_{stack}} = \sum_i \Delta p_{stack\_i} = \sum_i \left(p_{stack\_i+1} - p_{stack\_i}\right)$$

Where,

Δp_{stack} – Stack pressure rise (Pa); dPStack

Δp_{stack_i} – Stack pressure rise in segment *i*(Pa); dPStack

$p_{stack\_i+1} = p_{stack\_i} * e^{-g*\frac{\Delta h_i}{(R*(T_i+273.15))}}$ Stack Pressure in node *i+1*(Pa); PStack

p_{stack_1} – Static pressure in left node of section (Pa); PStack

Δh_i – Change of altitude in segment *i* (m); dH

g – 9.80665 – Acceleration of gravity (m/s^2);

T_i – Air temperature at node *i* (°C); TAir

R – 287 – Gas constant for air (J/kg/K);

$$\boldsymbol{\Delta p_{fire}} = -FPD * q_{fire}/1000000 * \delta_i$$

Where,

Δp_{fire} – Pressure drop across fire (Pa)

FPD – Pressure drop across fire per MW of fire power (Pa/MW) *FPD*

q_{fire} – Actual fire power (W)

δ_i – If fire in segment *i* then if $|m_{dot\_i}/A_i| > 0.1$ sign(m_{dot_i}) else

sin($\pi/2 \cdot m_{dot\_i}/A_i/0.1$) else 0

m_{dot_i} – Air mass flow in segment *i* (kg/s) m_dot

$$\boldsymbol{\Delta p_{fricv}} = \sum_i \sum_j \frac{\rho_i}{8} \frac{\lambda_{V\_j} * l_{V\_ij} * p_{V\_j}}{A_i\left(1 - A_{V\_j}/A_i\right)^3} \left(v_{V\_ij} - v_i\right) \left|v_{V\_ij} - v_i\right|$$

Where,

$$\lambda_{V\_j} = \lambda_{VS\_j} + \frac{c_{DTV\_j}}{4 l_{V\_j} p_{V\_j}}$$

Δp_{fricv} – Pressure change due to friction against vehicles (Pa); dPFricv

λ_{V_j} – Skin friction coefficient for vehicles of type *j;* lambda

λ_{VS_j} – Skin friction coefficient related to viscous drag for vehicles *j;* lambdas

c_{DTV_j} – Drag coefficient weighted total truck area of vehicle type *j* (m^2); cdTruck

l_{V_j} – Length of vehicles of type *j* (m); length

p_{V_j} – Perimeter of vehicles of type *j* (m); perim

$$\boldsymbol{\Delta p_{piston}} = \sum_i \sum_j \frac{\rho_i}{2} A_{V\_j} \left\{ \left[\frac{c_{DFV\_j}}{A_i} + \frac{\left(2A_i - A_{V\_j}\right)}{\left(A_i - A_{V\_j}\right)^2} \right] N_{front\_ij} + \left[c_{DBV\_j} \frac{A_i}{A_i - A_{V\_j}} - \frac{2}{A_i - A_{V\_j}} \right] N_{back\_ij} \right\} \left(v_{V\_ij} - v_i\right) \left|v_{V\_ij} - v_i\right|$$

Where,

$$c_{DBV\_j} = \frac{0.029}{\sqrt{0.5 \lambda_{VS\_j} l_{V\_j} p_{V\_j} / \left(4 A_{V\_j}\right)}}$$

Δp_{piston} – Piston pressure rise (Pa); dPPiston

c_{DBV_j} – Drag coefficient at back end of vehicle type *j;* cdBack

c_{DFV_j} – Drag coefficient at front end of vehicle type *j;* cdFront

N_{front_ij} – # of front ends (see below) of vehicle type *j* in segment *i;* nFront

N_{back_ij} – # of back ends (see below) of vehicle type *j* in segment *i;* nBack

The front end is defined as the end, either physical front or back, which has a headwind.

Thus, the aerodynamic drag force on each vehicle becomes:

$$\boldsymbol{F_{drag} = F_{fricv} + F_{piston}}$$

Where,

$$F_{fricv} = \frac{\rho}{8}\frac{\lambda_V l_V p_V}{(1 - A_V/A)^3}(v_V - v)|v_V - v|$$

$$F_{piston} = \frac{\rho}{2}A * A_V\left\{\frac{c_{DFV}}{A} + \frac{(2A - A_V)}{(A - A_V)^2} + c_{DBV}\frac{A}{(A - A_V)^2} - \frac{2}{A - A_V}\right\}(v_V - v)|v_V - v|;$$

$$= \frac{\rho}{2}A_V\left\{c_{DFV} + \frac{c_{DBV}}{(1 - A_V/A)^2} - \frac{A_V}{A(1 - A_V/A)^2}\right\}(v_V - v)|v_V - v|$$

Next, the contribution from the nodes, which cause discontinuities in the pressure profile along the section, are

$$\boldsymbol{\Delta p_{area}} = -\sum_i \frac{\rho_i}{2} * \zeta_i * v_i^2$$

Where,

i – Density of air at node i (kg/m3); Rho

v_i – Air velocity at node i (area Ai), positive from left to right (m/s); VAir

ζ_i – Resistance factor at node i, depends on area, shape of transition, direction of flow.

$\zeta_i = 1 - \left(1 - k_{\text{exp\_}i}\right) * (A_i/A_{i-1})^2$ if $A_i/A_{i-1} > 1$ and $v_i > 0$ kPos

$\zeta_i = 1 - \left(1 + k_{\text{cnt\_}i}\right) * (A_i/A_{i-1})^2$ if $A_i/A_{i-1} > 1$ and $v_i < 0$ kNeg

$\zeta_i = 1 + k_{\text{cnt\_}i} - (A_i/A_{i-1})^2$ if $A_i/A_{i-1} \le 1$ and $v_i > 0$ kPos

$\zeta_i = 1 - k_{\text{exp\_}i} - (A_i/A_{i-1})^2$ if $A_i/A_{i-1} \le 1$ and $v_i < 0$ kNeg

k_{exp_i} – Expansion loss coefficient at node i; kExp

k_{cnt_i} – Contraction loss coefficient at node i; kCntr

Ai – Cross-section area at node i – Cross-section area of segment to the right (m^2)

$$\boldsymbol{\Delta p_{fan}} = \sum_i \sum_j \delta_{ij} * \rho_i * k_{f\_j} * \left(sign(c_{act\_j}) * v_{fan\_j} - v_i\right) * \left|c_{act\_j} * v_{fan\_j}\right|$$

$$= \sum_i \sum_j \delta_{ij} * \rho_i * k_{f\_j} * \left(c_{act\_j} * v_{fan\_j} - v_i\right) * \left|c_{act\_j} * v_{fan\_j}\right|$$

Where,

Δp_{fan} – Fan pressure rise (Pa); dPFan

δ_{ij} – 1 if fans *j* is in node *i*, otherwise 0;

$k_f j$ – $N_{fan\_j} * k_{fan\_j} * A_{fan\_j} / A_i$ = efficiency factor of fans *j;* kF

N_{fan_j} – Number of jet fans *j* at node *i;* mult

A_{fan_j} – Cross section area of jet fan *j* (m^2); area

k_{fan_j} – Pressure rise coefficient (installation factor) of jet fan *j;*

v_{f_j} – $c_{act\_j} * v_{fan\_j}$ – Outlet velocity of fan *j*, positive from left to right (m/s);

c_{act_j} – $-\tau * dc_{act\_j}/dt + c_{tr\_j}$ – delayed fan capacity control; cntrAct

c_{tr_j} – Fan capacity control in interval [-1, 1], -1 = right to left action; cntr

τ – Time constant for startup (s); tau

v_{fan_j} – jet speed of fan *j* (m/s); v

$Q_{f\_j} = N_{fan\_j} * A_{fan\_j} * \rho_i * v_{fan\_j}^2 / Tp_{fan\_j\,i} * \left|c_{act\_j}\right|$ if thrust control PowerCons

$= N_{fan\_j} * A_{fan\_j} * \rho_i * v_{fan\_j}^2 / Tp_{fan\_j\,i} * {c_{act\_j}}^2$ if speed control [kW]

Power consumption of fans *j* (W);

T_{pfan_j} – Total performance (thrust/fan power ratio) of fan *j* (N/W); TotPerform

The air density ρ_i at node *i* is assumed to satisfy the perfect gas law and is given as follows:

$$\boldsymbol{\rho_i} = \frac{p_i}{R * (T_i + 273.15)}$$

Where,

R – 287 – Gas constant for air (J/kg/K);

p_i – Static pressure at node *i* (Pa);

T_i – Air temperature at node *i* (°C); TAir

The tunnel area is initially computed at the nodes between the segments. The relation between the mass flow m_{dot_i} and the velocity v_i at the node *i* or in a segment *i*, is given as:

$$\boldsymbol{v_i} = \frac{m_{dot\_i}}{\rho_i A_i}$$

A.1.1.2. Plenum

Applying the mass conversation at Plenum:

$$V * \frac{d\rho_{dry}}{dt} = \sum_j m_{dot\_i}$$

Where,

ρ_{dry} – Density of dry air = $\rho\ (1 + w)^{-1}$ (kg/m^3);	RhoDry
ρ – Density of air (kg/ m^3);	Rho
w – Humidity ratio of air (= 0 in IDA RTV);	xHum
m_{dot_j} – Mass flow from tunnel j (kg/s) tunnel;	m_dot
V – Volume of Plenum (m3);	VEncl

Also, the static pressure is:

$$p = \rho * R * (T + 273.15)$$

Where,

T – Air temperature in plenum (˚C);	Tair

A.1.1.3. Tunnel Entry (Entry)

On the *IDA Tunnel* software, the tunnel entry phenomenon is modelled as a 'flanged entrance' for airflow and an 'abrupt exit' for airflow moving out of the tunnel. The reduction in the wind pressure as a result of a vehicle in the tunnel entry is neglected. Now, given a total pressure p_{out} outside the entry the Bernoulli equations take the following form:

$\boldsymbol{p_{out}} = p_{tunnel} + \frac{\rho_{mean}}{2} * (1 + k_c) * v_{tunnel}^2$ - for airflow entrainment;

$\boldsymbol{p_{out}} = p_{tunnel} + \frac{\rho_{mean}}{2} * (1 - k_d) * v_{tunnel}^2$ - for airflow leaving tunnel.

Where,

$p_{out} - p_{height} + p_{wind}$	P1

Total pressure outside tunnel relative reference level (Pa);

p_{tunnel} – Static pressure inside tunnel relative reference level (Pa); tunnel.P

$p_{height} = p_{amb}\left(e^{-gh/R(T_{amb}+273.15)} - 1\right)$ PHeight

ambient static pressure relative reference level (Pa);

p_{wind} – Wind pressure outside tunnel (Pa) PWindCalc

p_{amb} – Ambient pressure at reference level (Pa) amb.P

ρ_{mean} – Mean air density at entry (kg/m3) Rho

k_c – Loss coefficient for ingoing flow (into tunnel), default = 0.5 kPos

k_d – Loss coefficient for outgoing flow (out of tunnel), default = 1 kNeg

v_{tunnel} = Air velocity in tunnel inside entrance (m/s) VAir

T_{amb} – Ambient temperature (˚C) amb.T

h – Height relative reference level (m) hTun

g – 9.80665 – Acceleration of gravity (m/s2)

R – 287 – Gas constant for air (J/kg/K).

A.1.1.4. Tunnel Portal (Portal)

The openings in tunnels to either stations or plenums are modelled on *IDA Tunnel* in a similar fashion as that of pointed earlier, Tunnel entry regarding Airflow. Therefore, in this case the Bernoulli equation become:

$$\boldsymbol{p_{station}} = p_{tunnel} + \frac{\rho_{mean}}{2} * (1 + k_c) * v_{tunnel}^2 - \Delta p_{height}$$ - for airflow entrainment;

$$\boldsymbol{p_{station}} = p_{tunnel} + \frac{\rho_{mean}}{2} * (1 - k_d) * v_{tunnel}^2 - \Delta p_{height}$$ - for airflow entering station/plenum ;

Where,

$p_{station}$ – Total pressure outside tunnel at floor level station.P

relative reference level (Pa);

p_{amb} – ambient at reference level (Pa); amb.P

$\Delta p_{height} = (p_{station}) + p_{amb}\left(e^{-gh/R(T_{amb}+273.15)} - 1\right)$ PHeight

Static pressure relative to station/plenum floor level (Pa);

ρ_{mean} – Mean air density at portal (kg/m3); Rho

k_c – Loss coefficient for flow entering tunnel, default = 0.5; kPos

k_d – Loss coefficient for flow leaving tunnel, default = 1; kNeg

v_{tunnel} – Air velocity in tunnel (m/s); VAir

T – Temperature in station/plenum (°C); station.T

h – Height to tunnel from station floor (m); hTun

g – 9.80665 – Acceleration of gravity (m/s2);

R – 287 – Gas constant for air (J/kg/K).

A.1.1.5. Damper

For this section, the Pressure difference is represented as a function of Mass flow. In case of a fully open position the flow phenomenon is governed by a loss coefficient, whereas for the case of closed scenario by an Equivalent Leakage Area. It can be defined as asymmetric too.

$$\boldsymbol{\Delta p} = sign(m_{dot}) * \left|\frac{m_{dot}}{c_{Act}}\right|^{\frac{1}{n_{Act}}}$$

Where,

m_{dot} – Mass flow (kg/s); left.m_dot

n_{Act} – **if** powerLawLeakage **then** 0.5 + f_{closed}^{k} (n − 0.5) **else** 0.5; nAct

c_{Act} – **if** m_{dot} > 0 **then** $c_{open} + f_{closed}^{k}\left(c_{closed} - c_{open}\right)$ cAct

else $c_{open} + f_{closed}^{k}\left(c_{closR2L} - c_{open}\right)$

$f_{closed} = -\tau_{open} * \frac{df_{closed}}{dt} + \left(1 - f_{openSig}\right)$ – Delayed opening/closing; partClosed

$f_{openSig}$ – Opening control, 1 for fully open and 0 for closed; partOpen

$\tau open$ – Time constant for opening/closing (s); tau

n – Power law exponent at closed; n

c – Power law coefficient at closed; c

k – Integer exponent in linear combinations; k

$c_{open} = \sqrt{2\rho_{air}/k_{loss}} * A$ c_open

c_{closed} = **if** powerLawLeakage **then** c **else** $\sqrt{2\rho_{air}} * A_{el} * C_d$ c_closed

$c_{closR2L}$ = **if** powerLawLeakage **or** symmetric **then** c_{closed} c_closR2L

else $\sqrt{2\rho_{air}} * A_{elR2L} * C_d$;

Cd – Discharge coefficient; cd

Δp – Static pressure difference between left and right (Pa); dPtot

ρair – Density of air (kg/m^3); Rho_air

$kloss$ – Loss coefficient at fully open; kLoss

A – Cross section area (m^2); tArea

A_{el} – Equivalent leakage area (m^2); ela

A_{elR2L} – Equivalent leakage area for air flow from right to left if not symmetric (m^2). elaR2L

A.1.1.6. Axial Fan

Finally, the description of axial fan is presented by a fan curve as a spline, where the pressure rise is basically a function of the air volume flow:

$$\boldsymbol{\Delta p} = f_{spline}(V_f/f_{vAct}) * |f_{vAct}| * f_{vAct} * \rho/\rho_{nom}$$

Where,

Δp – Static pressure difference between inlet and outlet (Pa); dPtot

V_f – Air volume flow (m^3/s); VFAir

$f_{spline}(Vf)$ – Spline giving pressure rise as a function of air volume flow (Pa) spline

f_{vAct} – $-\tau * df_{vAct}/dt + f_{vRel}$ = delayed f_{vRel} speedAct

f_{vRel} – Quotient fan speed to nominal fan speed in interval [0 : 1] speedRel

τ – Time constant (s); tau

ρ = Air density (kg/m^3);

ρ_{nom} – Air density at which the fan performance is defined (kg/m3) RhoNom

Q_{sup} – Max(0, $V_f * \Delta p$)/ eff = power supplied (W) PowerSup

eff – $espline(V_f / f_{vAct})$ = fan efficiency effic

$e_{spline}(V_f)$ – Spline giving fan efficiency as a function of air volume flow; spline

A.1.2. Calculation of Heat Flow:

On *IDA Tunnel* software the temperature fields are not only computed for the air medium within the tunnel but also the surrounding walls. The effects such as heat from equipments, people, temperature of trains are integrated together and included.

Following sections describe in detail the main approach used by the software for this project work:

A.1.2.1. Rail Tunnel Section heat balance (Rail Section)

The heat transport phenomenon along the tunnel is modelled with the help of the discretised advection equation. The heat exchange with the tunnel wall is represented with convection and radiation.

$$\rho_i l_i A_i \frac{dE_i}{dt} + \Delta(m_{dot}E)_i = Q_{air\_i} + Q_{cond\_i} + Q_{veh\_i} + Q_{equi\_i} - Q_{evap_i} + Q_{fire_i} + Q_{trans_i} - Q_{pipe\_i}$$

Where,

E_i – Air enthalpy ($c_{pAir}\ Ti$) in segment *i* (J/kg); EntAir

ρ*i* – density of air in segment *i* (kg/m3); Rho

$\Delta(m_{dot}\ E)_i$ – **(if** $m_{dot\_i+1/2} > 0$ **then** $m_{dot\_i+1/2}\ E_i$ **else** $m_{dot\_i+1/2}\ E_{i+1}$)

-(if $m_{dot\_i-1/2} > 0$ **then** $m_{dot\_i-1/2}\ E_{i-1}$ **else** $m_{dot\_i-1/2}\ E_i$)

$m_{dot\_i-1/2}$ – Air mass flow at node between segment *i*-1 and *i* (kg/s);

$Q_{air\_i} = l_i * \left(4 * \frac{A_i}{d_i}\right) * U_i * \left(T_{wall\_i} - T_i\right)$ Qair

T_i – Air temperature in segment *i* (°C) TAir

$T_{wall\_}i$ – Wall temperature in segment *i* (°C) TWall

U_i – Total heat transfer coefficient in segment *i* containing UTot convection and radiation depending on temperature, air velocity, extinction coefficient and hydraulic diameter (W/ m²°C);

Q_{cond_i} – Heat from condensation of moisture in segment *i* (= 0 in IDA RTV) (W)

Q_{veh_i} – Heat from cars/trains in segment *i* (W); Qtraffic

Q_{equi_i} – Heat from equipment in segment *i* (W);

Q_{evap_i} – Heat for evaporation of liquid water mist from equipment in segment *i.* (= 0 in IDA RTV) (W)

$Q_{trans\_i} = c_{pAir}\left(m_{TrIn\_i} * T_{TrIn\_i} - m_{TrOut\_i} * T_i\right)$

Heat from transverse ventilation in segment *I* (W);

m_{TrIn_i} – Total supplied air mass flow into segment *i* (kg/s); m_trin_tot

m_{TrOut_i} – Total exhausted air mass flow from segment *i* (kg/s); m_trout

T_{TrIn_i} – Temperature of supplied airflow in segment *i* (°C); TWall

Q_{fire_i} – $f_{air} \cdot q_{fire} \cdot \delta_i$ = heat from fire to air in segment *i* (W);

q_{fire} – Fire power (W); FirPower

f_{air} – Fraction of fire power directly to air (the rest goes to wall); fire2air

δ_i – 1 if fire in segment *i*, otherwise 0;

l_i – Length of tunnel segment *i* (m); lTun

A_i – Cross-section area of tunnel segment *i* (m^2); aTun

Q_{pipe_i} – $Q_{airP} \cdot l$ QAirPl2r

heat to cooling pipes in segment *i* (see 2.2.9) (W) QAirPr2l

The heat transfer coefficient U_i depends on both radiation and convection:

$$\boldsymbol{U} = U_{rad} + U_{conv}$$

With,

$$U_{rad} = em_{gas} * \sigma * (K_{air}^2 + K_{wall}^2) * (K_{air} + K_{wall})$$

Where,

$$U_{conv} = k_1 * max\left(h, U_{film}\right)$$

Where,

h – $Nu * k_{air} / d$ = Convective heat transfer coefficient ($W/m^2°C$)

U_{film} – Heat transfer coefficient at low air velocities computed as a function of the temperature difference between air and wall. From IDA Indoor Climate and Energy 3.0 ($W/m^2°C$);

k_1 – factor (e.g. for surface enlargement); k1

$Nu = 0.7\left(\frac{\lambda_T}{8}\right) Re / \left(1 + 1.592\left(15.217\left(\frac{\lambda_T}{4}\right) Re^{\frac{1}{5}} - 1\right) / Re^{\frac{1}{8}}\right)$ Nusselt

Nusselt Number;

Re – $|v_{air}|*\rho_{air}*d$ / μ_{air} = Reynolds number; Reynold

Pr – $c_{pAir}*\mu_{air}$ / k_{air} = Prandtl number;

λ_T – Darcy friction factor for tunnel wall;

c_{pAir} – Specific heat of air (J/kg°C); CP_AIR

$k_{air}(T)$ – Thermal conductivity in air (W/m°C);

$\mu_{air}(T)$ – Dynamic viscosity in air (Pa s);

K_{air} – $(T_{air}$ +273.15) – Absolute temperature of air (K);

K_{wall} = absolute temperature of wall (K)

em_{gas} = 1 – $e^{-ext \cdot d}$ = gas emission; GasEmiss

ext = extinction coefficient (m^{-1}) extinc

σ = 5.6697 · 10-8 = constant of Stefan-Boltzmann (W/m^2K^4);

d = hydraulic diameter (m); dTun

$vair$ = air velocity (m/s); VAir

A.1.2.2. Plenum

As pointed out earlier the air in the plenum is taken to be 'well mixed. As a result, the temperature is computed using:

$$c_{pAir} V \frac{d(\rho_{dry} T)}{dt} = \sum_j Q_j + Q_{air} + \sum_j Q_{equi\_j} + Q_{fire}$$

Where,

T – Temperature in plenum (°C); TAir

c_{pAir} – Specific heat of air (J/kg°C); CP_AIR

ρ_{dry} – Density of dry air = $\rho\ (1 + w)^{-1}$ (kg/m^3); RhoDry

ρ – Density of air (kg/m^3); Rho

w – Humidity ratio (= 0 in IDA RTV); xHum

V – Volume of Plenum (m^3); VEncl

Q_j – Heat flow from tunnel *j* into Plenum (W) Q [kW]

$Q_{air} - A_{wall} * U * (T_{wall} - T)$= heat flow from wall into Plenum (W) QAir [kW]

$U - U_{rad} + U_{film}$ = total heat transfer coefficient. Utot

Urad and *Ufilm* are computed as in sections (W/ m²°C)

A_{wall} – wall area (2 * length * (width + height)) (m²); Awall

T_{wall} – wall temperature (˚C); Twall

m_{dot_j} – mass flow from tunnel *j* (kg/s); tunnel.m_dot

A – Cross-section area of Plenum (m²); VEncl

Q_{equi_j} – Heat from equipment *j* (W) equip.Q2air

$Q_{fire} - f_{air} * q_{fire}$ = Heat from fire to air in Plenum (W)

q_{fire} – Fire power (see 2.2.6) (W) FirPow [MW]

f_{air} – Fraction of firepower directly to air (rest is radiated to the wall) (default = 0.7).

A.1.2.3. Wall

The computation of temperature around sections/platforms/plenums takes into account the temperature of the air within the sections/platforms/plenums but also the temperatures in neighboring sections/platforms/plenums. As a result, superposition principal is used where different fields of temperature are superimposed which are basically 1D temperature fields. The following assumptions are made:

a. The cross sections of sections/platforms can be approximated as circular;
b. Heat conduction in ground parallel to section/platform can be neglected;
c. The thermal properties are homogeneous outside a thin region close to section/platform; The distances to the neighbor section/platform and ground surface are large, so that the gradients of the temperature fields caused by these are small, i.e. within the thin layer the total temperature is well approximated by radial depth (and time) dependence;
d. The ground surface above each segment/platform is approximated by a horizontal plane;
e. In simulations containing inclined tunnels be careful to get all tunnel parts defined as close to ground surface beneath the ground surface;

The undisturbed ground temperature is computed using the one-dimensional heat equation with Dirichlet boundary conditions at ground surface and at a depth, such that variations at the ground level are handled in a correct way.

$$\rho_{gr} c_{pgr} \frac{\partial T_z}{\partial t} = \frac{\partial}{\partial z}\left(k_{gr} \frac{\partial T_z}{\partial z}\right)$$

with boundary conditions,

$T_z = T_{amb}(T)$ at ground surface $z = 0$

$T_z = \overline{T_{amb}}$ at bottom of computational domain

where,

T_z – Undisturbed temperature in ground (˚C)

ρ_{gr} – Density in ground (kg/m3)

c_{pgr} – Specific heat in ground (J/kg˚C)

k_{gr} – Thermal conductivity in ground (W/m˚C).

$\overline{T_{amb}}$ – Mean of T_{amb} (˚C) TWall0

The Geothermal effects are modelled by a constant vertical temperature gradient.

$$T_g = gradT\, z$$

Where,

T_g – temperature in ground due to geothermal effects (0 at ground surface) (˚C)

$gradT$ – geothermal temperature gradient (˚C/m) geoTGrad

z – vertical coordinate starting from ground surface (m)

“The temperature fields are computed using the 1D conduction-advection equation in cylindrical coordinates and is carried out around each segment. The size of the computational domain in radial direction is estimated by looking at the 1D heat equation with constant properties. To achieve ‘equal’ properties in all layers the thickness of each layer is adjusted by a dimensional analysis. Given a typical time scale one can decide where to set the outer boundary condition (Dirichlet or no-flow B.C.) with an error smaller than a given tolerance as compared to an infinite domain.” [53]

$$2\pi r \rho_{wall}(r) c_{pwall}(r) \frac{\partial T_r}{\partial t} = 2\pi \frac{\partial}{\partial r}\left(k_{wall}(r) r \frac{\partial T_r}{\partial r}\right) + m_{seep} c_{pWat} \frac{\partial T_r}{\partial r}$$

with boundary conditions,

$$-2\pi k_{wall}(r_0) r_0 \frac{\partial T_r}{\partial t} = \alpha(T_{air} - T_{wall}) + Q_{wall}/l \text{ at wall surface } r_0$$

$\frac{\partial T_r}{\partial t} = 0 \quad or \quad T_r = 0$ at outer boundary of computational domain.

Where,

T_r – Temp. change in wall caused by conditions in segment/platform/plenum (˚C);

T_{wall} – temperature in wall surface (˚C);

$\rho_{wall}(r)$ – density in wall (kg/m3);

$c_{pWall}(r)$ – specific heat in wall (J/kg˚C);

c_{pWat} – specific heat of water (J/kg˚C); CP_WAT

m_{seep} – water seepage/meter out of wall (= 0 in IDA RTV) (kg/sm); mSeep

$k_{wall}(r)$ – thermal conductivity in wall (W/m˚C);

α – $U^* Awall / l$ = heat transfer coefficient between wall and segment/platform/plenum (W/m˚C); Alfa

U – Total heat transfer coefficient containing convection and radiation depending on temperature, extinction coefficient and hydraulic diameter (W/ m2˚C); Utot

A_{wall} – Wall area of segment/platform/plenum (m^2); aTun/AWall

l – Length of segment/platform/plenum (m); lTun/length

r_0 – Half the hydraulic diameter (m); rPlat

T_{air} – Air temperature in segment/platform/plenum (˚C); Tair

$$\boldsymbol{Q_{wall}} = Q_{fire} + Q_{equip} + Q_{evap} + Q_{occ} - Q_{pipe} + Q_{window} \text{ (W)}$$

Where,

Q_{fire} – $(1\text{-}f_{air})^* q_{fire}$ = Heat from fire to wall in segment/platform/plenum (W);

q_{fire} – Fire power (W);

Q_{equip} – $s_{equip} * q_{equipNom}$ = radiation heat from equipment to wall (W); Q2wall

s_{equip} – schedule;

$q_{equipNom}$ – nominal radiation load (W); Q2wallNom

Q_{evap} – $HFvap \cdot mcond \cdot l$ = heat from air to wall through condensation/evaporation (= 0 in IDA RTV) (W);

m_{cond} – Humidity flow between air and wall (= 0 in IDA RTV) (kg/sm); Humf

HF_{vap} – $2.501*10^6$ = water vaporization heat at 0 ˚C (J/kg) ; HF_VAP

Q_{occ} – $s_{occ}*N_{occ}*1.8*(3.96E^{-8}*f_{cl}*((T_{cl}+273.15)^4-(T+273.15)^4))$; QOcc2wall

Radiation from occupants to wall in platform (Q_{occ} = 0 in sections and plenums; [kW]

N_{occ} – Maximum number of persons on platform; nOcc

s_{occ} – Occupancy coefficient (schedule); schedOcc

T_{cl} – Temperature of clothes (˚C) TCl

f_{cl} – Area increase factor; fCl

f_{air} – Fraction of firepower directly to air (the rest goes to the wall);

Q_{pipe} – $Q_{wallP}*l$ in sections, otherwise 0 QWallPl2r

heat to cooling pipes (see 2.2.9) (W); QWallPr2l

Q_{window} – $Q_{wall} = \sum Q_{dir\_j} + Q_{diff\_j} + Q_{back\_j} + Q_{win\_j}$

heat radiation through and from windows to wall (platform only) (W);

Q_{dir_j} – Direct inward radiation through window *j* (platform only) (W); winRad[j].Q_dir

Q_{diff_j} – diffuse inward radiation through window *j* (platform only) (W); winRad[j].Q_diff

Q_{back_j} – - Outward radiation through window *j* (platform only). winRad[j].Q_back

Computed from Q_{dir} and Q_{diff} (W)

Q_{win_j} – $5A_{win\_j}(T_{win\_j} - T_{wall})$ win[j].Qlw

Long wave radiation from window *j* (platform only) (W)

A_{win_j} – Area of window *j* (m^2); win[j].area

T_{win_j} – Temperature of window *j* (˚C); win[j].TGlass

The partial differential equations are discretized using finite difference methods in space. The discretization is governed by a grid factor (quotient between consecutive cell lengths) to yield finer grid at segment/platform and ground surfaces. The detailed solution of this can be seen from the *IDA Tunnel* Reference [53].

A.1.2.4. Fire model

Usually, fires can be located and specified in different sections, plenums and even platforms. For a section, the fire is limited to one segment where the developed firepower q_{fire} is limited by temperature and the available air. This limitation of air is because air has 23.2% of oxygen and the energy that is developed per kg consumption of oxygen is 13.1 MJ thereby giving a maximum firepower of 3.04*m_{dot} MW.

$$q_{fire} = q_{sup} * f_{\lim\ T} * f_{\lim\ Air} * cq_1$$

Where,

q_{sup} – $q_{sup}(t)$ Supplied Maximum Fire power (W); FirPow

f_{limT} – **if** T_i <1500 -1 **else if** T_i >2000 - 0.1

else 0.1 + 0.9(1+ cos(π (T_i – 1500)/500))/2 = factor in interval [0.1 : 1] limiting power for high temperatures;

f_{limAir} – **if** |3.04m_{dot}| > q_{sup} 1 **else** 1 - f_{red} (1+ cos (π 3.04 m_{dot}/ q_{sup})) /2 =

factor in interval [1- f_{red}: 1] limiting power due to oxygen supply;

f_{red} – Reduction factor (default = 0.9) redF

cq_1 – Factor used for numerical reasons, integrated by a 1st order ODE with time constant τ_{fire} from zero to one if q_{sup} > 0 in a segment and back to zero when $qsup$ = 0. CQ1

The firepower in platform or plenum is q_{fire} = q_{sup}. The firepower q_{fire} is distributed to the air and wall:

f_{air} * q_{fire}	*to air &*
(q-f_{air}) * q_{fire}	*to wall.*

A.2. Fire Modelling on *ANSYS Fluent*

The section 4.4.2 in Chapter 4 talks about the representation of the fire *ANSYS Fluent*. The fire is not represented by any combustion mechanism but rather as a volumetric source of energy based on the principal conservation laws of mass balance. The selected combustion model reduces the complexity, uncertainty and burden of replicating the fire behaviour. Also, previous studies from Hue et.al. [52] demonstrate similar accuracy of same order when modelling the fire source as volumetric heat source or dedicated combustion model. The ideology is shown below in the Figure A.2.1, where the fire source is represented by a simple rectangular slab with the top surface emitting the combustion products and the mass balance being achieved by the entrainment of air through the sidewalls.

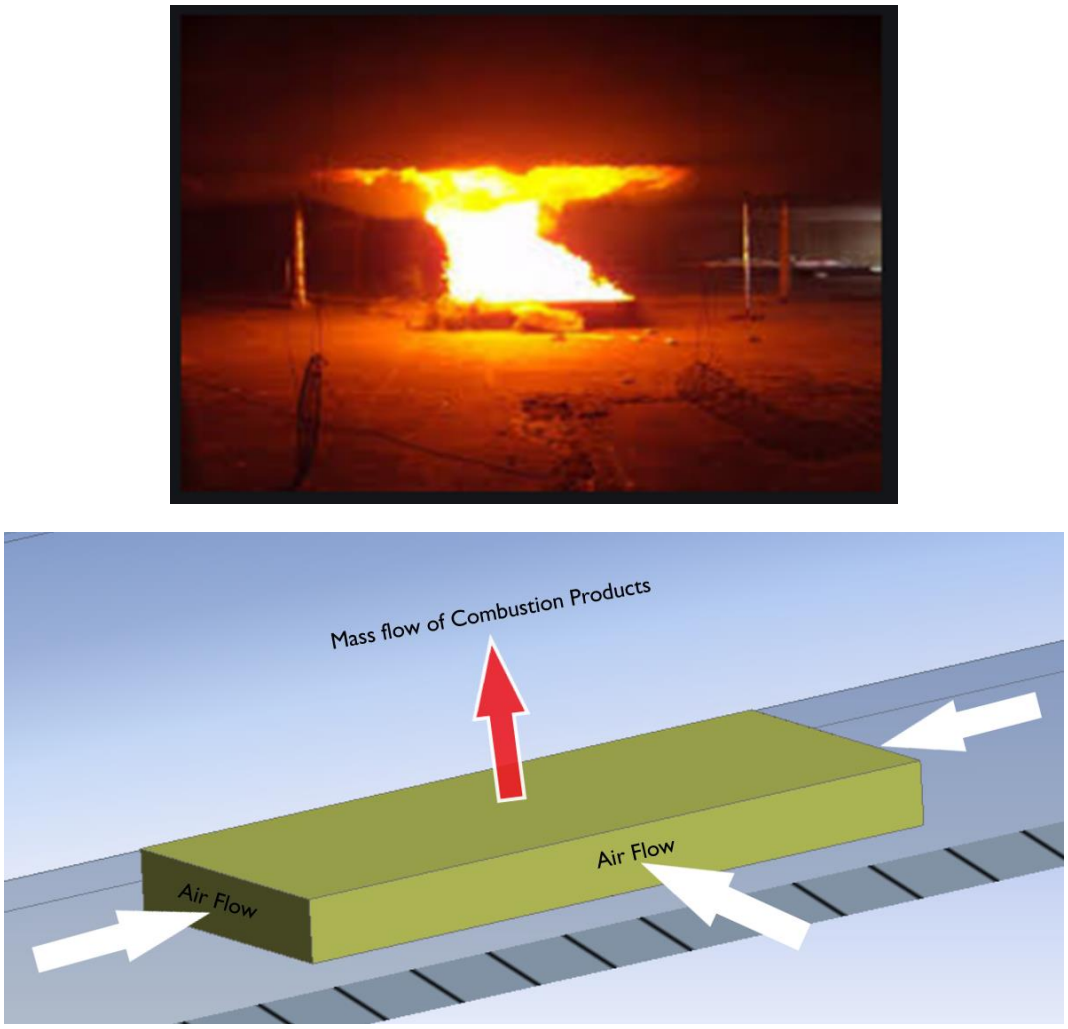

Figure A.1. Fire model for 20 MW fire: Top – Realization of a fire; Bottom – Set-up on *Fluent*

The fire source is kept as close as possible with respect to the ground so as to allow the fire source to evolve and spread naturally depending upon the ventilation present inside the tunnel. In order to obtain such a state of representation, where specific amount of HRR from the fire is released a simple calculation is carried out taking into account some thermal properties of the fire like Heat of combustion, Combustion Temperature, Yield of certain

species, etc. This is then used to calculate the minimum surface area needed to produce 20 MW and 250 MW fire for both the cases with and without LEP. The results of the calculations carried out for all the cases are shown below:

A.2.1. 20 MW fire with LEP

Input data for the 20 MW fire with LEP:

Heat of combustion	H	25.4	MJ/kg
Heat Release Rate	Q	20	MW
Soot Yield	Y_s	0.13	kg_s/kg_f
Combustion efficiency	K_{ic}	70.00%	-
Energy developed per consumed kg of O_2	E_{O2}	13.1	MJ/kg_{O2}
Mass of O_2 per kg of air	M_{O2}	23.14%	kg_{O2}/kg_{AIR}
CO Yield	Y_s	0.031	kg_{CO}/kg_f
Supply Temperature (from *IDA Tunnel* Simulation)	T_{air}	37.699	°C
Heat of combustion for sqm	H_{sqm}	800	kW/m^2

Table A.1. Input Data for the 20 MW fire with LEP.

Fuel mass loss rate	q_c	1.12	kg/s
Soot mass production rate	$\dot{m}_s$	0.15	kg/s
Combustion air mass loss rate	$\dot{m}_{air}$	6.6	kg/s
Total combustion mass rate	$\dot{m}_{combustion}$	7.7	kg/s
CO mass production rate	$\dot{m}_{CO}$	0.03	kg/s
Combustion mixture Temperature (K)	T_g	2271.43	K
Combustion Surface	Ac	25.00	m^2
Side surfaces for combustion air	A_A	7.92	m2
CO_2 mass production rate	$\dot{m}_{air}$	2.4	kg/s
Residual air rate (N_2, i.e.)	$\dot{m}_{N2}$	5.2	kg/s
Specific heat mixture	C_p	1.321	kJ/kgK

Table A.2. Results of the Calculations for the 20 MW fire with LEP.

A.2.2. 20 MW fire without LEP

Similarly, for the case of the 20 MW fire without the LEP the calculations are carried out with the input values as describe below. The data were obtained from previous research and experiments from reference [33], [35], [36] and [37].

Input data for the 20 MW fire without LEP:

Heat of combustion	H	25.4	MJ/kg
Heat Release Rate	Q	20	MW
Soot Yield	Y_s	0.13	kg_s/kg_f
Combustion efficiency	K_{ic}	70.00%	-
Energy developed per consumed kg of O_2	E_{O2}	13.1	MJ/kg_{O2}
Mass of O_2 per kg of air	M_{O2}	23.14%	kg_{O2}/kg_{AIR}
CO Yield	Y_s	0.031	kg_{CO}/kg_f
Supply Temperature (from *IDA Tunnel* Simulation)	T_{air}	37.609	°C
Heat of combustion for sqm	H_{sqm}	800	kW/m^2

Table A.3. Input Data 20 MW fire without LEP.

Fuel mass loss rate	q_c	1.12	kg/s
Soot mass production rate	$\dot{m}_s$	0.15	kg/s
Combustion air mass loss rate	$\dot{m}_{air}$	6.6	kg/s
Total combustion mass rate	$\dot{m}_{combustion}$	7.7	kg/s
CO mass production rate	$\dot{m}_{CO}$	0.03	kg/s
Combustion mixture Temperature (K)	T_g	2271.34	K
Combustion Surface	A_c	25.00	m^2
Side surfaces for combustion air	A_A	7.92	m2
CO_2 mass production rate	$\dot{m}_{air}$	2.4	kg/s
Residual air rate (N_2, i.e.)	$\dot{m}_{N2}$	5.2	kg/s
Specific heat mixture	C_p	1.321	kJ/kgK

Table A.4. Results of the Calculations 20 MW fire without LEP.

A.2.3. 250 MW fire with LEP

For the case of 250 MW fire the area needed to represent the HRR is quite high. As a result, the rectangular slab is divided into two sub-sections wherein combustion products are released from the top slab surface and the air entrainment takes place through the walls of the bottom slab, thereby respecting the conservation of mass. The representation is also verified to a fine extent so as to avoid representing the fire source as a jet stream which would contradict our analysis.

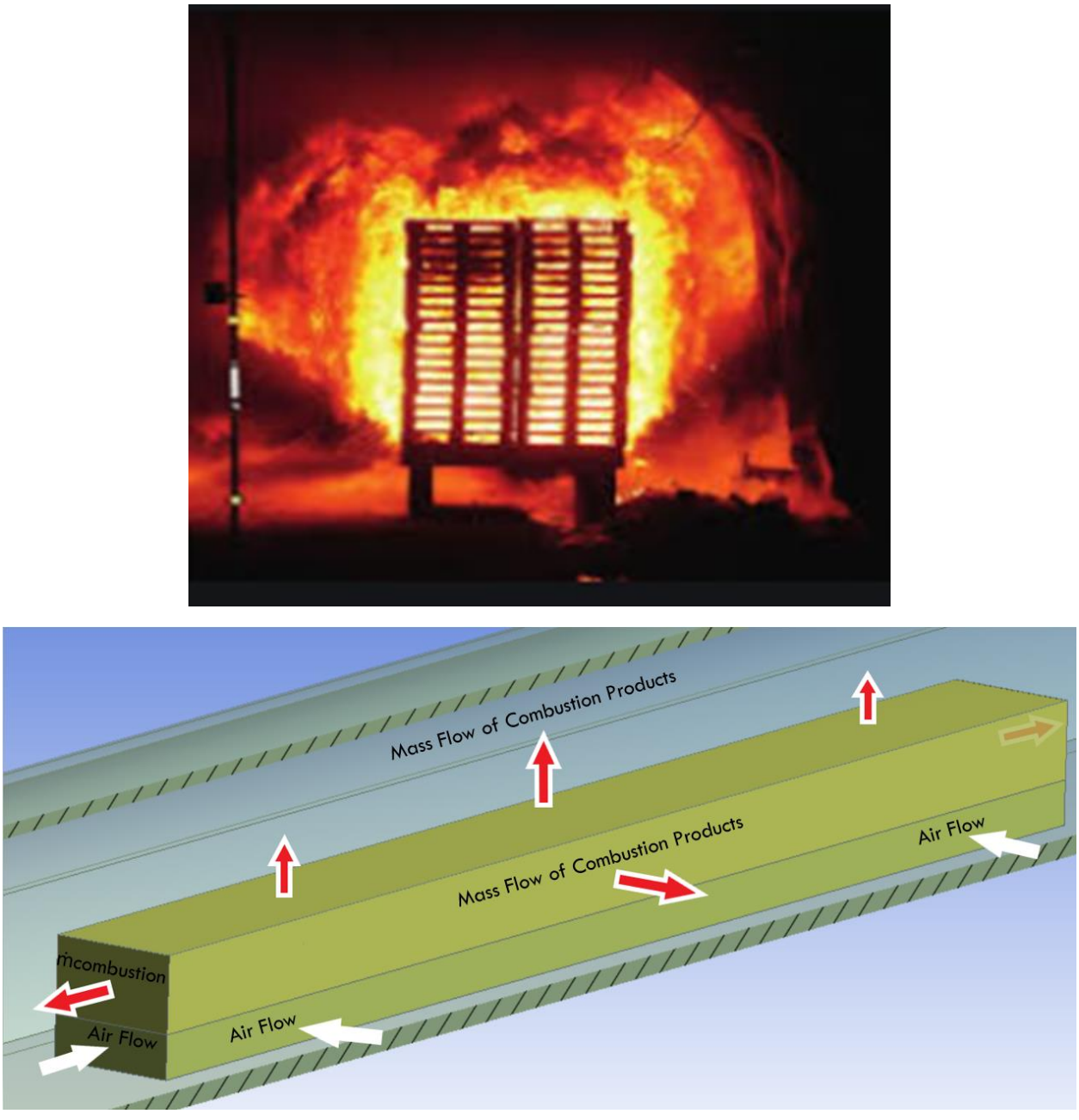

Figure A.2. Fire model for 250 MW fire: Top – Realization of a fire; Bottom – Set-up on *Fluent*

Input data for the 250 MW fire with LEP:

Heat of combustion	H	25.4	MJ/kg
Heat Release Rate	Q	250	MW
Soot Yield	Y_s	0.13	kg_s/kg_f
Combustion efficiency	K_{ic}	70.00%	-
Energy developed per consumed kg of O_2	E_{O2}	13.1	MJ/kg_{O2}
Mass of O_2 per kg of air	M_{O2}	23.14%	kg_{O2}/kg_{AIR}
CO Yield	Y_s	0.031	kg_{CO}/kg_f
Supply Temperature (from *IDA Tunnel* Simulation)	T_{air}	39.579	°C
Heat of combustion for sqm	H_{sqm}	800	kW/m^2

Table A.5. Input Data for 250 MW fire with LEP.

Fuel mass loss rate	q_c	14.06	kg/s
Soot mass production rate	$\dot{m}_s$	1.83	kg/s
Combustion air mass loss rate	$\dot{m}_{air}$	82.5	kg/s
Total combustion mass rate	$\dot{m}_{combustion}$	96.5	kg/s
CO mass production rate	$\dot{m}_{CO}$	0.44	kg/s
Combustion mixture Temperature (K)	T_g	2273.31	K
Combustion Surface	Ac	312.50	m^2
Side surfaces for combustion air	A_A	98.97	m2
CO_2 mass production rate	$\dot{m}_{air}$	29.5	kg/s
Residual air rate (N_2, i.e.)	$\dot{m}_{N2}$	64.7	kg/s
Specific heat mixture	C_p	1.321	kJ/kgK

Table A.6. Results of the Calculations for 250 MW fire with LEP.

A.2.4. 250 MW fire without LEP

Input data for 250 MW fire without LEP:

Heat of combustion	H	25.4	MJ/kg
Heat Release Rate	Q	250	MW
Soot Yield	Y_s	0.13	kg_s/kg_f
Combustion efficiency	K_{ic}	70.00%	-
Energy developed per consumed kg of O_2	E_{O2}	13.1	MJ/kg_{O2}
Mass of O_2 per kg of air	M_{O2}	23.14%	kg_{O2}/kg_{AIR}
CO Yield	Y_s	0.031	kg_{CO}/kg_f
Supply Temperature (from *IDA Tunnel* Simulation)	T_{air}	44.372	°C
Heat of combustion for sqm	H_{sqm}	800	kW/m^2

Table A.7. Input Data for 250 MW fire without LEP.

Fuel mass loss rate	q_c	14.06	kg/s
Soot mass production rate	$\dot{m}_s$	1.83	kg/s
Combustion air mass loss rate	$\dot{m}_{air}$	82.5	kg/s
Total combustion mass rate	$\dot{m}_{combustion}$	96.5	kg/s
CO mass production rate	$\dot{m}_{CO}$	0.44	kg/s
Combustion mixture Temperature (K)	T_g	2278.10	K
Combustion Surface	Ac	312.50	m^2
Side surfaces for combustion air	A_A	98.97	m2
CO_2 mass production rate	$\dot{m}_{air}$	29.5	kg/s
Residual air rate (N_2, i.e.)	$\dot{m}_{N2}$	64.7	kg/s
Specific heat mixture	C_p	1.321	kJ/kgK

Table A.8. Results of the Calculations for 250 MW fire without LEP.

A.3. Results of the CFD Simulations – Temperature Distributions:

A.3.1. Scenario 1: Train on fire stopped in the tunnel at ch. 5+100 with HRR of 20 MW:

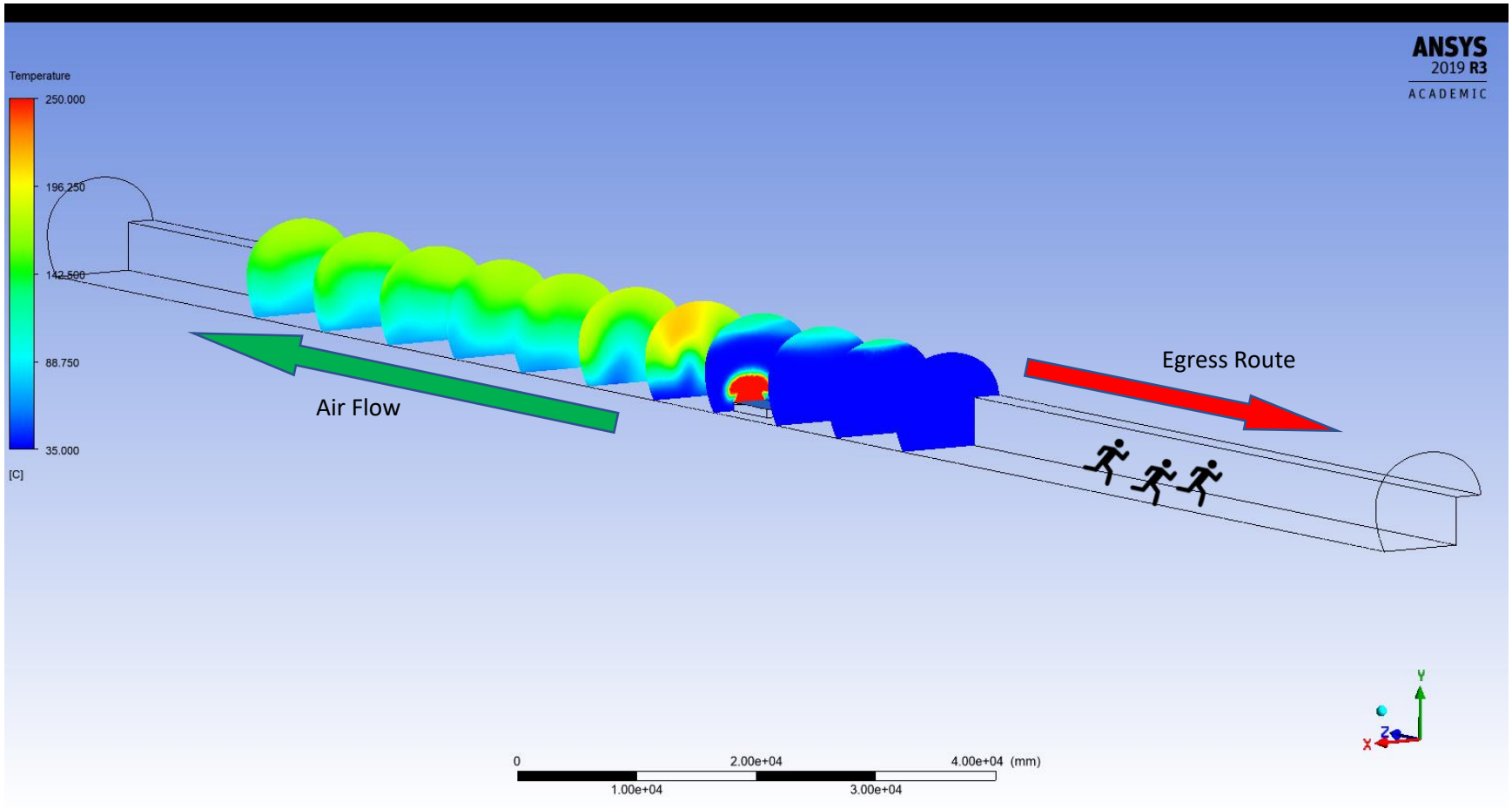

Figure A.3. Temperature Distribution for Scenario 1.

A.3.2. Scenario 2: Train on fire stopped in the tunnel at ch. 5+100 with HRR of 250 MW

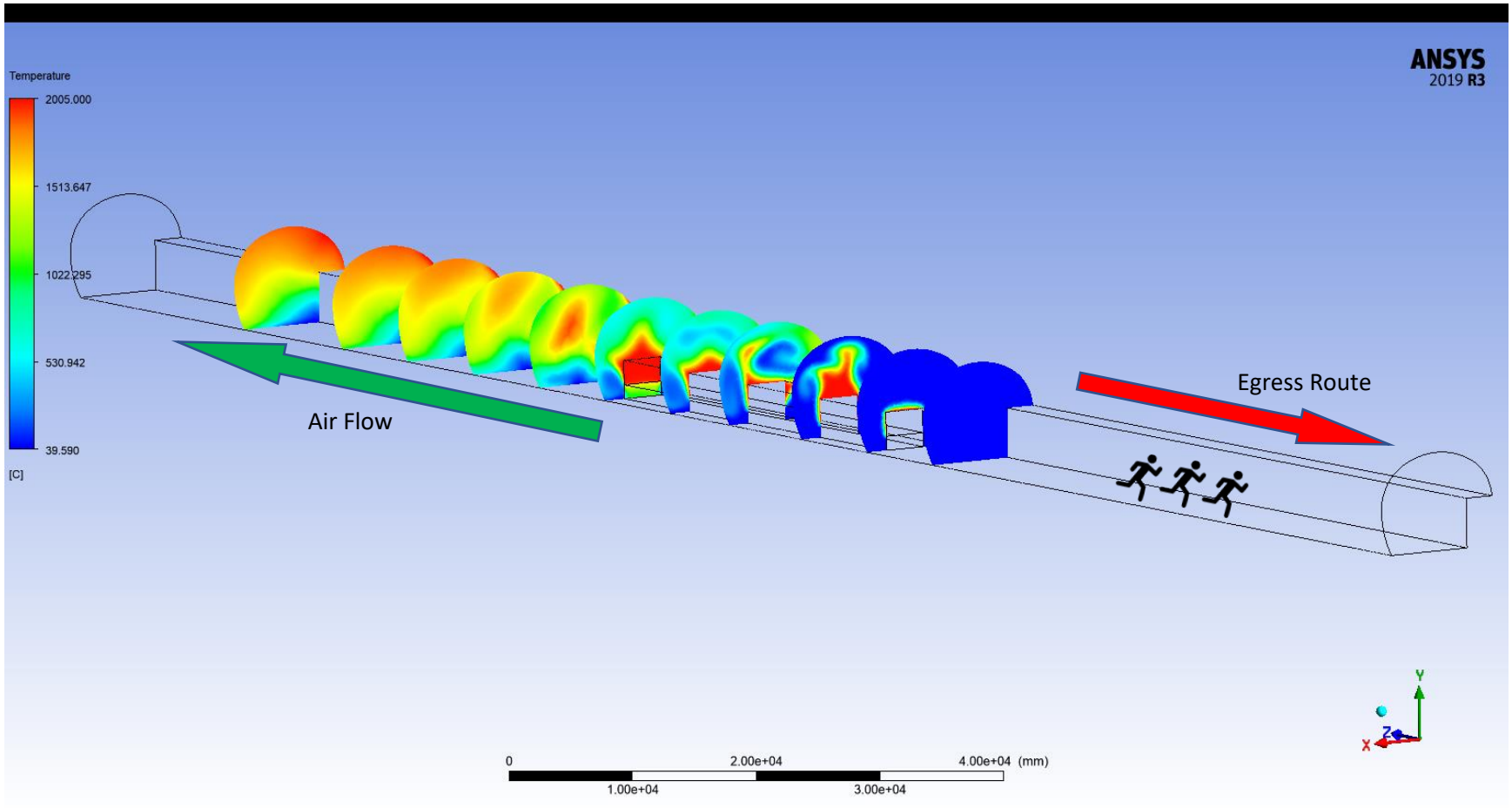

Figure A.4. Temperature Distribution for Scenario 2.

A.3.3. Scenario 3: Train on fire stopped in the tunnel at ch. 6+450 with HRR of 20 MW

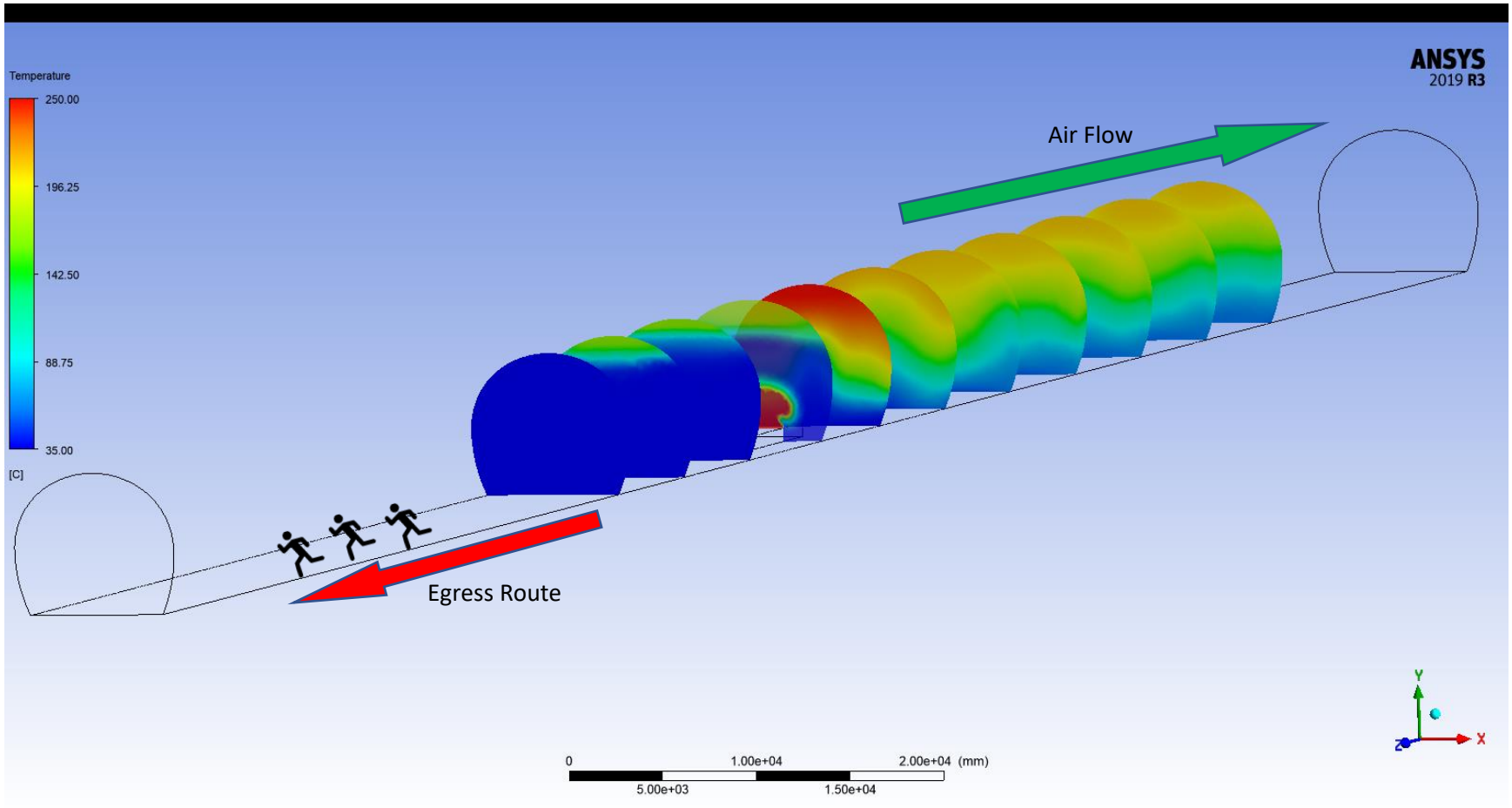

Figure A.5. Temperature Distribution for Scenario 3.

A.3.4. Scenario 4: Train on fire stopped in the tunnel at ch. 6+450 with HRR of 250 MW

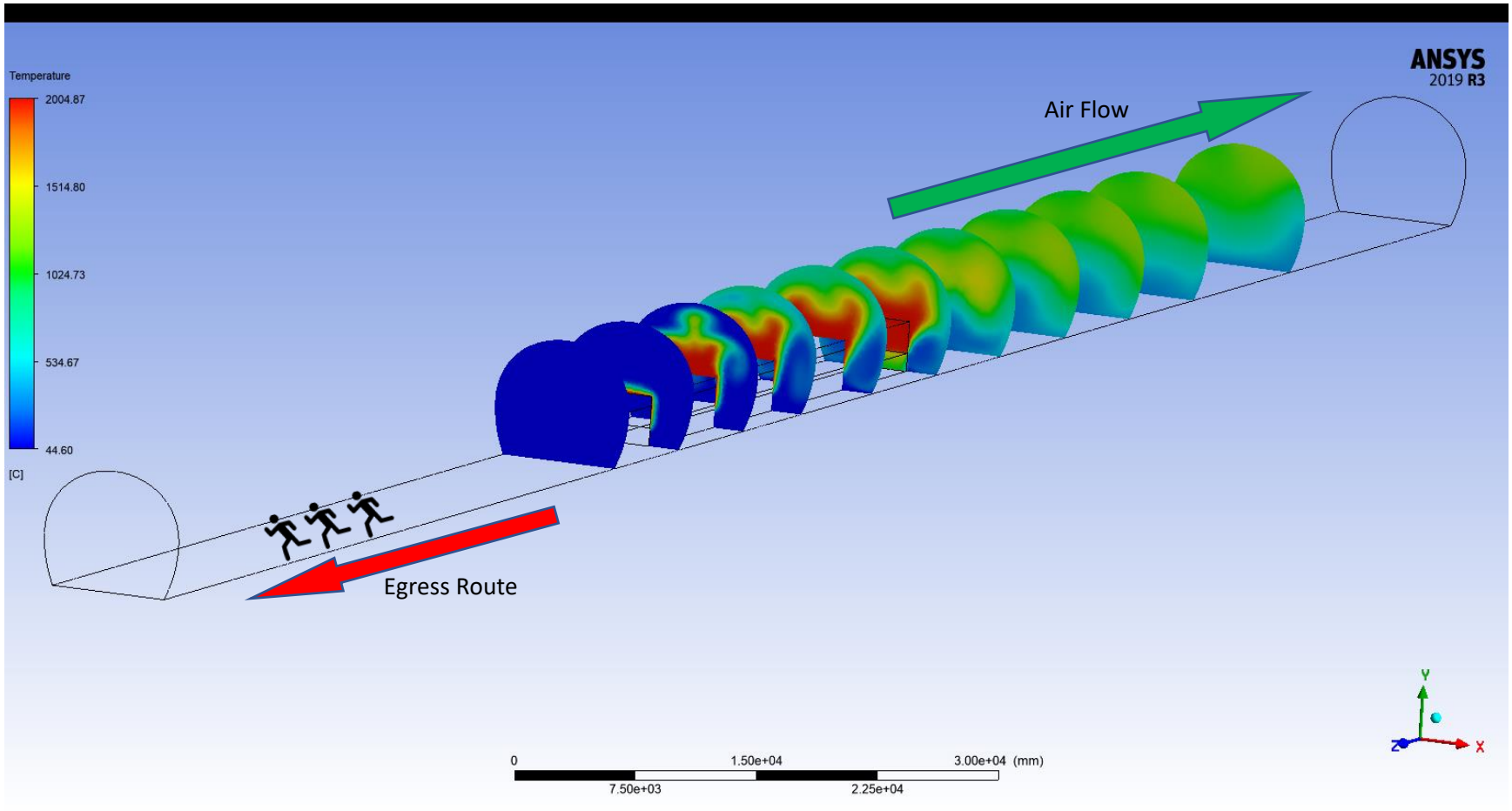

Figure A.6. Temperature Distribution for Scenario 4.